

INFORMATION TO USERS

This manuscript has been reproduced from the microfilm master. UMI films the text directly from the original or copy submitted. Thus, some thesis and dissertation copies are in typewriter face, while others may be from any type of computer printer.

The quality of this reproduction is dependent upon the quality of the copy submitted. Broken or indistinct print, colored or poor quality illustrations and photographs, print bleedthrough, substandard margins, and improper alignment can adversely affect reproduction.

In the unlikely event that the author did not send UMI a complete manuscript and there are missing pages, these will be noted. Also, if unauthorized copyright material had to be removed, a note will indicate the deletion.

Oversize materials (e.g., maps, drawings, charts) are reproduced by sectioning the original, beginning at the upper left-hand corner and continuing from left to right in equal sections with small overlaps.

**ProQuest Information and Learning
300 North Zeeb Road, Ann Arbor, MI 48106-1346 USA
800-521-0600**

UMI[®]

**BUOYANCY EFFECTS ON BUILDING PRESSURIZATION
IN EXTREME COLD CLIMATES**

**A
DISSERTATION**

**Presented to the Faculty
of the University of Alaska Fairbanks
in Partial Fulfillment of the Requirements
for the Degree of
DOCTOR OF PHILOSOPHY**

**By
Harold Edward Bargar, BSME, MSME, PE**

Fairbanks, Alaska

May 2003

UMI Number: 3079036

UMI[®]

UMI Microform 3079036

Copyright 2003 by ProQuest Information and Learning Company.
All rights reserved. This microform edition is protected against
unauthorized copying under Title 17, United States Code.

ProQuest Information and Learning Company
300 North Zeeb Road
P.O. Box 1346
Ann Arbor, MI 48106-1346

Buoyancy Effects on Building Pressurization

In Extreme Cold Climates

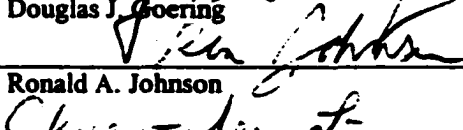
By

Harold Edward Bargar, P.E.

RECOMMENDED:



Douglas J. Goering



Ronald A. Johnson



Chuen-Sen Lin



Pham X. Quang



Deendra K. Das, Advisory Committee Chair



Jonah H. Lee, Mechanical Engineering Department Head

APPROVED:



David M. Woodall, Dean, CSEM



Joseph R. Kan, Dean, Graduate School

4-3-03

Date

ABSTRACT

This research investigates building pressurization due to buoyancy effect. The American Society of Heating, Refrigeration, and Air Conditioning Engineers (ASHRAE) presents an idealized equation to calculate the buoyancy effect. This dissertation compares differential pressure measurements from an actual building exposed to extremely cold temperatures to this idealized model. It also presents new statistical models based on the collected data. These new models should provide engineers with improved tools to properly account for building pressurization for designs in extreme cold climates.

Building pressurization, the differential pressure between the interior of a building and its exterior surroundings, is an important design consideration. Pressurization is the driving force in building infiltration/exfiltration. It also affects air flow within building zones. Improper calculation of pressurization can result in under-sizing the building's heating and cooling systems, improper operation of air distribution systems, improper operation of elevators, and freezing and failure of water distribution and circulation systems.

Building pressurization is affected by: wind (speed and direction), exterior-to-interior temperature difference, and mechanical equipment operation. In extreme cold climates, the predominant effect is air buoyancy due to temperature differences across the building envelope. The larger the temperature difference, the larger the buoyancy effect. In extreme cold climates, the largest temperature differences often occur at times when wind speed is negligible.

This dissertation also demonstrates the use of existing data sources such as building automation systems to collect data for basic research. Modern systems automation provides a tremendous amount of data that, in the past, had to be collected through separate instrumentation and data acquisition systems. Taking advantage of existing

automation systems can provide the required data at greatly reduced costs when compared to previous industry practices.

The statistical analysis approach taken in this research expands the tools for engineering design. Actual interactions of real world variables are analyzed and used to produce prediction models. These techniques allow the model to incorporate relationships which may not be fully understood at the underlying principle level but are evidenced in the data collected from actual installations.

TABLE OF CONTENTS

Table of Contents	v
List of Figures	vii
List of Tables	x
List of Equations	xi
Acknowledgments	xii
1. Introduction	13
1.1 Wind Effect	13
1.2 Buoyancy Effect	19
1.3 Equipment Effect	31
1.4 Why Considering Building Pressurization is Important	33
1.5 Goals for this Research	36
2. Experimental Setup	38
2.1 Test Building	38
2.2 Instrumentation	41
2.3 Pressure Measurement Basics	46
2.4 Differential Pressure Instrumentation	52
3. Data	55
3.1 DDC Data Processing	55
3.2 Weather Data Processing	69
3.3 Combining the Data	76
3.4 Elimination of Wind Effect	81
3.5 Data Reorganization	83
3.6 Data Validation	87
4. Statistical Models	91
4.1 Simple Additive Model	91
4.2 Transformed Additive Model	98
4.3 Nonlinear Multiplicative Model	100

4.4 Nonlinear Inverse Temperature Model	107
4.5 Temperature Ratio Model	112
4.6 Additive Temperature Ratio Model	119
4.7 Additive Temperature Ratio with Intercept Model	125
5. Conclusions	131
5.1 Shortcomings of ASHRAE and Other Previous Methods	131
5.2 Models Developed in this Research	132
6. Recommendations	134
7. Appendix A – Data	140
References	141

LIST OF FIGURES

Figure 1 – Wind Stagnation	14
Figure 2 – Wind Flow Separation	14
Figure 3 – Basic Stack or Chimney Effect	20
Figure 4 – Simple Building NPL Location	23
Figure 5 – Flow Stream Pressure Analysis	24
Figure 6 – NPL for Simulated Building with Uniform Openings	25
Figure 7 – NPL Location	28
Figure 8 – Buoyancy Pressure Estimate Diagram, 8-Story Building	30
Figure 9 – West Elevation of the Ernest Gruening Building	38
Figure 10 – Typical Gruening Building Floor Plan	39
Figure 11 – DDC Control Panels and Terminal	42
Figure 12 – DDC Panel Internal View	42
Figure 13 – Differential Pressure (DP) Sensor Installation Schematic	45
Figure 14 – U-Tube Manometer	47
Figure 15 – Bourdon Tube Pressure Gage	49
Figure 16 – Diaphragm Pressure Transducer	50
Figure 17 – Variable Capacitance Pressure Transducer	51
Figure 18 – Differential Pressure Transmitter Installation	53
Figure 19 – Raw DDC Data Excerpt	57
Figure 20 – S-Function ddcExtract	67
Figure 21 – q1 DDC Data File Excerpt	68
Figure 22 – S-Function WeaExtract	75
Figure 23 – q1 Data File Excerpt	75
Figure 24 – S-Function MonMerg	77
Figure 25 – S-Function BldCombFile	78
Figure 26 – S-Function Ltrim	79
Figure 27 – q1 Combined Data File Excerpt	80

Figure 28 – S-Plus Interactive Command to Eliminate Wind Effect Records	83
Figure 29 – S-Plus Interactive Session to Create Serial Dataset	84
Figure 30 – S-Plus Interactive Session to Round Data	85
Figure 31 – Outlier Visualization	87
Figure 32 – Cook’s-D Evaluation of Data Points	89
Figure 33 – S-Plus Additive Model Report	92
Figure 34 – Additive Model – Residual vs. Fit Plot	94
Figure 35 – Additive Model Comparison at -40°F	95
Figure 36 – Additive Model Comparison at -20°F	95
Figure 37 – Additive Model Comparison at 0°F	96
Figure 38 – Additive Model Comparison at $+15^{\circ}\text{F}$	96
Figure 39 – Additive Model Comparison at $+40^{\circ}\text{F}$	97
Figure 40 – Additive Model Comparison at $+60^{\circ}\text{F}$	97
Figure 41 – S-Plus Transformed Additive Model Report	99
Figure 42 – Transformed Additive Model – Residual vs. Fit Plot	100
Figure 43 – S-Plus Multiplicative Model Report	101
Figure 44 – Multiplicative Model – Residual vs. Fit Plot	102
Figure 45 – Multiplicative Model Comparison at -40°F	103
Figure 46 – Multiplicative Model Comparison at -20°F	104
Figure 47 – Multiplicative Model Comparison at 0°F	104
Figure 48 – Multiplicative Model Comparison at $+15^{\circ}\text{F}$	105
Figure 49 – Multiplicative Model Comparison at $+40^{\circ}\text{F}$	105
Figure 50 – Multiplicative Model Comparison at $+60^{\circ}\text{F}$	106
Figure 51 – S-Plus Nonlinear Inverse Temperature Model Report	107
Figure 52 – Inverse Temperature Model – Residual vs. Fit Plot	108
Figure 53 – Inverse Temperature Model Comparison at -40°F	109
Figure 54 – Inverse Temperature Model Comparison at -20°F	110
Figure 55 – Inverse Temperature Model Comparison at 0°F	110
Figure 56 – Inverse Temperature Model Comparison at $+15^{\circ}\text{F}$	111

Figure 57 – Inverse Temperature Model Comparison at +40°F	111
Figure 58 – Inverse Temperature Model Comparison at +60°F	112
Figure 59 – S-Plus Temperature Ratio Model Report	114
Figure 60 – Temperature Ratio Model – Residual vs. Fit Plot	115
Figure 61 – Temperature Ratio Model Comparison at –40°F	116
Figure 62 – Temperature Ratio Model Comparison at –20°F	116
Figure 63 – Temperature Ratio Model Comparison at 0°F	117
Figure 64 – Temperature Ratio Model Comparison at +15°F	117
Figure 65 – Temperature Ratio Model Comparison at +40°F	118
Figure 66 – Temperature Ratio Model Comparison at +60°F	118
Figure 67 – S-Plus Additive Temperature Ratio Model Report	120
Figure 68 – Additive Temperature Ratio Model – Residual vs. Fit Plot	121
Figure 69 – Additive Temperature Ratio Model Comparison at –40°F	122
Figure 70 – Additive Temperature Ratio Model Comparison at –20°F	122
Figure 71 – Additive Temperature Ratio Model Comparison at 0°F	123
Figure 72 – Additive Temperature Ratio Model Comparison at +15°F	123
Figure 73 – Additive Temperature Ratio Model Comparison at +40°F	124
Figure 74 – Additive Temperature Ratio Model Comparison at +60°F	124
Figure 75 – S-Plus Additive Temperature Ratio w/Intercept Model Report	126
Figure 76 – Additive Temperature Ratio w/Intercept Model – Residual vs. Fit Plot	126
Figure 77 – Additive Temperature Ratio w/Intercept Model Comparison at –40°F	127
Figure 78 – Additive Temperature Ratio w/Intercept Model Comparison at –20°F	128
Figure 79 – Additive Temperature Ratio w/Intercept Model Comparison at 0°F	128
Figure 80 – Additive Temperature Ratio w/Intercept Model Comparison at +15°F	129
Figure 81 – Additive Temperature Ratio w/Intercept Model Comparison at +40°F	129
Figure 82 – Additive Temperature Ratio w/Intercept Model Comparison at +60°F	130

LIST OF TABLES

Table 1 – ASHRAE Load Calculation Manual C_p Values	17
Table 2 – Typical Wind Surface Pressure Estimates	19
Table 3 – Typical Buoyancy Pressure Estimates	30
Table 4 – Research Data DDC Point Names	44
Table 5 – Monthly DDC Data Excerpt	65
Table 6 – Raw Weather Data Excerpt (Jan-Jul Form)	70
Table 7 – Raw Weather Data Excerpt (Aug-Dec Form)	71
Table 8 – Monthly Weather Data Excerpt (Jan-Jul Form)	73
Table 9 – Monthly Weather Data Excerpt (Aug-Dec Form)	74
Table 9 – Wind Elimination Criteria	82
Table 10 – Serial Structure Dataset Excerpt	86
Table 11 – Cook’s-D Influential Point Details	89

LIST OF EQUATIONS

Equation (1) – Bernoulli’s Equation Along a Flow Line	14
Equation (2) – ASHRAE 1997 Equation for Wind Pressurization (P_w)	16
Equation (3) – Normalized Wind Surface Pressure Coefficient ($C_{p,n}$)	17
Equation (4) – Theoretical Chimney Draft	21
Equation (5) – Bernoulli for Simple Flow Analysis Across the Envelope	23
Equation (6) – Stack Effect Pressurization	25
Equation (7) – ASHRAE Stack Effect Pressurization	27
Equation (8) – Stack Effect Pressurization with Draft Coefficient	29
Equation (9) – Manometer Equation	47
Equation (10) – Simplified Manometer Equation	48
Equation (11) – Variable Capacitance Transducer	51
Equation (12) – Simple Additive Model Form	91
Equation (13) – Additive Model Fit	92
Equation (14) – Transformed Additive Model Form	99
Equation (15) – Multiplicative Model Form	101
Equation (16) – Multiplicative Model Fit	103
Equation (17) – Nonlinear Inverse Temperature Model Form	107
Equation (18) – Nonlinear Inverse Temperature Model Fit	109
Equation (19) – Nonlinear Temperature Ratio Model Form	113
Equation (20) – Nonlinear Temperature Ratio Model Fit	114
Equation (21) – Additive Temperature Ratio Model Form	119
Equation (22) – Additive Temperature Ratio Model Fit	121
Equation (23) – Additive Temperature Ratio w/Intercept Model Form	125
Equation (24) – Additive Temperature Ratio w/Intercept Model Fit	127

ACKNOWLEDGMENTS

The author wishes to thank the members of his Graduate Advisory Committee. The guidance provided and questions raised by Drs. Das, Goering, Johnson, Lin, and Quang not only assisted in developing the research but also aided in making the findings more understandable.

The author also wishes to thank Los Alamos National Laboratory (LANL) for the use of data from their instrument package located on the University of Alaska Fairbanks campus. Having this data available on the World Wide Web through LANL's NEWNET Project saved the expense of duplicate instrumentation for this research. Thanks also to Mr. Larry Sanders of LANL for his assistance with questions about the data from the NEWNET Web site.

1. Introduction

Building pressurization can be viewed as the pressure gradient between the inside and outside of a building or as the pressure gradient between different zones and/or levels within a building. These are related phenomenon. The American Society of Heating, Refrigeration, and Air Conditioning Engineers (ASHRAE, 1997) attributes the pressure gradient to three primary driving forces: pressure differences across the building envelope created by wind; air density differences between the air inside and outside the building envelope; and the operation of mechanical equipment such as combustion equipment and forced ventilation equipment within the building.

The first two driving forces mentioned above are environmental considerations. Their effect is not only dependent on the building's design but also on the site at which the building is located. The third driving force is generally environment and site independent. This pressurization effect is driven solely by decisions made concerning the mechanical equipment and system designs.

This dissertation deals primarily with buoyancy effect pressurization. However, a general consideration of the other two pressurization effects has been taken into account in interpreting and analyzing the data obtained for the test building.

1.1 Wind Effect

The external surfaces of a building are subjected to various pressures as wind flows around the building.

The windward surfaces, those surfaces facing into the wind, experience positive pressure forces as the velocity stagnates against the surface. Consider a small particle of air contained in the wind stream (Fig. 1). At location A, the particle is exposed to the local barometric or static pressure, P_A , and has a velocity of V_A . At

the building surface, location B, the particle stagnates. The pressure is P_B and the velocity is zero.

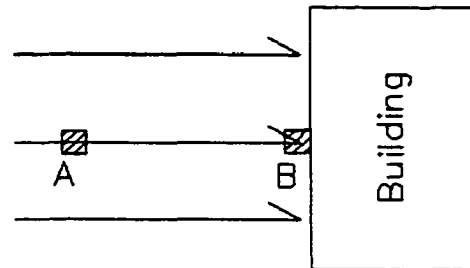


Figure 1. Wind Stagnation

Applying Bernoulli's Equation along the flow stream yields:

$$P_B = P_A + \frac{\rho V_A^2}{2} \quad (1)$$

The second term on the right hand side of Eq. (1) is generally referred to as the dynamic or velocity pressure. Since the barometric pressure is relatively stable for a given location, we see that the pressure exerted on a windward building surface is equal to the barometric pressure plus the dynamic pressure.

But the wind does not just stagnate on the windward side of a building. The flow streams bend around the structure causing shear flow on the sides of the structure and separate causing back eddies on the leeward side of a building as shown in Figure 2.

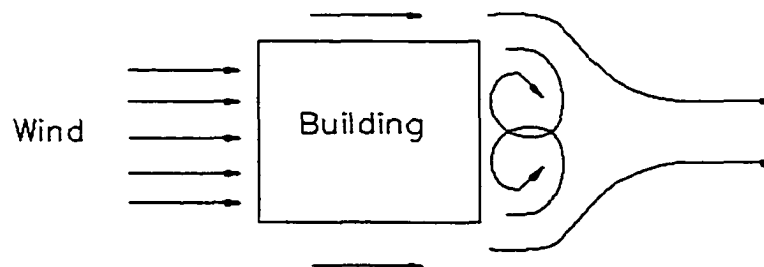


Figure 2. Wind Flow Separation

Another way to state Eq. (1) is that the total pressure at any point along a flow streamline is the sum of the static and dynamic pressures at that point. As the flow stream bends to move around the building, the streamlines move closer together thus compressing the flow tube. The law of continuity then requires that the velocity of the air increases in order to move the same quantity of air through the restricted flow tube. Since the velocity increases, the dynamic pressure also increases, but the total pressure must remain the same along the streamline. This means that the static pressure must decrease. This static pressure is the normal pressure that is exerted on the wind shear faces (those faces which are neither windward nor leeward) of the building. Finally, the static pressure exerted on the leeward surface of a building is a function of the separated flow and velocities of the eddy currents. These velocities, while slower than the free stream velocity, are always greater than the stagnation velocity on the windward side and thus the leeward pressure is always lower than that on the windward surface.

This variation in pressure on the building surfaces due to the flow of wind around the structure is known as wind effect pressurization.

Much research has been done on wind effect pressurization. One of the primary difficulties is determining the wind velocity at the building site. Wind data obtained from meteorological reports is at best a gross approximation of wind speed and direction at any given building site. Wind speed and direction recorded for meteorological reports are generally measured at 33 ft (10 m) above ground level in a clear field. That is, there are no obstructions to interfere with the wind.

At the ground surface, the laws of fluid mechanics dictate that the no-slip condition applies and the wind speed is zero. The wind speed tends to increase from zero at ground level to a maximum value approximately 2000 ft (600 m) above the ground

provided that there are no obstructions to the flow. The meteorological wind velocity is, therefore, only the velocity at a single point in this velocity profile.

The other problem with using meteorological wind data has to do with obstruction to wind flow at the building site. If a building is tall enough or in an otherwise relatively clear location, direct use of meteorological wind data may be acceptable (Tamura and Wilson, 1968). However, wind flow can be changed near the building by the terrain (Lee et al., 1980). Outcroppings, trees and vegetation, and other geographic features can change the wind flow locally around the building. Other buildings adjacent to a building being analyzed can shadow the building thus shielding it from direct impingement of the wind. Adjacent buildings can also channel the wind causing the local speed to be greater or the direction to be different than that reported in the meteorological data. Finally, the shape of the building itself can change the wind flow patterns. L-shapes, U-shapes, and wing walls can cause the building to be self-shielded from the wind or can amplify the wind's effect.

Based on previous research, the American Society of Heating, Refrigeration, and Air Conditioning Engineers (ASHRAE, 1997) recommends the following equation for estimating the wind effect surface pressure:

$$P_w = C_1 C_p \rho \frac{V^2}{2} \quad (2)$$

where: P_w = wind surface pressure [in. H₂O]
 ρ = air density [lbm/ft³]
 V = wind speed [mi/hr]
 C_p = wind surface pressure coefficient [unit less]
 C_1 = unit conversion factor = 0.0129

The key to using this equation is to determine the appropriate wind surface pressure coefficient, C_p . There are various methods of determining C_p depending on the building type, building environment and surroundings, and wind conditions. All methods are based on the underlying restrictions of the original research building(s) and so adoption of any method will undoubtedly result in some compromise of the true value.

A very simple approach is presented in ASHRAE's Load Calculation Manual (ASHRAE, undated). Table 5.5 of this manual lists C_p values for a rectangular footprint building with wind normal to the windward surface as:

Table 1. ASHRAE Load Calculation Manual C_p Values

	C_p
Windward	0.95
Leeward	-0.15
Sides	-0.40

A statistical study of 544 wind surface pressure coefficients by Swami and Chandra (1988) from several buildings yielded the following relationship:

$$C_{p,n} = Ln \left[\begin{array}{l} 1.248 - 0.703 \sin\left(\frac{\alpha}{2}\right) - 1.175 \sin^2(\alpha) \\ + 0.131 \sin^3(2\alpha G) + 0.769 \cos\left(\frac{\alpha}{2}\right) \\ + 0.07G^2 \sin^2\left(\frac{\alpha}{2}\right) + 0.717 \cos^2\left(\frac{\alpha}{2}\right) \end{array} \right] \quad (3)$$

where: $C_{p,n}$ = normalized C_p

α = angle between wind and wall outward normal [°]

G = natural log of the wall width to the adjacent wall width

This normalized C_p value is based on a zero incidence reference value of 0.6. To get the actual value of C_p for a given surface, multiply the result from Eq. (3) by 0.6. The relationship in Eq. (3) modeled all of the data in the study with a correlation coefficient of 0.80. However, even with this complex equation, the authors of the study note that the wind surface pressure coefficient predicted is likely to vary from an actual building surface's value due to complexities introduced by building geometry and geographic site conditions.

Tamura and Wilson (1968), Malik (1978), and many others also made similar observations concerning surface pressure coefficients and the complex relationship between the wind and a building's location within its surroundings. All references found on the prediction of wind surface pressure coefficients invariably conclude that to estimate wind effect pressurization accurately requires a wind tunnel test. Moreover, the model tested is not just a model of the building under analysis but also must consider features of the building's location such as adjacent buildings and geographic attributes.

Even with the uncertainties mentioned above, these methods can be used to obtain values indicative of the magnitude of the pressurizations due to wind effect. Table 2 shows values for wind surface pressure, P_w , for several wind speeds on the windward surface of the building. The building footprint is square (wall aspect ratio is 1) and the wind angle is normal to the building face. The windward surface with a normal wind will have the highest wind surface pressure. The values of C_p are taken to be 0.95 from the recommendations in Table 1 and 0.603 from calculation using Eq. (3).

Note that the wind pressurization effect is low until wind speeds become high (> 20 mph). Since wind speeds at these levels are generally short lived, the wind pressurization effect at these higher magnitudes is also short lived.

Table 2. Typical Wind Surface Pressure Estimates

Wind Speed [mph] ([km/hr])	Wind Surface Pressure [in. H ₂ O] ([Pa])	
	C _p = 0.95	C _p = 0.603
1.0 (1.6)	0.00046 (0.11)	0.00029 (0.07)
2.0 (3.2)	0.00184 (0.46)	0.00117 (0.29)
5.0 (8.0)	0.01149 (2.87)	0.00729 (1.82)
10.0 (16.1)	0.04596 (11.46)	0.02917 (7.27)
20.0 (32.2)	0.18383 (45.84)	0.11668 (29.10)
30.0 (48.3)	0.41361 (103.14)	0.26253 (65.47)

1.2 Buoyancy Effect

Air density differences due to temperature differences between the inside and outside of a building contribute to pressure gradients across the building envelope. This effect has been referred to by many names over the years including: buoyancy effect, stack or chimney effect, and density or gravimetric effect.

The mechanism behind this effect is the same as that which causes the draft in a chimney as shown in Fig. 3 (thus the name reference to chimney or stack effect). Warm (less dense) air rises and exits at the top of a structure, cooler (denser) air enters at the bottom of the structure to replace the air exiting. This air is heated, becoming less dense, and the cycle continues.

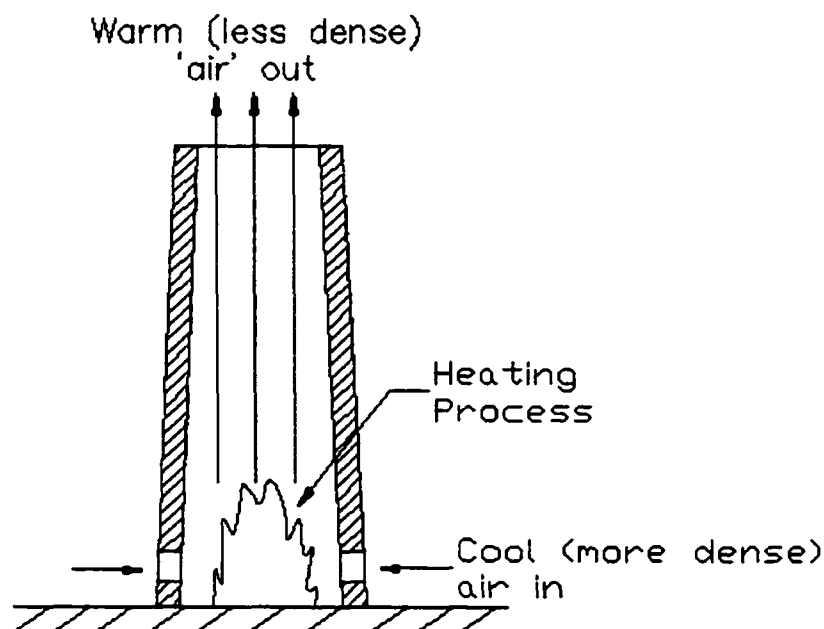


Figure 3. Basic Stack or Chimney Effect

For building buoyancy effect, this description is true for the heating season. That is, when the building's interior temperature is greater than the temperature of the environment surrounding the building. The opposite circulation of air takes place during the cooling season. At these times, the air within the building is cooler, and thus denser, than the air surrounding the building. So in the cooling season, the denser interior air sinks and exits at the lower levels of the building and is replaced by warmer, less dense, air at the higher levels of the building. While this effect does indeed occur, the temperature differences encountered are relatively small compared to those in the heating season. Therefore, buoyancy pressurization effects are generally greater during the heating season. For the remainder of this dissertation, heating season conditions will be assumed.

Building envelopes are not sealed structures. There are openings between the inside and outside of a building across the envelope that provide air flow paths. Doors and

windows in the envelope provide obvious air flow paths across the envelope. These flow paths are large when these appurtenances are open. But, even when closed, there are flow paths created at the door and window joints and the connection at the envelope's rough opening. Flow paths are also created at wall penetrations, structural cracks, and building expansion joints. Lastly, building materials themselves are porous to a greater or lesser extent and allow air flow when a driving pressure gradient exists across the structure.

These same flow paths exist in the interior of a structure and are augmented by design features to allow traffic flow such as corridors, stairwells, and elevator hoistways. These interior flow paths allow air to circulate within the building whenever there is a driving pressure gradient. This internal air flow is both horizontal at a given building level and vertical between levels of the building. Buoyancy effect building pressurization is concerned more with the vertical flow of air within a structure.

The theoretical draft in a chimney (or building) can be determined by the following equation as cited by Tamura and Wilson (1966):

$$P_c = 0.52PH \left(\frac{1}{T_o} - \frac{1}{T_i} \right) \quad (4)$$

where: P_c = pressure difference across the envelope [in. H₂O]

P = absolute pressure [lbf/in²]

H = height [ft]

T_o = absolute outside temperature [°R]

T_i = absolute inside temperature [°R]

The distribution of this pressure gradient across the building envelope is dependent on the location and magnitude of the air flow paths in the building's envelope and internally throughout the building.

Investigation of the pressure distribution across the envelope leads to the concept of the neutral pressure level (NPL). The pressure gradient causes air to flow into (infiltration) and out off (exfiltration) the building through the envelope's air flow paths. At steady state conditions, the mass flow of air must be conserved. Therefore, as much air must flow out of the building as flows into the building. If the interior and exterior temperatures are assumed to be constant over the building's height, then the variation in pressure is a function of the elevation at which the gradient across the envelope is measured. Therefore, at some elevation, the pressure difference must change form negative (infiltration) to positive (exfiltration). This elevation is called the NPL. Below the NPL, air infiltrates into the building. Above the NPL, air exfiltrates from the building. Note that this relationship is reversed during the cooling season.

The investigation of buoyancy effect pressurization (the pressure distribution on the envelope) is inextricably tied to the investigation of infiltration and exfiltration and the location of the NPL.

The simplest case would be a building with a perfectly sealed envelope except for one opening at its lowest level, another opening of equal area at its highest level, and no interior restrictions to air flow.

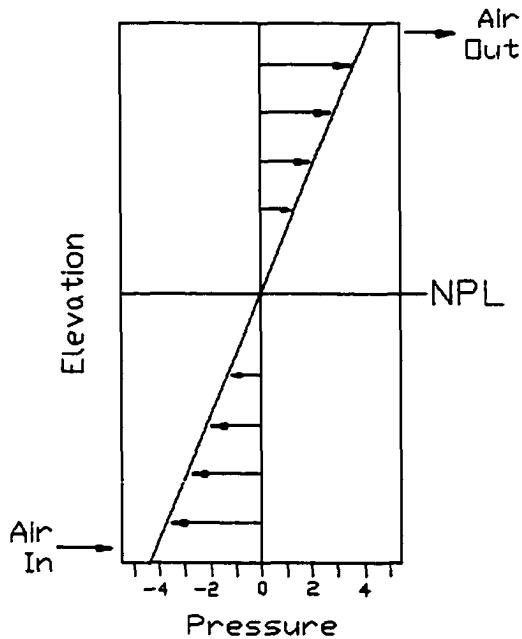


Figure 4. Simple Building NPL Location

As shown in Fig. 4, air infiltrates at the lower opening, an equal quantity of air exfiltrates at the upper opening, the pressure gradient is uniform over the elevation (lowest at the base of the building to highest at the top of the building), and the NPL is at the mid-point in the building's elevation.

Applying Bernoulli's Equation along a flow stream as shown in Fig. 5 will confirm the pressure gradients. The relation between points 1 and 2 is:

$$\frac{P_1}{\rho_1} + \frac{V_1^2}{2g} + Z_1 = \frac{P_2}{\rho_2} + \frac{V_2^2}{2g} + Z_2 + h_f \quad (5)$$

The elevation is the same for points 1 and 2 so the Z terms cancel. If points 1 and 2 are taken to be a significant distance from the flow opening through the envelope, then V_1 and V_2 are essentially zero and the velocity terms vanish. Since the density

of the cold air at 1 is greater than the density of the warmer air at 2, it follows that P_2 must be less than P_1 and the pressure gradient causes air to infiltrate provided that the gradient is sufficient to overcome the friction loss, h_f , for the flow path. A similar analysis could be carried out between points 2 and 3 and points 3 and 4. Thus a simple analysis based on fluid dynamics law, confirms the conditions observed in practice.

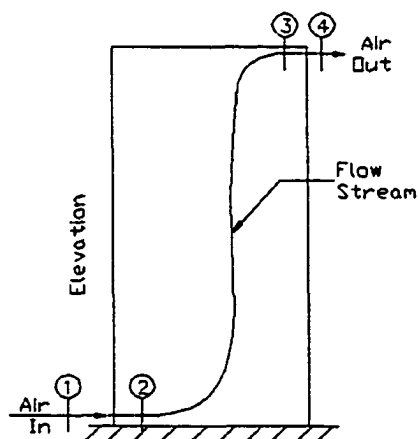


Figure 5. Flow Stream Pressure Analysis

A slightly more complicated model (Lee et al., 1985) simulated a tall building with a length of copper tubing. Holes in the tubing at specific elevations allowed infiltration/exfiltration at locations other than just the lowest and highest elevations. The holes were distributed in a uniform manner along the elevation. The tube contained no interior obstructions to impede the air flow vertically. The pressure distribution displayed in Fig. 6 resulted.

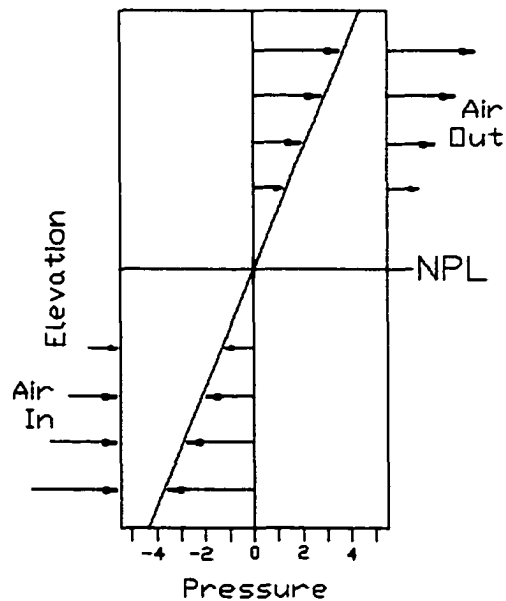


Figure 6. NPL for Simulated Building with Uniform Openings

The NPL remains at the mid-height of the simulated building because the openings are uniformly distributed along the elevation. The infiltration and exfiltration are proportional to the pressure difference at each elevation and there is no air flow at the NPL because there is no driving pressure differential. In other tests where the distribution and sizes of the openings were changed, the authors found that the location of the NPL could be significantly affected. It was found that the air flow behaved as predicted by ideal gas and fluid dynamics laws.

From this simulation, Lee et al. (1985) derived the following equation for the stack or buoyancy effect pressurization:

$$\Delta P_{Stack} = K_1 \left(\frac{1}{T_o} - \frac{1}{T_i} \right) (NPL - Z) \quad (6)$$

This relation shows that the pressure difference, ΔP , across the envelope at some elevation, Z , is a function of the inverse absolute temperature difference and the difference in elevation between the point in question and the elevation of the NPL. The problem now becomes one of determining the proper coefficient, K_1 , and location of the NPL for a given building's air flow openings and distribution.

Subsequent research by these same authors (Lee et al., 1988) modified the simulation to include internal floor partitioning. They concluded that accurate estimation of the buoyancy effect pressurization was possible if the distribution and geometry of the air flow openings in both the interior partitioning and the exterior envelope can be properly taken into account.

It is this in-depth knowledge of the air flow paths that makes calculation of buoyancy effect pressurization so difficult for "real world" buildings. The air flow paths in an actual building are not constant. Openings in the envelope and interior partitioning change over time. As the building expands and contracts due to changes in temperature, the geometry of the cracks and penetrations change. As the building settles, new cracks may form and older crack geometries may change or totally seal. Air flow paths due to operable doors and windows change as the doors and windows are used by the building occupants. All of these affect the elevation of the NPL, the amount of infiltration/exfiltration, and thus building pressurization at any given time. Studies by Min (1958), Tamura and Shaw (1976), and Kiel and Wilson (1986), to name just a few, have looked at the effects of door design and operation and exterior wall tightness on building pressurization due to buoyancy. But each study is specific to the building and/or specific geometry investigated.

Even though all of these investigations and simulations do not truly represent "real world" buildings, the 1997 ASHRAE Fundamentals Handbook recommends the

following equation based on this research to approximate the maximum stack effect that may occur.

$$\Delta P_s = C_2(\rho_o - \rho_i)g(h - h_{NPL}) = C_2\rho_i g(h - h_{NPL}) \left(\frac{T_i - T_o}{T_o} \right) \quad (7)$$

where: ΔP_s = pressure difference across the envelope [in. H₂O]
 ρ = air density [lbm/ft³]
 g = gravitational acceleration = 32.2 ft/s²
 h = height of observation [ft]
 h_{NPL} = height of NPL [ft]
 T = average absolute temperature [°R]
 C_2 = unit conversion factor = 0.00598
 i = subscript denoting indoor
 o = subscript denoting outdoor

It is left up to experience and similarities to prior research to determine the appropriate value for the elevation of the NPL. This uncertainty as to the location of the NPL for any given building or design can cause problems when applying Equation (7). In the practice of building design, the mid-height of the building is often taken as the location of the NPL. This is especially true for a new building design where there is no observed behavior from the building to contradict this assumption. The argument for this assumption is that the air pathways above and below the NPL are generally equal. If the infiltration must equal the exfiltration as stated above for steady state conditions, then the portion of the building above the NPL should equal the portion below the NPL. This results in the building's mid-height being the location of the NPL.

This reasoning also argues that the location of the NPL should not be effected by inside or outside temperature changes as long as the temperatures remain constant throughout and around the structure. Any changes in density due to temperature changes should act equally above and below the NPL. Thus the location of the NPL should remain unchanged.

Problems in estimating the location of the NPL are demonstrated by data from the test building for this dissertation. Figure 7 shows a plot of the NPL (differential pressure across the envelope equals zero) from the data collected for this research.

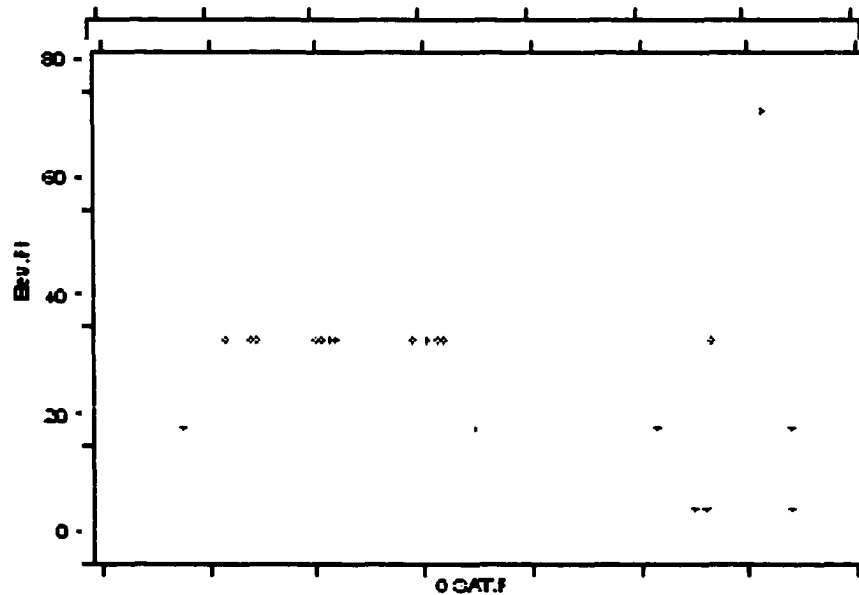


Figure 7. NPL Location

At the colder outside air temperatures (OSAT.F < 20°F) where the density differences between inside and outside air are greatest, the NPL is located just below 40 ft in elevation. This is the pressure sensor at the ceiling level of the 3rd story. This is

slightly below the mid-height of the building which is approximately 50 ft. However, the plot shows that the NPL drifts greatly at outside air temperatures of 40°F and above.

The statistical models developed in this dissertation will utilize the building's mid-height as the reference elevation to eliminate the uncertainty in the location of the NPL. Some of the models will include terms to attempt to account for the location of the NPL not being at the building mid-height.

Other references such as McQuiston et al. (2000) introduce a draft coefficient, C_d , to try to account for the air flow restrictions due to vertical partitioning within the building. Adding this coefficient to the theoretical draft equation results in:

$$\Delta P_s = \frac{C_d P_o h g}{R_a g_c} \left(\frac{1}{T_o} - \frac{1}{T_i} \right) \quad (8)$$

- where: ΔP_s = pressure difference across the envelope [in. H₂O]
 C_d = draft coefficient [unit less]
 P_o = outside pressure [lbf/in²]
 h = distance between observation and NPL [ft]
 T = average absolute temperature [°R]
 R_a = gas constant for air [ft-lbf/lbm-°R]
 g = gravitational acceleration = 32.2 ft/s²
 g_c = conversion factor = 32.2 ft-lbm/lbf-s²
 i = subscript denoting indoor
 o = subscript denoting outdoor

But this method still requires knowledge of the elevation of the NPL and estimation from experience or previous research of an appropriate value for a draft coefficient.

Even with all of the uncertainties, Eq. (7) can be used to establish buoyancy effect pressurization values to compare with pressurization due to wind effect and equipment effect. Assuming an eight story building as shown in Fig. 8 and letting the NPL reside at mid-height, the pressurization values for the top and bottom floors at the temperatures shown in Table 3 are obtained.

Note that the buoyancy effect pressure magnitudes are greater than those caused by wind effect (Table 2) for cold temperatures and low to moderate wind speeds.

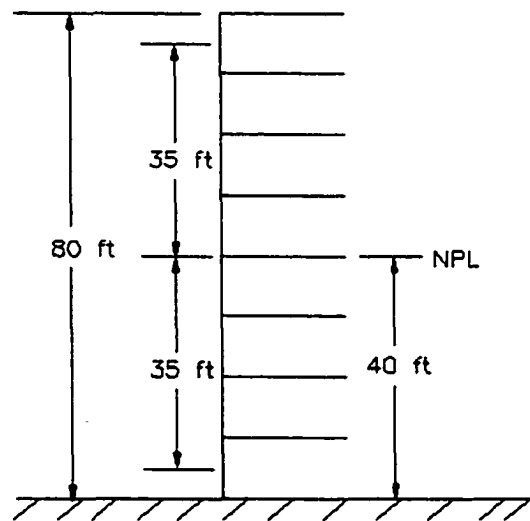


Figure 8. Buoyancy Pressure Estimate Diagram, 8-Story Building

Table 3. Typical Buoyancy Pressure Estimates

Outside Temp [°F] (°C)	Buoyancy Pressurization [in. H ₂ O] ([Pa])	
	Story -1	Story -8
50 (10)	-0.01982 (-4.94)	0.01982 (4.94)
30 (-1)	-0.04126 (-10.28)	0.04126 (10.28)
10 (-12)	-0.06453 (-16.08)	0.06453 (16.08)
-10 (-23)	-0.08986 (-22.39)	0.08986 (22.39)
-30 (-34)	-0.11755 (-29.29)	0.11755 (29.29)
-50 (-46)	-0.14794 (-36.86)	0.14794 (36.86)
Inside Temp = 70°F		

1.3 Equipment Effect

The final major contributor to building pressurization is equipment operated within the building. The two primary sources for overall building pressurization of this type are equipment which draws combustion air from within the building and ventilation equipment which either exhausts air from or introduces outside air into the building. Heating, ventilating, and air conditioning (HVAC) equipment and devices can also affect pressurization locally within a building by changing air temperatures and moving air between locations.

Combustion appliances, by using air in the combustion process and then exhausting the combustion products along with excess air, cause a building to be negatively pressurized. Outside air must enter the building to offset the air lost in the combustion appliance. If insufficient air enters the building, the combustion process can be starved and an unsafe combustion situation can ensue. For this reason, safety codes require that building designs include combustion air inlets for rooms containing combustion equipment or air inlets directly to the combustion appliance.

Building codes also require that outside ventilation air be introduced to a building. This makeup air replaces contaminated air that is exhausted and dilutes those contaminants that remain in order to provide a healthy and acceptable indoor air quality for the occupants. This outside ventilation air tends to positively pressurize the building. This building-wide pressurization tends to increase the overall exfiltration and drive the NPL lower in the building.

Equipment effect pressurization is very complex and interacts with wind and buoyancy effect at any point in time. It is also a function of the design of the air delivery and return systems, HVAC zoning, and interior building partitioning. Equipment effect is generally considered separately from the two environmental

pressurization effects during the design of the building's HVAC system and its control.

However, it is important not to fall into the trap of assuming that the HVAC system will be able to bring in enough outside air to positively pressurize the entire building. Explanation of this issue is presented by Bargar and Das (2001). This design attempt is often undertaken to avoid having to deal with infiltration heating loads at the lower levels (below the NPL). There are two major problems with this approach.

First, even if enough outside air is introduced to a building to force the pressure gradient across the envelope at the lowest level to be positive with respect to the outside, there will still be a pressure gradient within the building with respect to elevation within the building. This is due to the arguments based on Bernoulli's equation mentioned previously. In essence, this results in a shifting of the sloped line in Figs. 4 and 6 to the right so that the horizontal intercept is at zero pressure. Under these conditions, the NPL is forced to the zero elevation level and pressure gradients at all elevations above this zero level are positive with respect to the outside. Because buoyancy effect pressure gradients within a building at extreme cold temperatures can be very large, this results in a extremely high positive pressurization (> 1 in. H_2O) with respect to the outside in the upper floors of the building. This can cause occupant discomfort as well as equipment malfunction.

The second problem with this design attempt has to do with building and system dynamics. As noted, buoyancy pressurization at any level is a function of the location of the NPL. The elevation of the NPL is not fixed. As doors in the lower envelope open, the NPL moves down, and as these doors close, the NPL moves back up. The NPL is also affected by changes in air flow paths interior to the building as doors open and close. Wind effect will also change the NPL. The NPL will tend to cant upward on the windward side of the building and downward on the leeward side.

These changes in the NPL occur with a comparatively short time response. On the other hand, changing damper positions, speeding up and slowing down supply fans, and delivering air to the space is a relatively long time response operation. Therefore, it is not effective to try to use equipment pressurization to overpower environmental pressurization effects. This conclusion is borne out by the design for a recent tall building in Fairbanks. The building's pressurization controls and HVAC system cannot adequately overcome the buoyancy effect pressurization. As a result, substantial infiltration occurs at the building entries on the lowest level. Since the design assumed that the system would overpower the environmental pressurization effects, the heating capacity is inadequate and the temperatures regularly fall to unacceptable levels.

While it is difficult to quantify building pressurization due solely to equipment effect, Modera et al. (1991) did measure pressure difference across the envelope on the order of 0.012 to 0.024 in. H₂O (2.986 to 5.972 Pa) for low-rise residential buildings.

1.4 Why Considering Building Pressurization is Important

Buildings designed without proper consideration for environmental pressurization effects are likely to experience problems. These problems run the gamut from minor occupant discomfort to major facility damage.

In the heating season, infiltration of cold outside air will occur for building zones below the neutral pressure level. If the heating system in these zones is not designed to provide sufficient heat to counteract this infiltration load then the temperatures will fall below setpoint. At best, this may result in discomfort to the occupants and an associated loss in productivity. At worst, the temperature may fall below freezing and cause damage to various building systems.

An example of this worst case scenario (Phillips, 1997) is the test building used for this research. For several weeks in the winter of 1997/98 the outside temperature remained below -20°F (-29°C). During this time, cold air continuously infiltrated into the building entryways. Since the heating system was not designed to account for this infiltration load, the entryway temperatures grew progressively colder. Eventually the ceiling space above the entryway dropped below freezing and the water in the fire sprinkler system froze and burst the pipe. The thousands of gallons of water which discharge from the broken pipe before the firefighters could respond and shut off the system caused tens of thousands of dollars of damage to the entryway and surrounding spaces. In addition to the costs to repair the physical damage, there were also costs associated with the lost use of the facility while repairs were completed.

The case cited in Section 1.3 of the building design that tried to overpower the environmental pressurization effects by using the HVAC system is another example. While at first glance the problem would appear to be solely one of discomfort to the occupants and loss of productivity, other costs are also incurred. Even though the HVAC system time response prevents it from keeping up with the pressure fluctuations at the entryways, the control system still modulates the dampers, fan speed controls, and heating control valves in an attempt to meet the fluctuating load. This causes instability in the space conditions and wastes energy. In addition, the continued actuation of the dampers and valves will require increased maintenance for these devices and decrease their life necessitating early replacement.

At the opposite end of the spectrum, excessive positive pressure developed in the upper levels of the building can also create problems. An example (Phillips, 1997) is the case of a malfunctioning elevator on the University of Alaska Fairbanks campus. The elevator was located in an eight-story building. The elevator technician reported an increase in trouble calls when the outside temperatures became extremely cold and

again when the temperatures returned to more moderate ranges. The technician found that at the extreme cold temperatures, the elevator car would be stuck at an upper floor, its doors failing to close, and a large discharge of air from the elevator hoistway through the open doors. The internal pressure gradient due to pressurization effects was transporting air upward through the relatively unobstructed path of the hoistway and out the doors. The motor for the door operator was unable to develop sufficient torque to overcome the out rush of air. The technician adjusted the door operator to deliver more torque to the motor and all was well until the outside temperatures moderated. At more moderate outside temperatures, the trouble calls again increased. In this case, the elevator car was stuck at a floor with the doors closing rapidly and then bouncing back open. As the outside temperatures moderated, the pressure gradient within the building had decreased. Thus the quantity of air transiting the hoistway also decreased. The motor torque was now too great causing the doors to slam shut and rebound open. The solution was to decrease the torque on the door operator motor. Unfortunately, this readjustment of the door motor torque must be repeated several times throughout the winter season as the temperatures fluctuate. Not only does this add to the cost of maintaining the elevator but it also hinders occupant traffic flow within the building and decreases productivity.

Improper consideration of pressure gradients within the building can also adversely affect the HVAC air distribution systems. Ductwork systems are designed to provide the pressure required at the inlet side of diffusers, registers, and grilles (outlets) so that these devices can provide the proper air quantity and throw (distribution) to condition the space. The pressure at the outlet discharge is usually considered to be neutral. If the pressure in a zone varies greatly from neutrality due to building pressurization, zones below the NPL could receive excess air and those above the NPL could have their air delivery curtailed. This could result in the system not adequately meeting the temperature requirements of the space or not meeting the ventilation requirements prescribed by the building safety codes.

1.5 Goals for this Research

There are several goals for this dissertation's research. One is to compare buoyancy effect pressurization measured in an actual test building to the prediction obtained from the ASHRAE Method (Eq. 7). Another goal is to develop a new prediction model using statistical modeling techniques from the data gathered from the test building. In so doing, this dissertation will demonstrate the use of statistical analysis tools to compliment the usual engineering approach of mathematical theory and underlying physical principles.

This research will also demonstrate the use of existing data sources rather than the installation of instrumentation and data acquisition systems dedicated to a single research project. While these dedicated systems are sometimes required, they can be costly and short lived. This research will use existing building control systems and data acquisition systems to obtain the required data while reducing the cost of performing the research.

Instead of the statistical approach taken in this dissertation, computational fluid dynamics (CFD) could be used to construct models of buoyancy effect pressurization. Patankar (1980) presents a CFD algorithm called SIMPLE which is widely used by researchers in industry and academia. The researcher can build computer modeling code based on SIMPLE and similar algorithms or obtain commercial CFD codes constructed on these algorithms. Commercial codes include FIDAP (Fluid Dynamics International) and several CFD packages such as COMPACT (Innovative Research, Inc.). Computer modeling with techniques such as CFD is becoming more prevalent as the power of computers continues to increase while the costs associated with the use of computers continue to fall. CFD codes are becoming both more specialized and easier to apply. CFD modeling of the air flow through buildings can investigate the overall flow such as is done in this dissertation and can also take a more detailed look at the flows within the space both horizontally and vertically between floors.

The model could predict the flow within a zone, say a single story from perimeter walls to interior core as well as predict the flow patterns' "short circuits" such as when the air flow enters a vertical passage as in a stairwell or elevator hoistway. As with any type of modeling, it would be critical to calibrate and validate the model against actual test data similar to that obtained for this research.

It is unlikely that CFD modeling will be commonly used in the near future as a replacement for the ASHRAE Method or statistical model developed in this dissertation for the design of most buildings. The time and costs to develop such a model could not be justified. However, a complex CFD model might be justified for specialized or unique structures such as skyscrapers which would otherwise require wind tunnel modeling. As the CFD field advances, physical modeling is being supplanted by computer modeling. Several examples of CFD modeling in the areas of building air flow and buoyancy are discussed in Section 6, Recommendations, at the end of this dissertation.

2. Experimental Setup

Pressure and temperature data was collected for an existing building to compare to the buoyancy effect pressurization predicted by Eq. (7) as recommended in the ASHRAE Fundamentals Handbook. Wind data for the site was also collected in order to eliminate those data points in which wind effect pressurization would have been a factor.

2.1 Test Building

The Ernest Gruening Building (Bldg. FS314) on the University of Alaska Fairbanks campus in Fairbanks, Alaska was selected for this research. The Gruening Building is an eight story facility which was constructed in 1973. This building is one of the tallest buildings in interior Alaska and is regularly exposed to extremely cold temperatures which were important to the research for this dissertation.

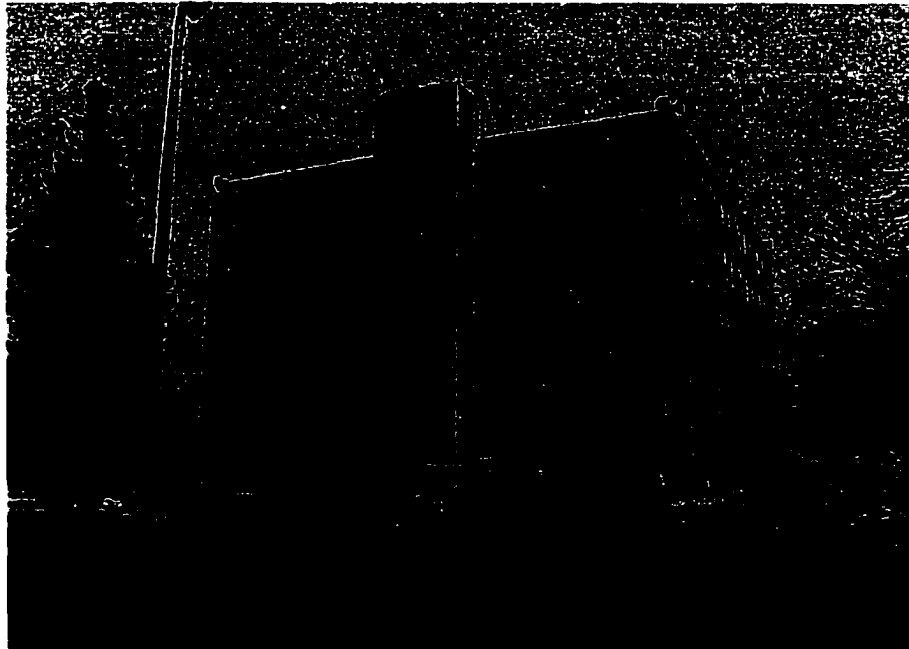


Figure 9. West Elevation of the Ernest Gruening Building

The Gruening Building is comprised of 102,263 ft² (9,500 m²) of classroom and office space. The building's footprint is square at 118 ft x 118 ft (36 m x 36m) and the major building axes are oriented along the primary compass points. A typical floor plan is shown in Fig. 10.

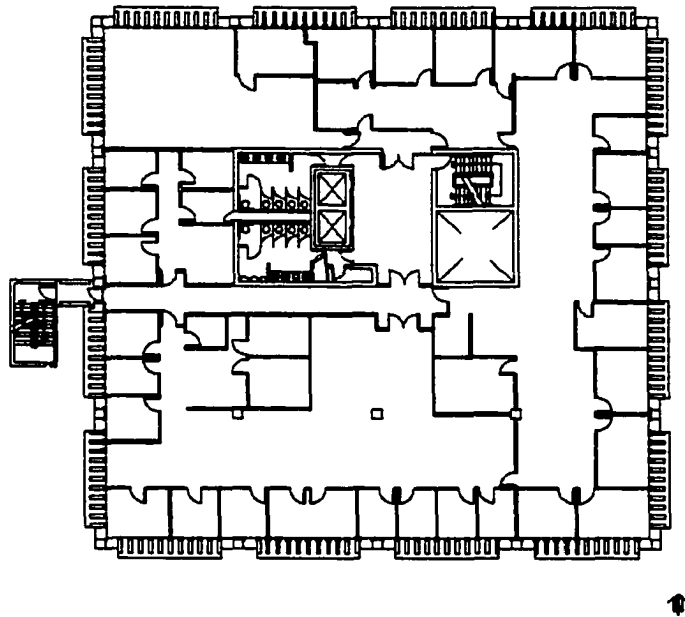


Figure 10. Typical Gruening Building Floor Plan

Exterior walls are constructed of heavy reinforced concrete structural members with reinforced concrete infill panels. Additional concrete finish panels are hung from the structure in order to obtain the desired architectural effects as seen in Fig. 9. The lowest two stories of the Gruening Building are below grade thus the third story is the ground floor. Openings in the exterior envelope consist of windows, doors, building expansion joints, and penetrations for fire suppression system piping and electrical conduit.

The windows are fixed (non-operable), double-pane units with reflective solar treatment. Double-door, all glass, vestibules provide entry and exit for the building on all four faces at the third level ground floor. The glass panels are similar to the window assemblies. There are emergency exit doors on all floors other than the ground floor on the west face of the building. These doors connect via walkways to the fire tower which can be seen on the photograph in Fig. 9 and the floor plan in Fig. 10. This fire tower is of heavy reinforced concrete construction which is open to the environment and serves all building levels including the roof. The fire tower provides exposure to the ambient environment for stories one and two.

The core services area on each floor, which contains the restrooms, elevators, elevator lobby, stairway, and mechanical chases, are separated from the rest of the level by concrete partitions. All other interior partitioning consists of gypsum wallboard and stud construction. Story separation is a 6 inch (15 cm) concrete slab with a suspended ceiling system in all finished areas (those areas except for the mechanical and electrical equipment rooms).

All major mechanical equipment for the facility is located on level one which is below grade. Building heating is obtained from the campus central power plant so there are no combustion appliances within the building. The HVAC system is an all air system. Constant volume air handlers provide cooling, ventilation, and heating to the perimeter zones. Variable air volume air handlers provide ventilation and cooling to the interior zones. There are a total of seven supply air handlers with a single return air fan serving all zones. The total system capacity is 94,300 cfm (44,500 L/s) with approximately 6,000 cfm (2,830 L/s) of outside ventilation air. It should be noted that since the HVAC system is of an all air type, the system remained operational during the data collection. This was required to provide code required ventilation air during the occupied periods and to prevent the temperature in the building from dropping due to lack of heat.

Vertical air flow within the building is relatively unobstructed. 580 ft² (54 m²) of each floor's 11,990 ft² (1,114 m²) is comprised of vertical openings between levels for stairwells, return air shafts, mechanical and electrical equipment chases, and elevator hoistways. In addition, there is an open mezzanine and stairway between the third and fourth floors and various other floor ceiling penetrations to run building services.

2.2 Instrumentation

Several data items were required in order to evaluate pressurization in the test building. Previous research and the ASHRAE recommended method to which the collected data will be compared, present buoyancy effect pressurization as a function of elevation and inside and outside temperature. Therefore, the differential pressure across the building's envelope was recorded at several elevations. Also, the outside air temperature and inside air temperature were recorded for the building. This research deals only with buoyancy effect pressurization. Therefore, any wind influence needed to be negated. In order to do this, wind speed and direction data were also recorded for the building site.

The Gruening Building's HVAC system utilizes a direct digital control (DDC) system (Fig. 11 and 12). In a DDC system, a digital computer replaces the controller that is found in more traditional (pneumatic, electronic) control systems. The computer obtains data such as temperatures, pressures, and flow rates from sensors located throughout building. This information is generally referred to as point data. This information is compared to setpoint values stored in or calculated by the computer which state what each point's value should be at any given time. If the setpoint value is not equal to the measured data, the computer sends output signals to control

devices such as heating valves, cooling valves, flow controllers, etc. in order to adjust the system so that the measured points are brought to the setpoint values.



Figure 11. DDC Control Panels and Terminal

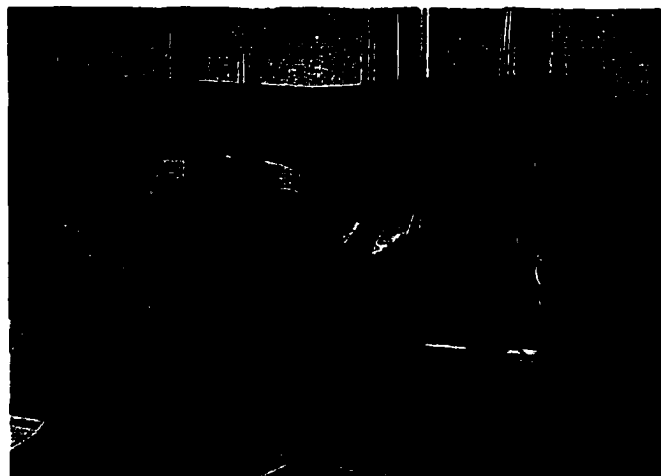


Figure 12. DDC Panel Internal View

There are several advantages to having a digital computer acting as the controller for an HVAC system. DDC systems offer many of the advantages inherent to digital computers. Making changes to a control strategy can be as simple as changing the

program on the computer. Complicated component change outs and re-wiring/re-piping can often be avoided. Data read from the sensors, signals sent to the actuators, even the state of a point (e.g. within range, in alarm, malfunctioning) can be stored in the computer's memory. This stored information can be used to initiate time-based control strategies and it can also be extracted from the DDC system for other uses. In essence, DDC systems provide the built-in capabilities of a data logger for the facility.

In order to manage all of the information needed to monitor and control the building, the DDC system needs a method to refer to each individual data point. As inferred above, a data point may be a temperature sensor, a valve actuator, or a setpoint to name but a few. The following discussion is particular to the Landis & Steafa (now Siemens Technology) DDC system installed in the Gruening Building. However, many of the concepts are similar to other manufacturer's DDC systems.

There are two major classifications of data points, more commonly referred to as just points. These classifications are physical points and virtual points. Physical points are those points associated with actual hardware. Examples of physical points are sensors and actuators. These devices are wired to specific locations on the DDC control boards and transmit signals to the system or carry out instructions from the system. Virtual points represent concepts or information needed for the control algorithms to function properly. They are not connected to a hardware device nor are they wired to the control boards. Examples of virtual points include setpoint values and scheduling points (e.g. ON/OFF, Occupied/Unoccupied).

Information about points is maintained in the DDC computers' point database. Each database record contains a point's name, its address, how to interpret its signal if it's a physical point (e.g. how to convert a 4 – 20 mA signal into a temperature value), its current value, and various status flags (e.g. alarm, malfunction). A physical point's

address is a map to where the device wires are connected to the control board. A virtual point's address can be thought of as a memory address where the information is stored, although this is not strictly correct.

To manage large DDC systems, it is important to develop a logical point naming nomenclature. Since the points discussed later in this dissertation will sometimes be referred to by their point names, a brief overview of the University of Alaska Fairbanks point naming conventions will be helpful. All DDC point names are constructed of six alphanumeric digits. The first two digits represent the building; the second two digits, the system within the building; and the final two digits the specific point in the system. Table 4 lists the primary point names for the data collected for this research.

Table 4. Research Data DDC Point Names

Point Name	Description
GROSAT	Outside Air Temperature
GRBG1P	Differential Pressure Level 1
GRBG2P	Differential Pressure Level 2
GRBG3P	Differential Pressure Level 3
GRBG4P	Differential Pressure Level 4
GRBG5P	Differential Pressure Level 5
GRBG6P	Differential Pressure Level 6
GRBG7P	Differential Pressure Level 7
GRBG8P	Differential Pressure Level 8

The first two digits, "GR", represent Gruening; the second two digits, say "BG", represent the "building" system; and the final two digits, say "5P", represent fifth level pressure.

The Gruening Building DDC system included return air and outside air temperature sensors prior to beginning this research. The return air (or space) sensors are single-

point thermistor type sensors (Landis & Gyr Model 535-741) with a range of 40-150°F (4-66°C). The outside air temperature sensor is a platinum RTD (Landis & Gyr Model 533-381) with a range of -58-122°F (-50-50°C). In support of this research, pressure sensors to monitor the pressure difference across the building envelope were installed at each level as shown in the schematic in Fig. 13.

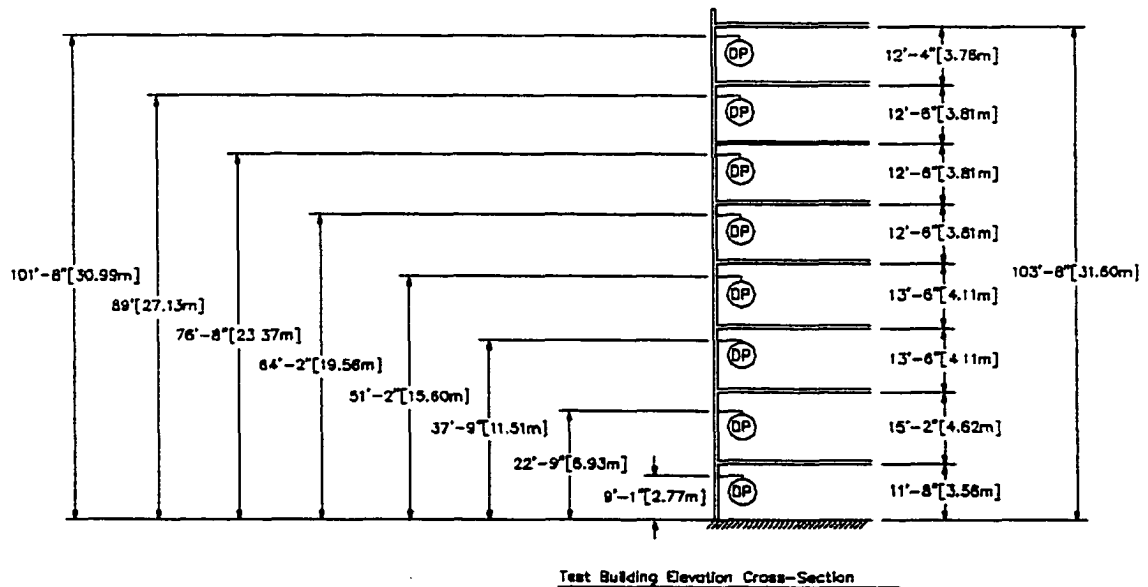


Figure 13. Differential Pressure (DP) Sensor Installation Schematic

In using the DDC system to log the data, the decision of how often each data point should be recorded needs to be made. Collecting data at short time intervals provides a more exact picture of conditions. However, recording at short time intervals results in more data which requires more memory in the DDC system. More data also entails more time in the data analysis phase, however, the computer based analysis described later in this dissertation made this less of a factor. Because outside air temperatures do not change rapidly, a 15 minute time interval for data recording was deemed adequate. This required that the data be downloaded from the DDC system every one to two days so as not to overtax the DDC system's memory capacity.

The test building did not include instrumentation to measure wind speed and direction. However, there was an instrument package located approximately ½ mile (0.80 km) from Gruening maintained by Los Alamos National Laboratory (LANL) that was collecting this data. This data was also being collected on a 15 minute time interval so merging with the data collected by the Gruening DDC system was eased. Since the wind data was used solely as an elimination factor, to remove those data points where wind pressurization might be a significant factor in the differential pressure recorded, the short distance between the instrument package and building sites was not significant.

Data from both the building DDC system and the LANL instrument package were downloaded periodically to a personal computer (PC) for long term storage and data analysis.

2.3 Pressure Measurement Basics

Since very resolute pressure measurements are a main focus of this research, a review of various pressure measurement technologies is in order to help explain why particular instrumentation was selected.

Pressure is a parameter that is usually not sensed directly. Pressure is generally measured by understanding that pressure is a force acting on a unit area. There are many instruments available to measure pressure and many considerations in selecting the proper pressure sensor for a particular application. Pressure measurement is accomplished by measuring how the forces due to pressure interact with some media or element used as a pressure transducer. Most pressure transducers can be grouped into two categories: gravimetric transducers and elastic element transducers.

Gravimetric pressure measuring instruments are based on a force balance acting on a fluid column. One of the most common of this type of pressure measuring device is the U-tube manometer shown in Fig. 14. The openings of each leg of the U-tube are exposed to pressures P_1 and P_2 respectively. These pressures act on the fluid in the manometer causing a shift. The differential height, h , of the manometer fluid in the legs reaches equilibrium when the gravitational forces acting on the manometer fluid are balanced by the pressure forces acting on the fluid surfaces.

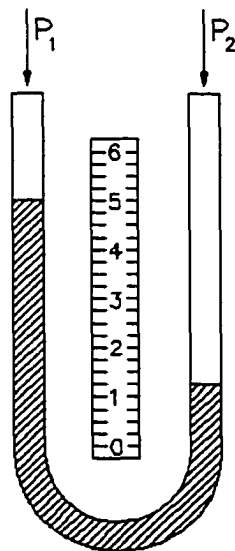


Figure 14. U-Tube Manometer

The general manometer equation is:

$$P_1 - P_2 = h(\rho_m - \rho_f) \left(\frac{g}{g_c} \right) \quad (9)$$

where: P_1 = pressure in leg 1
 P_2 = pressure in leg 2
 h = differential elevation of manometer fluid
 ρ_m = density of manometer fluid
 ρ_t = density of transmitting fluid
 g = gravitational acceleration
 g_c = conversion factor

In practice, the manometer fluid is often chosen to have a much higher density than the transmitting fluid. This is the case when the transmitting fluid is air and the manometer fluid is water or when the transmitting fluid is water and the manometer fluid is mercury. In these situations, Eq. (9) can be reduced to that shown in Eq. (10) without a significant loss in accuracy.

$$P_1 - P_2 = h\rho_m \left(\frac{g}{g_c} \right) \quad (10)$$

Figure 14 shows an example where P_2 is greater than P_1 . Thus the manometer fluid has been depressed in the leg exposed to P_2 and the fluid has risen in the other leg. If P_2 is atmospheric pressure, then the pressure depicted by the manometer can be directly read as gage pressure. If one of the legs is sealed and exposed to a vacuum, then the manometer becomes a barometer which depicts atmospheric pressure (note that barometers are not generally constructed in U-tube form).

Gravimetric type pressure transducers have the advantage of being simple to construct and understand. Also, they can be constructed (say by inclining one of the legs) so that small changes in differential pressure can be easily discernable. Disadvantages of this type of transducer include a limited range, they do not adapt well to large differential pressures due to their reliance on the density of the

manometer fluid and the height of a fluid column, and they have relatively slow response times.

Many pressure transducers rely on pressure causing an elastic deformation in an element or mechanism. This deformation is then converted by the transducer into a change in electrical signal proportional to the mechanical translation of the mechanism.

One of the oldest forms of this type of pressure transducer is the Bourdon tube pressure gage (Fig. 15). This is a fully mechanical transducer. The pressure to be measured is exposed to the gage stem which is attached to a curved tube of flat oval cross-section. The internal forces caused by the pressure in the tube try to deform the tube to a circular cross-section. This deformation, in turn, attempts to straighten the curve in the tube. This causes the free end of the tube (the end not attached to the stem) to move linearly. This linear motion is translated through a gear and linkage mechanism and causes the indicator needle on the pinion to rotate over a scale which has been calibrated to read directly in units of pressure.

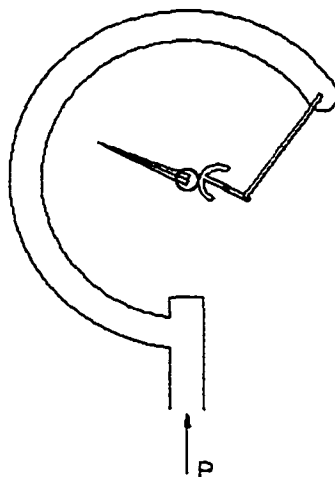


Figure 15. Bourdon Tube Pressure Gage

Other types of elastic deformation type pressure transducers recognize the deformed element is placed under strain when exposed to pressure. By measuring the strain on the element, the pressure can be deduced. Common examples of this type of transducer are pressure cells which affix strain gages to closed tubes and admit pressure into the tube element and diaphragm transducers that affix strain gages to a diaphragm that is deformed under pressure (Fig. 16). Cantilever beam and load cell pressure gages can also be constructed using this principle.

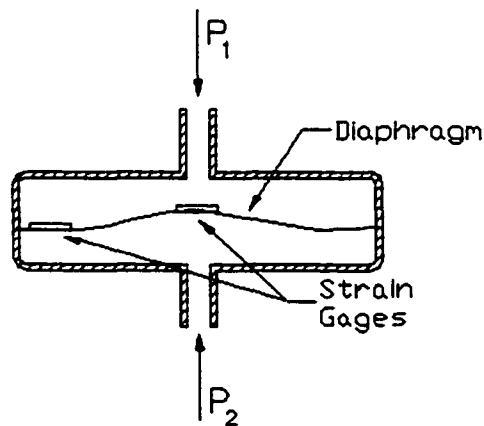


Figure 16. Diaphragm Pressure Transducer

Another type of elastic deformation transducer relies on measuring a change in capacitance which is proportional to the pressure. In this transducer (Fig. 17), the plates of a capacitor are exposed to a differential pressure causing them to deform. As the distance between the plates changes, so does the capacitance of the device.

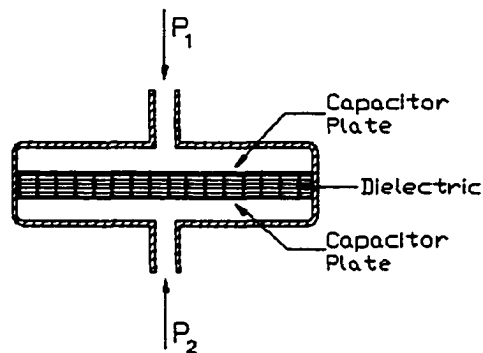


Figure 17. Variable Capacitance Pressure Transducer

The equation behind the variable capacitance transducer is:

$$C = \frac{0.2249KA(n-1)}{d} \quad (11)$$

- where: C = capacitance [pF]
 K = dielectric constant (1 for air)
 A = area of one side of one plate [in²]
 n = number of plates
 d = plate separation [in]

Elastic deformation type pressure transducers offer a wide range of capabilities from very small to extremely large pressures and include a wide range of time responses. They can also easily be adapted into electronic instrument systems since many of them transduce the pressure into a proportional electrical (e.g. voltage, current, or resistance) signal.

2.4 Differential Pressure Instrumentation

A variable capacitance differential pressure transducer/transmitter was selected for this research for several reasons. Variable capacitance transducers are capable of measuring the small pressure differences resulting from building pressurization. The units are durable with good repeatability and are relatively inexpensive to produce when compared to other alternatives. And finally, previous experience with this type of unit had shown that they performed well even in extremely cold weather.

The particular transducer/transmitter installed is the Model C264 with Option 717 manufactured by Setra Systems, Inc. This transmitter produces a 4-20 mA output signal which is proportional to the differential pressure sensed. It is easy to connect to the DDC system and program into the point database. This model has a sensor range of 0 to ± 0.5 in. H₂O (0 to ± 124.6 Pa) with a resolution of 0.0025 in. H₂O (0.6229 Pa). Another advantage to using the Setra transducer is that various models of Setra's pressure transducers are used throughout the campus-wide DDC system. This means that the University's technicians are familiar with their use and maintenance. This resulted in no maintenance problems during the research period and allows the continued use of these transducers in future building control strategies.

A single differential pressure transmitter was installed at each level of the building, generally above the suspended ceiling (Fig. 18b), adjacent to the doors on the west face of the building. The 'high' port of each transmitter was connected to a pneumatic tube which opened into an enclosure mounted on the suspended ceiling to sense interior building pressure (Fig. 18a). The port on the entry level was installed in the corridor inside of the entry vestibule to insure that the building and not the vestibule pressure was measured. The 'low' port of each transmitter was connected to a pneumatic tube and run in conduit through the exterior concrete wall where it was terminated in an electrical LB fitting (Fig. 18c).

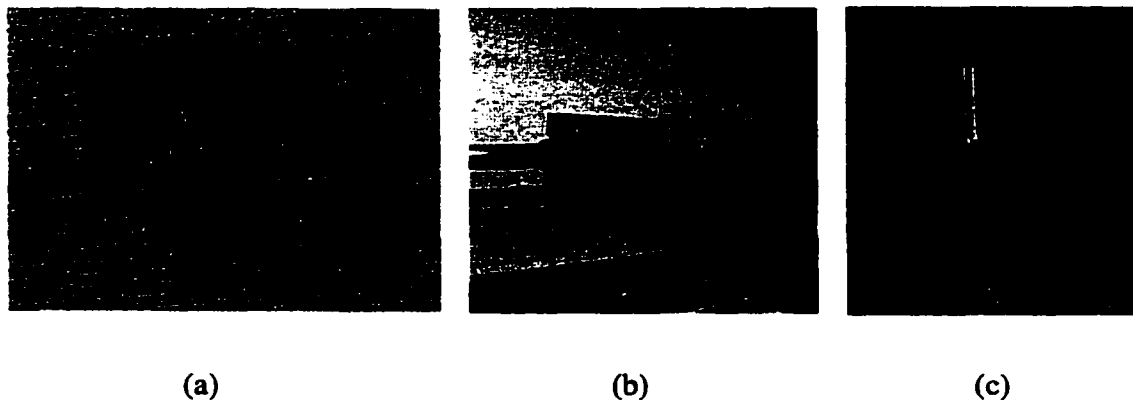


Figure 18. Differential Pressure Transmitter Installation

The signal wires from each transmitter were routed to a DDC control panel on the eighth floor and terminated to the analog input bus. The point database was programmed so that the system interpreted the 4-20 mA input signal and processed the differential pressure directly in units of in. H₂O. The orientation of the “low” and “high” ports resulted in the pressure reading as a negative value when the pressure inside the building is less than the pressure outside the building and vice versa.

Care was taken in how the port openings to detect the inside and outside pressure were configured to preclude false readings and maintenance problems. The pneumatic tubing used was a ¼” (6.4mm) polyethylene tube commonly referred to in the industry as “poly-tube”. To transmit the static pressure at the desired location to the Setra transmitter, this poly-tube need only have an open end exposed at the location. However, experience has shown that this simple installation will result in many operational problems.

For the inside location, an exposed open ended black poly-tube is often viewed by building occupants and non-technical staff as something that has been disconnected. This often results in the tube being removed or pushed above the ceiling so as to improve the appearance in the finished space. To prevent this from happening, the

tubes were terminating in a control sensor housing mounted to the suspended ceiling (Fig. 18a) so that the installation has a finished appearance. Use of a housing in this manner also prevents localized pressure perturbations due to corridor traffic.

For the outside location, the open end of the poly-tube is installed in an electrical LB fitting (Fig. 18c). This fitting is part of the metal conduit system used to penetrate the outside wall. The end of the LB not connected to the conduit is fitted with a screen to expose the port to the ambient pressure while protecting it from insect blockage and damage. It is also critical to completely seal the conduit penetration to the wall system and the interior of the conduit to the poly-tube with a flexible caulk. During the heating season, the air inside the building has a higher moisture content than the outside air. Without these seals, moisture will migrate into the LB enclosure, freeze, and block the port.

3. Data

As mentioned previously, the data came from two primary sources, the test building direct digital control system and a LANL weather instrument package. The DDC system data was collected at one and two day intervals and each data collection increment was stored in a separate text file. The weather instrument data was stored in monthly text files. Prior to analysis, this data needed to be combined into a single cohesive dataset and tested for validity.

While excerpts of the data are shown in the body of this dissertation (e.g. Fig. 19), it would not be practicable to show all of the thousands of data points in the written text. Appendix A contains a compact disk (CD) which includes all of the data, both raw and processed, used for this research. The data is stored in various file formats which makes it available for viewing and for possible use in future studies.

A discussion of terminology might help clarity at this time. A *dataset* is a collection of data. This data may be in almost any form from highly organized tables to simple lists. A dataset may exist in written form, volatile memory, or electronic permanent storage. A *data file* is data that is organized in some manner and stored as a computer file (permanent electronic storage). Therefore, all data files are, by definition, datasets. But, all datasets need not be data files.

3.1 DDC Data Processing

The raw DDC data containing information on temperature and building pressurization is stored in standard text files with names such as "Gru011999x.cap". This particular file contains the Gruening DDC data downloaded on 01/19/99. The "cap" file extension indicates that this data was "captured" during an interactive session with the DDC system. The total DDC data was captured in 52 of these files.

Figure 19 shows an excerpt of this data. Because the data was downloaded or captured during an interactive session, the file contains not only the data of interest but also the commands and responses to and from the DDC operating system. The lines beginning with the ">" prompt show commands issued by the operator to instruct the system what data to report. The system then responds with "Command Successful", reports the data, and concludes with "End of Report".

The first trend data report in each raw data file contains the outside air temperature data, DDC point GROSAT (Gruening Bldg outside air temperature). The next eight trend data reports contain the differential static pressure readings for each story of the building, DDC points GRBG1P (Gruening Bldg level 1 differential pressure) through GRBG8P (Gruening Bldg level 8 differential pressure). The final trend data in each file is a check to insure that the fan systems that supply air to the occupied zones of the test building remained running during the entire period of data collection. This insures that the equipment effect building pressurization remains relatively constant across all of the collected data. During each download operation, the building space and return air temperature trends were also checked to insure that they remained constant. It was found that the DDC system was doing an excellent job of controlling space temperatures and these values remained constant at 70°F (21°C). Because these values did not vary, they were not downloaded in order to conserve space in the raw data files.

```

>Point, Time, Message, Cancel, Hello ?P
>Log, Display, Monitor, Trend, Subptlog, Alarm ?T
>Display, Listpoints, Quit ?D
>Here, Printer ?H
>Start date (e.g. 19-Jan)? 18-JAN
>Start time (e.g. 00:00)?
1>Point name? GROSAT
Command successful
1 GROSAT (LOW OA TEMP) Time: 15 minute(s) 100 samples

```

```

1>Which trend (<CR> for 1st or ex#)?
2>Next point name?
Command successful

```

```

Trend Data Report      Name:GROSAT      20:05 19-Jan-1999
-----

```

```

GROSAT (LOW OA TEMP ) DEG F
18-Jan 19:11:54 -13.84 -N- P:NONE
18-Jan 19:26:54 -13.84 -N- P:NONE
18-Jan 19:41:54 -14.06 -N- P:NONE
18-Jan 19:56:54 -13.95 -N- P:NONE
18-Jan 20:11:54 -13.95 -N- P:NONE
... ..
... ..
... ..
19-Jan 19:56:55 -19.46 -N- P:NONE

```

End of Report

```

>Display, Listpoints, Quit ?D
>Here, Printer ?H
>Start date (e.g. 19-Jan)? 18-JAN
>Start time (e.g. 00:00)?
1>Point name? GRBG1P
Command successful
1 GRBG1P (1ST FLSTATIC) COV      100 samples
2 GRBG1P (1ST FLSTATIC) Time: 15 minute(s) 100 samples

```

```

1>Which trend (<CR> for 1st or ex#)? 2
2>Next point name?
Command successful

```

```

Trend Data Report      Name:GRBG1P      20:06 19-Jan-1999
-----

```

```

GRBG1P (1ST FLSTATIC) IN H2O
18-Jan 19:12:45 -0.034408 -N- P:NONE
18-Jan 19:27:45 -0.035656 -N- P:NONE
18-Jan 19:42:45 -0.035868 -N- P:NONE
18-Jan 19:57:45 -0.035032 -N- P:NONE
18-Jan 20:12:45 -0.039088 -N- P:NONE
... ..
... ..
... ..
19-Jan 19:57:45 -0.036903 -N- P:NONE

```

End of Report

Figure 19. Raw DDC Data Excerpt

```

>Display, Listpoints, Quit ?D
>Here, Printer ?H
>Start date (e.g. 19-Jan)? 18-JAN
>Start time (e.g. 00:00)?
1>Point name? GRBG2P
Command successful
1 GRBG2P (2ND FLSTATIC) COV          100 samples
2 GRBG2P (2ND FLSTATIC) Time: 15  minute(s) 100 samples

```

```

1>Which trend (<CR> for 1st or exit)? 2
2>Next point name?
Command successful

```

```

Trend Data Report          Name:GRBG2P          20:06 19-Jan-1999
-----

```

```

GRBG2P (2ND FLSTATIC) IN H2O
18-Jan 19:22:45 -0.015688 -N-  P:NONE
18-Jan 19:37:45 -0.013504 -N-  P:NONE
18-Jan 19:52:45 -0.023487 -N-  P:NONE
18-Jan 20:07:45 -0.018808 -N-  P:NONE
18-Jan 20:22:45 -0.01444  -N-  P:NONE
....
....
....
19-Jan 20:07:45 -0.016624 -N-  P:NONE

```

End of Report

```

>Display, Listpoints, Quit ?D
>Here, Printer ?H
>Start date (e.g. 19-Jan)? 18-JAN
>Start time (e.g. 00:00)?
1>Point name? GRBG3P
Command successful
1 GRBG3P (3RD FLSTATIC) COV          100 samples
2 GRBG3P (3RD FLSTATIC) Time: 15  minute(s) 100 samples

```

```

1>Which trend (<CR> for 1st or exit)? 2
2>Next point name?
Command successful

```

```

Trend Data Report          Name:GRBG3P          20:07 19-Jan-1999
-----

```

```

GRBG3P (3RD FLSTATIC) IN H2O
18-Jan 19:12:45 0.000379 -N-  P:NONE
18-Jan 19:27:45 -0.0  -N-  P:NONE
18-Jan 19:42:45 -0.001335 -N-  P:NONE
18-Jan 19:57:45 0.001159 -N-  P:NONE
18-Jan 20:12:45 -0.001959 -N-  P:NONE
....
....
....
19-Jan 19:57:45 0.001940 -N-  P:NONE

```

End of Report

Figure 19. Raw DDC Data Excerpt (continued)

```

>Display, Listpoints, Quit ?D
>Here, Printer ?H
>Start date (e.g. 19-Jan)? 18-JAN
>Start time (e.g. 00:00)?
1>Point name? GRBG4P
Command successful
1 GRBG4P (4TH FLSTATIC) COV          100 samples
2 GRBG4P (4TH FLSTATIC) Time: 15   minute(s) 100 samples

1>Which trend (<CR> for 1st or exit)? 2
2>Next point name?
Command successful

Trend Data Report          Name:GRBG4P          20:07 19-Jan-1999
-----
GRBG4P (4TH FLSTATIC) IN H2O
18-Jan 19:12:45 0.034232 -N- P:NONE
18-Jan 19:27:45 0.033608 -N- P:NONE
18-Jan 19:42:45 0.029083 -N- P:NONE
18-Jan 19:57:45 0.035636 -N- P:NONE
....
....
....
19-Jan 19:57:45 0.039067 -N- P:NONE

End of Report

>Display, Listpoints, Quit ?D
>Here, Printer ?H
>Start date (e.g. 19-Jan)? 18-JAN
>Start time (e.g. 00:00)?
1>Point name? GRBG5P
Command successful
1 GRBG5P (5TH FLSTATIC) COV          100 samples
2 GRBG5P (5TH FLSTATIC) Time: 15   minute(s) 100 samples

1>Which trend (<CR> for 1st or exit)? 2
2>Next point name?
Command successful

Trend Data Report          Name:GRBG5P          20:07 19-Jan-1999
-----
GRBG5P (5TH FLSTATIC) IN H2O
18-Jan 19:12:45 0.075572 -N- P:NONE
18-Jan 19:27:45 0.072139 -N- P:NONE
18-Jan 19:42:45 0.068708 -N- P:NONE
18-Jan 19:57:45 0.077287 -N- P:NONE
....
....
....
19-Jan 19:57:45 0.081187 -N- P:NONE

End of Report

```

Figure 19. Raw DDC Data Excerpt (continued)

```

>Display, Listpoints, Quit ?D
>Here, Printer ?H
>Start date (e.g. 19-Jan)? 18-JAN
>Start time (e.g. 00:00)?
1>Point name? GRBG6P
Command successful
1 GRBG6P (6TH FLSTATIC) COV          100 samples
2 GRBG6P (6TH FLSTATIC) Time: 15   minute(s) 100 samples

```

```

1>Which trend (<CR> for 1st or exit)? 2
2>Next point name?
Command successful

```

```

Trend Data Report          Name:GRBG6P          20:08 19-Jan-1999
-----

```

```

GRBG6P (6TH FLSTATIC) IN H2O
18-Jan 19:12:45 0.119095 -N- P:NONE
18-Jan 19:27:45 0.116755 -N- P:NONE
18-Jan 19:42:45 0.113323 -N- P:NONE
18-Jan 19:57:45 0.121435 -N- P:NONE
....
....
....
19-Jan 19:57:45 0.129703 -N- P:NONE

```

End of Report

```

>Display, Listpoints, Quit ?D
>Here, Printer ?H
>Start date (e.g. 19-Jan)? 18-JAN
>Start time (e.g. 00:00)?
1>Point name? GRBG7P
Command successful
1 GRBG7P (7TH FLSTATIC) COV          100 samples
2 GRBG7P (7TH FLSTATIC) Time: 15   minute(s) 100 samples

```

```

1>Which trend (<CR> for 1st or exit)? 2
2>Next point name?
Command successful

```

```

Trend Data Report          Name:GRBG7P          20:08 19-Jan-1999
-----

```

```

GRBG7P (7TH FLSTATIC) IN H2O
18-Jan 19:12:45 0.132824 -N- P:NONE
18-Jan 19:27:45 0.128924 -N- P:NONE
18-Jan 19:42:45 0.124556 -N- P:NONE
18-Jan 19:57:45 0.135007 -N- P:NONE
....
....
....
19-Jan 19:57:45 0.157315 -N- P:NONE

```

End of Report

Figure 19. Raw DDC Data Excerpt (continued)

```

>Display, Listpoints, Quit ?D
>Here, Printer ?H
>Start date (e.g. 19-Jan)? 18-JAN
>Start time (e.g. 00:00)?
1>Point name? GRBG8P
Command successful
1 GRBG8P (8TH FLSTATIC) COV          100 samples
2 GRBG8P (8TH FLSTATIC) Time: 15   minute(s) 100 samples

1>Which trend (<CR> for 1st or exit)? 2
2>Next point name?
Command successful

Trend Data Report          Name:GRBG8P          20:09 19-Jan-1999
-----
GRBG8P (8TH FLSTATIC) IN H2O
18-Jan 19:12:45 0.188515 -N-  P:NONE
18-Jan 19:27:45 0.184459 -N-  P:NONE
18-Jan 19:42:45 0.180404 -N-  P:NONE
18-Jan 19:57:45 0.189139 -N-  P:NONE
....
....
....
19-Jan 19:57:45 0.207547 -N-  P:NONE

End of Report

```

Figure 19. Raw DDC Data Excerpt (continued)


```

>Display, Listpoints, Quit ?D
>Here, Printer ?H
>Start date (e.g. 19-Jan)? 18-JAN
>Start time (e.g. 00:00)?
1>Point name? GRS2SS
Command successful
1 GRS2SS (START STOP ) COV          100 samples

1>Which trend (<CR> for 1st or exit)?
2>Next point name? GRS3SS
Command successful
1 GRS3SS (START STOP ) COV          100 samples

2>Which trend (<CR> for 1st or exit)?
3>Next point name? GRS4SS
Command successful
1 GRS4SS (START STOP ) COV          100 samples

3>Which trend (<CR> for 1st or exit)?
4>Next point name? GRS5SS
Command successful
1 GRS5SS (START STOP ) COV          100 samples

4>Which trend (<CR> for 1st or exit)?
5>Next point name? GRS6SS
Command successful
1 GRS6SS (START STOP ) COV          100 samples

5>Which trend (<CR> for 1st or exit)?
6>Next point name?
>Minutes between data lines? 15
Command successful

```

Trend Multi-point Report interval: 15 minute(s) 20:09 19-Jan-1999

```

-----
Name : GRS2SS GRS3SS GRS4SS GRS5SS GRS6SS
Units :
-----COV-----COV-----COV-----COV-----COV-----
18-Jan 00:00: ON ON ON ON ON
18-Jan 00:15: ON ON ON ON ON
18-Jan 00:30: ON ON ON ON ON
....
....
....
19-Jan 20:00: ON ON ON ON ON

```

End of Report

Figure 19. Raw DDC Data Excerpt (continued)

The trend data reports present the information on outside air temperature and differential pressure in five columns. The first two columns display the date and time at which the data was recorded. This information was used to group the data into 15-minute time bins as described later. It can be seen that each data point is not recorded at exactly the same “clock tick”, but may vary by a second or two. This is due to the manner in which the DDC system sequentially reads its programming instructions to record the data and also to the fact that the several data points collected were connected to different panels in the DDC system. While the DDC system synchronizes time settings between its individual panels each day, they may still not be coordinated to the exact clock tick at all times. The use of a 15-minute time bin also aided in combining the DDC data with the weather data. The weather data instrument package collected data based on its own internal clock. While both the DDC system and the LANL instrument package based their time settings on recognized time standards, it is likely that their internal clocks were not synchronized to the exact same time.

The third column in each trend report displays the data used in the analysis, either the outside air temperature or the differential pressure.

The final two columns report the status of the point in the DDC system. This information was used to eliminate data that may have been in error due to DDC system problems. A value of “-N-“ in the forth column indicates that the condition is “normal”. This column would display “-F-“, “-P-“, or “-A-“ if the sensor was sensing a value outside of its prescribed range or there was some problem with the signal being sent. A value of “P:NONE” in the fifth column stands for “priority none”. This means that the point and system are under normal operation and control. A value other than “P:NONE” might mean that the value being recorded had been manually set by the operator rather than the actual value being sent by the sensor/

transmitter. Any data where the values in the last two columns were not “-N-“ and “P:NONE” were omitted from the dataset analyzed.

The next step in developing the cohesive dataset was to combine the data in the daily files into monthly files. This was done using Excel spreadsheet software. Through use of data import wizards and manual manipulation, the date, time, temperature, and differential pressure data was extracted from each daily file and combined into a monthly spreadsheet file in the tabular form. Table 5 shows an excerpt from the August 1999 file. Note that the complete file for August has over 2,400 data records. The raw date and time data was used to align the temperature and pressure data into the proper 15-minute time bin.

Table 5 points out another factor that needed to be considered when dealing with the date/time of data acquisition. The DDC system records data in “real time”. That is, data collected in the summer months are time stamped with a value in Alaska Daylight Time; winter values are time stamped in Alaska Standard Time.

Table 5. Monthly DDC Data Excerpt

Time Bin	Date	DT-ADT	DT-AST	OSAT	Lv 1 D.P.	Lv 2 D.P.	Lv 3 D.P.	Lv 4 D.P.	Lv 5 D.P.	Lv 6 D.P.	Lv 7 D.P.	Lv 8 D.P.
13:00	4-Aug-99	8/4/1999 13:00	8/4/1999 12:00	81	0.011767	0.035479	0.023468	0.027835	0.029864	0.032671	0.025183	0.026900
13:15	4-Aug-99	8/4/1999 13:15	8/4/1999 12:15	81	0.006464	0.038599	0.022687	0.025027	0.024248	0.027055	0.021439	0.023779
13:30	4-Aug-99	8/4/1999 13:30	8/4/1999 12:30	81	0.013639	0.037663	0.025651	0.030019	0.031423	0.032203	0.025340	0.026120
13:45	4-Aug-99	8/4/1999 13:45	8/4/1999 12:45	81	0.001783	0.032671	0.011456	0.013484	0.021439	0.019100	0.005995	0.007399
14:00	4-Aug-99	8/4/1999 14:00	8/4/1999 13:00	81	0.016448	0.021751	0.024092	0.028771	0.031423	0.034699	0.025963	0.024092
14:15	4-Aug-99	8/4/1999 14:15	8/4/1999 13:15	83	0.016759	0.035791	0.023935	0.025340	0.023468	0.030799	0.020503	0.025027
14:30	4-Aug-99	8/4/1999 14:30	8/4/1999 13:30	83	0.020503	0.012391	0.025651	0.037039	0.036260	0.035479	0.028147	0.027368
14:45	4-Aug-99	8/4/1999 14:45	8/4/1999 13:45	83	0.026120	-0.004455	0.024403	0.036415	0.039535	0.043435	0.032671	0.043124
15:00	4-Aug-99	8/4/1999 15:00	8/4/1999 14:00	83	-0.009136	0.025183	0.018787	0.026275	0.022844	0.016448	0.015200	0.009584
15:15	4-Aug-99	8/4/1999 15:15	8/4/1999 14:15	85	-0.024735	0.025807	0.014887	0.010208	0.040159	0.027679	0.005840	0.008960
15:30	4-Aug-99	8/4/1999 15:30	8/4/1999 14:30	85	0.000000	-0.013815	0.017383	0.020503	0.032360	0.023000	0.016291	0.018476
15:45	4-Aug-99	8/4/1999 15:45	8/4/1999 14:45	85	0.021751	0.017695	0.026900	0.044839	0.036884	0.021127	0.026744	0.018787
16:00	4-Aug-99	8/4/1999 16:00	8/4/1999 15:00	85	0.035167	0.137192	0.042500	0.059347	0.058723	0.054823	0.045776	0.050768
16:15	4-Aug-99	8/4/1999 16:15	8/4/1999 15:15	85	-0.027231	0.032671	0.013639	0.014576	0.029395	0.009584	0.005371	0.003655
16:30	4-Aug-99	8/4/1999 16:30	8/4/1999 15:30	85	0.003031	-0.026296	0.024716	0.018787	0.042032	0.028616	0.026587	0.035323
16:45	4-Aug-99	8/4/1999 16:45	8/4/1999 15:45	85	-0.003207	0.004903	0.005684	0.003655	0.011143	0.015824	0.011923	0.019879
17:00	4-Aug-99	8/4/1999 17:00	8/4/1999 16:00	85	-0.059368	0.014887	0.017539	0.025340	0.034388	0.020503	0.009427	0.036260
...
...
23:30	31-Aug-99	8/31/1999 23:30	8/31/1999 22:30	53	0.015200	0.028616	0.023935	0.039847	0.050144	0.064339	0.062936	0.079627
23:45	31-Aug-99	8/31/1999 23:45	8/31/1999 22:45	51	0.002407	0.014263	0.012391	0.035479	0.045619	0.062155	0.059971	0.074791

Since the thrust of this research is analysis during the cold weather months, Alaska Standard Time (AST) was chosen as the common time reference. Therefore, any date/time stamp referenced to a time zone other than AST must be corrected to AST. Date/time calculations are easy to do in most spreadsheet software once it is understood that date/time values are stored as sequential index integers from a specific reference date. For the Excel software used in this research, the index reference is January 1, 1900. That means that January 1, 1900 is stored as 0, January 2, 1900 is stored as 2, and so on. Time can be mathematically manipulated by recognizing that a day is composed of 24 hours, an hour is 60 minutes, and so on. So time of day becomes a fractional portion of the index reference.

The date/time stamp was the database key used to coordinate all of the data collected. Therefore, a great deal of attention was paid to converting all time stamps to the AST common time base so that the data from many individual files formed a cohesive dataset. This was critical to insure that differential pressures were not erroneously associated with the wrong outside air temperatures.

The monthly data was then stored in two file formats. The data was saved in standard spreadsheet file format (.xls) for ease of viewing and presentation. It was also stored in comma separated value (.csv) format. This format made the data easier to use in the analysis described later.

The final step in processing the DDC data was to extract only that data necessary for building pressurization analysis or required to combine the DDC derived data with the weather information obtained from the LANL instrument package. These fields consisted of the differential pressure data for each level (Table 5, Lvl n D.P.), the outside temperature (Table 5, OSAT), and the standardized time bin stamp (Table 5, DT-AST). This data was extracted from the monthly csv files and stored in a new csv file saved with a .q1 file extension using S-Plus software.

S-Plus (Insightful, Inc.) is an integrated development environment (IDE) and programming language (the S-Language). This software was chosen for use in this research because it was specifically designed for statistical analysis and includes many preprogrammed functions and routines to perform statistical modeling and dataset manipulation. Any functionality not provided in the IDE was easily added by writing custom functions in the S-Language. An S-function (Fig. 20) was written to create the q1 data files mentioned above.

```
function(MoNum = "01")
{
  # This function reads in the csv DDC files for the Gruening
  # Building DDC data. It assigns field headings and then
  # extracts the data needed for the Gruening Stack Effect
  # research project. That data is then written back to a new
  # data file of the form 'ddc01 99.q1'. This function works
  # with both versions of data files (DST and AST versions).
  # The input argument is the month number (i.e.; Jan = 01)
  # used to construct the file names for the input and output
  # data files.

  # 1st build the input & output file names.
  in.file <- paste("e:/Dphd/grueningdata/processedddcdata/ddc", MoNum, "99.csv", sep = "")
  out.file <- paste(substring(in.file, 1, 46), "q1", sep = "")

  # read the file & test for type.
  in.dat <- read.table(file = in.file, sep = ",", row.names = NULL, as.is = T, skip = 1)
  col.size <- length(in.dat[, ])
  if(col.size == 12)
    {names(in.dat) <- c("T-Bin", "Date", "DT-AST", "OSAT", "L1-DP", "L2-DP", "L3-DP",
      L4-DP", "L5-DP", "L6-DP", "L7-DP", "L8-DP")}
  else
    {names(in.dat) <- c("T-Bin", "Date", "DT-ADT", "DT-AST", "OSAT", "L1-DP", "L2-DP",
      L3-DP", "L4-DP", "L5-DP", "L6-DP", "L7-DP", "L8-DP")}
  Ex.Dat <- as.data.frame(cbind(in.dat["DT-AST"], in.dat["OSAT"], in.dat["L1-DP"],
    in.dat["L2-DP"], in.dat["L3-DP"], in.dat["L4-DP"], in.dat["L5-DP"], in.dat["L6-DP"],
    in.dat["L7-DP"], in.dat["L8-DP"]))

  # write the 'new' dataset to file.
  write.table(Ex.Dat, file = out.file, sep = ",", dimnames.write = "col")

  # msg to user.
  cat("Data processing is complete.\n\n")
}
```

Figure 20. S-Function ddcExtract

This function was run against each of DDC monthly data files in their csv format to generate a monthly data file in the q1 format that would later be combined with the weather data for each month. An excerpt of the data for January is shown in Figure 21.

```

DT-AST,OSAT,L1-DP,L2-DP,L3-DP,L4-DP,L5-DP,L6-DP,L7-DP,L8-DP
1/6/99 12:00, -5,-0.040336,-0.016936,-0.000712, 0.026275,
0.061219,0.096632 p.116755,0.153259
1/6/99 12:15, -5,-0.045639,-0.016624,-0.003520, 0.023624,
0.060595,0.098035 p.120967,0.160435
1/6/99 12:30, -4,-0.043143,-0.025672,-0.003207, 0.023311,
0.059816,0.097723 p.122995,0.165740
1/6/99 12:45, -2,-0.038775,-0.013815,-0.000400, 0.026900,
0.066056,0.104744 p.131887,0.175880
1/6/99 13:00, -2,-0.043456,-0.017560,-0.003831, 0.024403,
0.059816,0.100219 p.127987,0.168547
1/6/99 13:15, 0,-0.030975,-0.017872, 0.004436, 0.035167,
0.070735,0.109892 p.133291,0.174475
1/6/99 13:30, -2,-0.040023,-0.022552,-0.000712, 0.028459,
0.064339,0.103807 p.126739,0.169327
1/6/99 13:45, -3,-0.035344,-0.020056, 0.002407, 0.038443,
0.072919,0.117536 p.145771,0.191947
1/6/99 14:00, -3,-0.036280,-0.011008, 0.002407, 0.035323,
0.073543,0.117536 p.143275,0.188203
1/6/99 14:15, -2,-0.039399,-0.017248, 0.000223, 0.030175,
0.066835,0.106615 p.131107,0.175567
1/6/99 14:30, -4,-0.043767,-0.019119,-0.001803, 0.026900,
0.064495,0.104276 p.129079,0.170107
1/6/99 14:45, -5,-0.024735,-0.014440, 0.009271, 0.046243,
0.085088,0.126271 p.152791,0.202556
1/6/99 15:00, -5,-0.044391,-0.018184,-0.001959, 0.028616,
0.068863,0.110359 p.135787,0.177751
1/6/99 15:15, -6,-0.038775,-0.018184,-0.000400, 0.031268,
0.069800,0.111920 p.138440,0.182276
...
...
...
1/28/99 15:45,-29,-0.083079, 0.000223,-0.029416,-0.004612,
0.030488,0.088831 p.124087,0.177595
1/28/99 16:00,-29,-0.006016, 0.015200, 0.014732, 0.076820,
0.125023,0.182900 p.207080,0.266983

```

Figure 21. q1 DDC Data File Excerpt

The building pressurization and temperature data is now in a form that can be combined with the weather data to form a complete dataset.

3.2 Weather Data Processing

The wind speed and wind direction data was downloaded from the LANL NEWNET Project Web site where it was published after being collected by the LANL instrument package on the UAF campus. The data was downloaded and saved in standard text file format.

For the first two thirds of the test year of 1999, the wind data was displayed as north and east vector quantities. An excerpt of this data is shown in Table 6. Beginning in August of the test year, the published wind data changed to a wind speed and wind direction format. An excerpt of this form is shown in Table 7.

These raw data files contain a great deal of information other than the wind data which is required for this research and this data was removed during the data processing described later. It is important to note that the data was collected on a 15-minute time interval. This allows the wind data to be "binned" similar to the DDC data for combining into a coherent dataset. A data value displayed as a series of asterisks is an indication that the instrument was malfunctioning in some manner. Finally, the last column notes the minutes that the instrument package access door was open. A 'door open' condition means that the instrument is being inspected or adjusted by a technician. While this operation is underway, the sensed parameter may be interfered with by the proximity of the technician or the sensor may be disabled during a portion of the 15-minute reading interval. This would make the data recorded during these periods unreliable. Any data record that had asterisks in any field or that indicated the door had been opened was eliminated during processing.

Table 6. Raw Weather Data Excerpt (Jan – Jul Form)

Date	Time (GMT)	Gamma micror	East wind (mph)	North wind (mph)	wind STD	Baro. Press. mbars	Temp (C)	Humid (%)	Rain (in)	Door open Min.
01-JAN-1999	00:10:11	7.5	.9	.7	31.2	985.5	-18.2	85.3	*****	0
01-JAN-1999	00:25:11	7.2	.0	.8	43.7	985.5	-18.5	85.1	*****	0
01-JAN-1999	00:40:11	7.3	-.4	1.0	14.3	985.7	-18.8	84.8	*****	0
01-JAN-1999	00:55:11	7.2	-.6	1.5	14.0	985.9	-18.6	86.3	*****	0
01-JAN-1999	01:10:11	7.5	-.6	1.4	15.0	986.1	-18.1	85.9	*****	0
01-JAN-1999	01:25:11	7.4	-.3	.9	12.7	986.3	-17.9	86.1	*****	0
01-JAN-1999	01:40:11	7.6	-.2	.9	13.9	986.5	-17.9	85.9	*****	0
01-JAN-1999	01:55:11	7.7	.1	1.1	13.4	986.9	-19.1	86.0	*****	0
01-JAN-1999	02:10:11	7.7	-.9	1.0	21.3	986.9	-17.8	86.0	*****	0
01-JAN-1999	02:25:11	7.6	-.7	1.0	12.8	987.1	-17.8	86.3	*****	0
01-JAN-1999	02:40:11	7.7	-.4	.9	15.5	987.1	-17.8	86.9	*****	0
01-JAN-1999	02:55:11	7.8	-1.0	.9	11.6	987.1	-17.6	87.8	*****	0
....
....
....
20-JAN-1999	05:25:11	8.3	-2.3	1.6	8.6	1001.3	-32.7	79.5	*****	0
20-JAN-1999	05:40:11	*****	*****	*****	*****	*****	*****	*****	*****	*****
20-JAN-1999	05:55:11	*****	*****	*****	*****	*****	*****	*****	*****	*****
20-JAN-1999	06:10:11	*****	*****	*****	*****	*****	*****	*****	*****	*****
20-JAN-1999	06:25:11	*****	*****	*****	*****	*****	*****	*****	*****	*****
....
....
....
31-JAN-1999	23:25:12	8.3	.7	-.6	6.0	984.0	-34.4	71.4	*****	0
31-JAN-1999	23:40:12	7.9	.3	-.2	11.3	983.8	-34.2	72.1	*****	0
31-JAN-1999	23:55:12	7.7	.2	-.5	6.9	983.8	-34.2	71.8	*****	0

Table

Date	Time (GMT)	Gamma micror
----	----	-----
01-AUG-1999	00:10:13	8.5
01-AUG-1999	00:25:13	8.5
01-AUG-1999	00:40:13	8.2
01-AUG-1999	00:55:13	8.1
01-AUG-1999	01:10:13	8.5
01-AUG-1999	01:25:13	8.4
01-AUG-1999	01:40:13	8.4
01-AUG-1999	01:55:13	8.3
01-AUG-1999	02:10:13	8.2
01-AUG-1999	02:25:13	8.1
01-AUG-1999	02:40:13	8.4
01-AUG-1999	02:55:13	8.4
01-AUG-1999	03:10:13	8.6
01-AUG-1999	03:25:13	8.5
01-AUG-1999	03:40:13	8.3
01-AUG-1999	03:55:13	8.5
01-AUG-1999	04:10:13	8.4
01-AUG-1999	04:25:13	8.6
01-AUG-1999	04:40:13	8.7
01-AUG-1999	04:55:13	8.7
01-AUG-1999	05:10:13	8.8
....
....
....
31-AUG-1999	22:55:14	8.7
31-AUG-1999	23:10:14	8.5
31-AUG-1999	23:25:14	8.6
31-AUG-1999	23:40:14	8.6
31-AUG-1999	23:55:14	8.7

7. Raw Weather Data Excerpt (Aug – Dec Form)

Wind Speed (mph)	Wind Dir (deg)	Wind STD	Baro. Press. mbars	Temp (C)	Humid (%)	Rain (in)	Door Open Min.
4.1	161.6	32.2	1003.1	26.3	42.5	*****	0
4.7	262.7	23.3	1003.1	26.4	40.1	*****	0
2.5	198.4	43.2	1003.1	26.7	41.5	*****	0
5.2	188.9	31.1	1002.9	27.0	41.7	*****	0
4.0	247.9	32.5	1002.9	27.0	38.5	*****	0
3.1	266.3	36.6	1002.7	27.6	37.4	*****	0
4.9	232.4	30.9	1002.5	27.7	36.1	*****	0
3.3	280.6	32.7	1002.7	27.4	35.3	*****	0
4.8	283.2	29.2	1002.5	27.6	35.8	*****	0
2.9	277.9	40.2	1002.5	27.9	36.3	*****	0
2.9	301.0	34.9	1002.5	27.9	36.4	*****	0
4.4	271.3	32.7	1002.5	27.9	37.0	*****	0
7.0	314.4	22.6	1002.5	26.7	42.8	*****	0
6.9	308.5	19.9	1002.7	26.4	43.2	*****	0
6.1	317.7	21.9	1002.7	26.2	42.8	*****	0
5.9	305.3	19.4	1002.7	24.4	48.1	*****	0
7.2	317.2	21.0	1002.9	23.3	53.7	*****	0
6.8	318.6	24.0	1002.9	22.6	55.5	*****	0
6.4	312.5	22.6	1002.9	22.0	55.7	*****	0
5.5	320.9	21.6	1002.9	21.6	55.3	*****	0
6.8	321.6	20.9	1002.9	21.1	56.7	*****	0
....
....
....
3.0	147.4	30.3	997.8	16.7	47.4	*****	0
4.8	136.7	21.4	997.6	17.0	46.1	*****	0
3.4	163.1	27.4	997.8	16.7	43.0	*****	0
2.0	149.5	50.7	997.6	17.3	44.3	*****	0
4.4	133.2	28.0	997.6	17.4	42.2	*****	0

The first step in processing this raw data was again accomplished by importing the data into an Excel spreadsheet and eliminating the “Gamma microR” “Rain”, and “Door Open Min” fields. The barometric pressure, temperature and humidity fields were kept for informational purposes in this stage of data reduction. While this data was collected on a 15-minute interval, it should be noted that the time reference is Greenwich Mean Time (GMT). The spreadsheet included calculations to group the 15-minute data into a standard 15-minute bin and also convert from GMT to the standard AST time reference used for the DDC data. The spreadsheet also converted the North and East vector wind data into nominal wind speed and direction values for the January through July data files. Lastly, any questionable data fields, that is, those noted with asterisks, were converted to “na” to ease the next processing step.

Once this processing was completed, each monthly group of data was stored in a csv file for future processing. Since most spreadsheet software (including Microsoft Excel used here) considers csv formatting to be “native”, these monthly csv files also provide a method for easy viewing of this data. Excerpts of the January and August data files processed to this state are shown in Tables 8 and 9 respectively.

Next, the S-Function shown in Figure 22 was run against each monthly csv weather file to extract the date/time stamp, wind speed, and direction fields and store this data into a csv file saved with a .q1 extension. An excerpt of the January weather data file in this format is shown in Figure 23.

The weather data is now in a form that can be combined with the pressurization and temperature data to for a cohesive dataset.

Table 8. Monthly Weather Data Excerpts (Jan)

Date (GMT)	Time (GMT)	Time (local)	Date/Time (local)	Date/Time (GMT)	E/Wind (m/s)	N/Wind (m/s)	W/Wind (m/s)	W/Wind (from N) (m/s)	Wind Speed (m/s)	Barometer Temp (°C)	Temp (°F)	Humidity (%)
1-Jan-99	0:10:11	0:00	1/1/1999 0:00	12/31/1998 15:00	0.9	0.7	1.1	52	31.2	985.5	-18.2	85.3
1-Jan-99	0:25:11	0:15	1/1/1999 0:15	12/31/1998 15:15	0	0.2	0.2	0	43.7	985.5	-18.5	85.1
1-Jan-99	0:40:11	0:30	1/1/1999 0:30	12/31/1998 15:30	-0.4	1	1.1	338	14.3	985.7	-18.8	84.8
1-Jan-99	0:55:11	0:45	1/1/1999 0:45	12/31/1998 15:45	-0.6	1.5	1.6	338	16	985.9	-18.6	85.3
1-Jan-99	1:10:11	1:00	1/1/1999 1:00	12/31/1998 16:00	-0.6	1.4	1.5	337	15	986.1	-18.1	85.9
1-Jan-99	1:25:11	1:15	1/1/1999 1:15	12/31/1998 16:15	-0.3	0.9	0.9	342	12.7	986.3	-17.9	86.1
1-Jan-99	1:40:11	1:30	1/1/1999 1:30	12/31/1998 16:30	-0.2	0.9	0.9	347	13.9	986.5	-17.9	85.9
1-Jan-99	1:55:11	1:45	1/1/1999 1:45	12/31/1998 16:45	0.1	1.1	1.1	5	13.4	986.9	-19.1	86
1-Jan-99	2:10:11	2:00	1/1/1999 2:00	12/31/1998 17:00	-0.9	1	1.3	318	21.3	986.9	-17.8	86
1-Jan-99	2:25:11	2:15	1/1/1999 2:15	12/31/1998 17:15	-0.7	1	1.2	325	12.8	987.1	-17.8	86.3
1-Jan-99	2:40:11	2:30	1/1/1999 2:30	12/31/1998 17:30	-0.4	0.9	1	336	15.5	987.1	-17.8	86.9
...
...
...
20-Jan-99	5:40:11	5:30	1/20/1999 5:30	1/19/1999 20:30	na	na	na	na	na	na	na	na
20-Jan-99	5:55:11	5:45	1/20/1999 5:45	1/19/1999 20:45	na	na	na	na	na	na	na	na
20-Jan-99	6:10:11	6:00	1/20/1999 6:00	1/19/1999 21:00	na	na	na	na	na	na	na	na
...
...
...
31-Jan-99	21:26:12	21:15	1/31/1999 21:15	1/31/1999 14:15	0.7	-0.6	0.9	131	6	984	-34.4	71.4
31-Jan-99	21:40:12	21:30	1/31/1999 21:30	1/31/1999 14:30	0.3	-0.2	0.4	124	11.3	983.8	-34.2	72.1
31-Jan-99	21:55:12	21:45	1/31/1999 21:45	1/31/1999 14:45	0.2	-0.5	0.5	199	6.9	983.8	-34.2	71.8

Table 9. Monthly Weather Data Excerpt (Aug)

Date [GMT]	Time [GMT]	Time [h]	Date/Time [UTC]	Date/Time [PST]	Wind [m/s]	Wind [ft/min]	Wind [mph]	Wind [knots]	Wind [knots]	Barometer [hPa]	Barometer [inHg]	Temp [C]	Temp [F]	Humidity [%]
1-19-99	0:10:13	0:00	8/1/1999 0:00	7/31/1999 15:00	4.1	162	32.2	1003.1	26.3	79.3	42.5			
1-19-99	0:26:13	0:15	8/1/1999 0:15	7/31/1999 15:15	4.1	263	23.3	1003.1	26.4	79.5	40.1			
1-19-99	0:40:13	0:30	8/1/1999 0:30	7/31/1999 15:30	2.5	198	43.2	1003.1	26.7	80.1	41.5			
1-19-99	0:56:13	0:45	8/1/1999 0:45	7/31/1999 15:45	5.2	189	31.1	1002.9	27	80.6	41.7			
1-19-99	1:10:13	1:00	8/1/1999 1:00	7/31/1999 16:00	4	248	32.5	1002.9	27	80.6	39.5			
1-19-99	1:26:13	1:15	8/1/1999 1:15	7/31/1999 16:15	3.1	266	36.6	1002.7	27.6	81.7	37.4			
1-19-99	1:40:13	1:30	8/1/1999 1:30	7/31/1999 16:30	4.9	232	30.9	1002.5	27.7	81.9	36.1			
1-19-99	1:56:13	1:45	8/1/1999 1:45	7/31/1999 16:45	3.3	281	32.7	1002.7	27.4	81.3	36.3			
1-19-99	2:10:13	2:00	8/1/1999 2:00	7/31/1999 17:00	4.8	283	29.2	1002.5	27.6	81.7	36.8			
1-19-99	2:26:13	2:15	8/1/1999 2:15	7/31/1999 17:15	2.9	278	40.2	1002.5	27.9	82.2	36.3			
...			
31-19-99	23:25:14	23:15	8/31/1999 23:15	8/31/1999 14:15	3.4	163	27.4	997.8	16.7	62.1	43			
31-19-99	23:40:14	23:30	8/31/1999 23:30	8/31/1999 14:30	2	150	50.7	997.6	17.3	63.1	44.3			
31-19-99	23:55:14	23:45	8/31/1999 23:45	8/31/1999 14:45	4.4	133	28	997.6	17.4	63.3	42.2			

```

function(MoNum = "01")
{
# This function reads in the csv weather files for the LANL
# weather station data. It assigns field headings and then
# extracts the data needed for the Gruening Stack Effect
# research project. That data is then written back to a new
# data file of the form 'wea0199.q1'. This function works
# with both versions of data files from the LANL station.
# The input argument is the month number (i.e.; Jan = 01)
# used to construct the file names for the input and output
# data files.

# 1st build the input & output file names.
in.file <- paste("e:/Ophd/grueningdata/processedweatherdata/wea", MoNum, "99.csv", sep = "")
out.file <- paste(substring(in.file, 1, 50), "q1", sep = "")

# read the file & test for type.
in.dat <- read.table(file = in.file, sep = ",", row.names = NULL, as.is = T, skip = 2)
col.size <- length(in.dat[, ])
if(col.size == 14)
{
names(in.dat) <- c("D-GMT", "T-GMT", "T-Bin", "DT-Bin", "DT-AST", "E-Wind", "N-Wind",
"Wind", "W-Dir", "W-se", "Barom", "Temp-C", "Temp-F", "rh")
}
else
{
names(in.dat) <- c("D-GMT", "T-GMT", "T-Bin", "DT-Bin", "DT-AST", "Wind", "W-Dir",
"W-se", "Barom", "Temp-C", "Temp-F", "rh")
}
Ex.Dat <- as.data.frame(cbind(in.dat["DT-AST"], in.dat["Wind"], in.dat["W-Dir"]))

# write the 'new dataset to file.
write.table(Ex.Dat, file = out.file, sep = ",", dimnames.write = "col")

# msg to user.
cat("Data processing is complete.\n\n")
}

```

Figure 22. S-Function WeaExtract

```

DT-AST,Wind,W-Dir
12/31/98 15:00,1.1, 52
12/31/98 15:15,0.8, 0
12/31/98 15:30,1.1,338
12/31/98 15:45,1.6,338
12/31/98 16:00,1.5,337
12/31/98 16:15,0.9,342
12/31/98 16:30,0.9,347
12/31/98 16:45,1.1, 5
... ..
... ..
... ..
1/31/99 14:00,0.8,120
1/31/99 14:15,0.9,131
1/31/99 14:30,0.4,124
1/31/99 14:45,0.5,158

```

Figure 23. q1 Weather Data File Excerpt

3.3 Combining the Data

Next the monthly data files created above need to be combined into a single dataset (file) that is used to perform the statistical modeling. An interesting problem arose in the first attempt to merge this data due to the large quantity of data involved. The first approach was to merge all of the DDC data and all of the weather data into two respective intermediate files and then merge these two files into the final data file. The resultant two intermediate files containing a years worth of DDC and weather data became too large for the S-Plus memory allocation to address when performing the last merge operation. So a second approach, described below, was used to create the combined data file.

The S-Function shown in Figure 24 was used to first merge the monthly q1 DDC and weather data files into files containing pressurization data at each level, outside temperature, and wind data for each month. The key used for the merge operation was the 15-minute date/time stamp field (DT-AST). Records were written to the combined file only when each of the subordinate files contained data for the particular date/time stamp. That is, if weather data existed for a particular 15-minute bin but no DDC data was available or vice versa, that data was omitted from the combined output file. Once the individual monthly combined files were created, the S-Function shown in Figure 25 created a yearly data file. This avoided the memory allocation problems encountered in the first approach since some of the data was eliminated during the monthly merge process.


```

function(MoNum = "01")
{
# This function obtains data from the DDC & Weather
# data files for the Gruening Pressurization/Stack
# Effect research. It first LTrims the date/time
# field for each file and then merges these two files
# into a combined output file. The function's output
# is a combined data file written to disk and three
# data frames in an output list.

# Get DDC data and create a data frame:
  in.ddc <- paste("e:/Ophd/grueningdata/processedddcdata/ddc", MoNum, "99.q1", sep = "")
  mo.ddc <- as.data.frame(read.table(in.ddc, sep = ",", row.names = NULL, header = T, as.is = T))

# Find the number of records:
  ddc.len <- length(mo.ddc[, 1])

# LTrim the date/time field:
  cat("LTrim of DDC data in progress:\n\n")
  for(i in 1:ddc.len) {
    mo.ddc[i, "DT.AST"] <- LTrim(mo.ddc[i, "DT.AST"])
    if(i %% 10 == 0)
      cat("Processing ", mo.ddc[i, "DT.AST"], "\n")
  }
  cat("DDC data frame complete.\n\n")

# Get weather data and create a data frame:
  in.wea <- paste("e:/Ophd/grueningdata/processedweatherdata/wea", MoNum, "99.q1", sep = "")
  mo.wea <- as.data.frame(read.table(in.wea, sep = ",", row.names = NULL, header = T, as.is = T))

# Find the number of records:
  wea.len <- length(mo.wea[, 1])

# LTrim the date/time field:
  cat("LTrim of weather data in progress:\n\n")
  for(j in 1:wea.len) {
    mo.wea[j, "DT.AST"] <- LTrim(mo.wea[j, "DT.AST"])
    if(j %% 10 == 0)
      cat("Processing ", mo.wea[j, "DT.AST"], "\n")
  }
  cat("Weather data frame complete.\n\n")

# Merge the data frames and write to disk:
  cat("Merging data into a combined data frame:\n\n")
  mo.combined <- merge(mo.ddc, mo.wea, by = "DT.AST")
  out.comb <- paste("e:/Ophd/grueningdata/combineddata", MoNum, "99Combined.q1", sep = "")
  write.table(mo.combined, file = out.comb, sep = ",", dim.names.write = "col")

# Completion msg and return list:
  list(out.ddc = mo.ddc, out.wea = mo.wea, out.combined = mo.combined)
  cat("Data processing for this month is complete.\n\n")
}

```

Figure 24. S-Function MonMerg

```

function()
{
# This function imports combined data from individual month data files
# and uses it to build a data file for the entire year. It
# was written for the data in the Greening Pressurization/Stack Effect
# research project.

# Stub strings to construct path/file names.
pthnm1 <- "e:/dphd/grueningdata/combineddata/"
pthnm2 <- "99Combined.q1"

# Start a counted loop for 12 month iterations and build the annual file.
for(i in 1:12) {
  if(i == 1) {
cat("Processing January data.\n")
in.file <- paste(pthnm1, "D1", pthnm2, sep = "")
in.dat <- as.data.frame(read.table(file = in.file, sep = ";", header = T,
row.names = NULL, as.is = T))
out.file <- paste(substring(in.file, 1, 34), "1999Combined.q1", sep = "")
write.table(in.dat, file = out.file, sep = ";", dimnames.write = "col")
}
  if(i == 2) {
cat("Processing February data.\n")
in.file <- paste(pthnm1, "D2", pthnm2, sep = "")
in.dat <- as.data.frame(read.table(file = in.file, sep = ";", header = T,
row.names = NULL, as.is = T))
out.file <- paste(substring(in.file, 1, 34), "1999Combined.q1", sep = "")
write.table(in.dat, file = out.file, sep = ";", append = T, dimnames.write = F)
}
  if(i == 3) {
cat("Processing March data.\n")
in.file <- paste(pthnm1, "D3", pthnm2, sep = "")
in.dat <- as.data.frame(read.table(file = in.file, sep = ";", header = T,
row.names = NULL, as.is = T))
out.file <- paste(substring(in.file, 1, 34), "1999Combined.q1", sep = "")
write.table(in.dat, file = out.file, sep = ";", append = T, dimnames.write = F)
}
  if(i == 4) {
cat("Processing April data.\n")
in.file <- paste(pthnm1, "D4", pthnm2, sep = "")
in.dat <- as.data.frame(read.table(file = in.file, sep = ";", header = T,
row.names = NULL, as.is = T))
out.file <- paste(substring(in.file, 1, 34), "1999Combined.q1", sep = "")
write.table(in.dat, file = out.file, sep = ";", append = T, dimnames.write = F)
}
  if(i == 5) {
cat("Processing May data.\n")
in.file <- paste(pthnm1, "D5", pthnm2, sep = "")
in.dat <- as.data.frame(read.table(file = in.file, sep = ";", header = T,
row.names = NULL, as.is = T))
out.file <- paste(substring(in.file, 1, 34), "1999Combined.q1", sep = "")
write.table(in.dat, file = out.file, sep = ";", append = T, dimnames.write = F)
}
  if(i == 6) {
cat("Processing June data.\n")
in.file <- paste(pthnm1, "D6", pthnm2, sep = "")
in.dat <- as.data.frame(read.table(file = in.file, sep = ";", header = T,
row.names = NULL, as.is = T))
out.file <- paste(substring(in.file, 1, 34), "1999Combined.q1", sep = "")
write.table(in.dat, file = out.file, sep = ";", append = T, dimnames.write = F)
}
  if(i == 8) {
cat("Processing August data.\n")
in.file <- paste(pthnm1, "D8", pthnm2, sep = "")
in.dat <- as.data.frame(read.table(file = in.file, sep = ";", header = T,
row.names = NULL, as.is = T))
out.file <- paste(substring(in.file, 1, 34), "1999Combined.q1", sep = "")
write.table(in.dat, file = out.file, sep = ";", append = T, dimnames.write = F)
}
  if(i == 9) {
cat("Processing September data.\n")
in.file <- paste(pthnm1, "D9", pthnm2, sep = "")
in.dat <- as.data.frame(read.table(file = in.file, sep = ";", header = T,
row.names = NULL, as.is = T))
out.file <- paste(substring(in.file, 1, 34), "1999Combined.q1", sep = "")
}
}
}

```

Figure 25. S-Function BldCombFile

There was also another problem encountered during the merge operation. For the S-Plus “merge” function to work, the key-field values in each dataset, the DT-AST field in this instance, must match exactly. Recall that the DT-AST value in the original spreadsheet version of the data file existed as a sequence number from a specific reference point as explained earlier. When this field was saved to the csv format of the q1 files, the value was converted to a simple string value. It was discovered that the spreadsheet software was not consistent in how it created this string value. Sometimes the string value was created as the exact value such as “8/10/99 0:00”. However, sometimes empty space(s) were added at the beginning of the string such as “ 8/10/99 0:00”. This caused string values that should have been considered a match to be interpreted as unequal during the merge operation. To correct this, a custom S-Function (Fig. 26) was created to trim any leading spaces from the DT-AST field values. The call to this function is seen in the MonMerg function (Fig. 24) prior to the call to “merge”.

```
function(trimstr)
{
# This function trims the leading spaces from a string.
# The string is passed to the function as its sole argument.
# This function was written to trim the dateTime fields in the Gruening data.
  strlen <- nchar(trimstr)
  i <- 1
  for(i in 1:strlen) {
    chrpos <- i
    if(substring(trimstr, i, i) != " ")
      break
  }
  substring(trimstr, chrpos, strlen)
}
```

Figure 26. S-Function LTrim

An excerpt of the combine data file is shown in Figure 27. Note that the complete data file is comprised of over 700 data records.

```

DT ,AST ,OSAT ,L1 ,DP ,L2 ,DP ,L3 ,DP ,L4 ,DP ,L5 ,DP ,L6 ,DP ,L7 ,DP ,L8 ,DP ,Wind ,W ,Dir
1/1/99 12:45, 7, -0.026296, -0.004768, -0.000400, 0.022687, 0.053263, 0.087271, 0.104744, 0.143431, 3.6, 309
1/1/99 13:00, 7, -0.028367, -0.008512, 0.004436, 0.027679, 0.088099, 0.092732, 0.110359, 0.149204, 3.8, 311
1/1/99 13:15, 7, -0.026920, -0.003207, -0.000244, 0.021283, 0.049831, 0.086960, 0.104431, 0.141247, 3.3, 311
1/1/99 13:30, 9, -0.035359, -0.013504, 0.000379, 0.022063, 0.053731, 0.089299, 0.107551, 0.145927, 3.9, 312
1/1/99 13:45, 6, -0.015688, -0.013191, 0.006464, 0.031579, 0.062312, 0.098191, 0.117223, 0.154195, 3.5, 314
1/1/99 14:00, 7, -0.021912, -0.078711, -0.003051, 0.018943, 0.048896, 0.087427, 0.104900, 0.143275, 3.2, 326
1/1/99 14:15, 7, -0.007575, 0.001471, 0.012080, 0.038443, 0.070423, 0.104431, 0.123619, 0.158407, 3.3, 315
1/1/99 14:30, 7, -0.030664, 0.000223, -0.003831, 0.015043, 0.045619, 0.088407, 0.098815, 0.134539, 2.9, 316
1/1/99 14:45, 7, -0.016000, -0.007264, 0.006308, 0.028147, 0.057631, 0.081795, 0.109892, 0.145147, 2.7, 304
1/1/99 15:00, 7, -0.027855, -0.004768, -0.002896, 0.019724, 0.046555, 0.085088, 0.106927, 0.142340, 3.5, 320
...
...
...
9/1/99 9:00, 50, -0.026607, 0.016759, 0.009584, 0.033451, 0.042811, 0.058568, 0.064495, 0.077287, 1.0, 151
9/1/99 9:15, 50, 0.003031, 0.028927, 0.023000, 0.029240, 0.039380, 0.054044, 0.038599, 0.054355, 1.1, 195
9/1/99 9:30, 50, 0.010832, 0.022376, 0.020503, 0.039535, 0.050144, 0.064495, 0.073700, 0.086960, 1.9, 201
9/1/99 9:45, 50, -0.024111, 0.026744, 0.021283, 0.049207, 0.060595, 0.073855, 0.063560, 0.075259, 2.9, 190

```

Figure 27. ql Combined Data File Excerpt

3.4 Elimination of Wind Effect

This research focuses on building pressurization due to buoyancy effect. However, the combined data file includes data when the wind was blowing and when conditions were calm. The easiest way to eliminate wind effect pressurization from the study is to eliminate all data records when the wind speed was great enough to produce a significant wind effect pressure differential.

As noted in Section 2.4, the pressure transmitter has a resolution of 0.0025 in. H₂O (0.6221 Pa). Therefore, any data record with a wind speed capable of producing a differential pressure equal to or greater than this value should be eliminated from the dataset. Equation (2) is one method to relate wind speed to differential pressure created across the building envelope. One of the factors in this equation is the density of the air which is a function of the air temperature. The spreadsheet shown in Table 10, which shows the wind pressurization in the body of the table, was constructed to evaluate wind effect pressurization. A surface pressure coefficient of 0.95 was used in this spreadsheet. This should represent a worst case scenario for pressurization which is on the windward side of the building (Table 1).

The calculations show that for a wind speed of 2 mph (0.9 m/s) and the most dense (coldest) air, the differential pressure due to wind effect is 0.0024 in. H₂O (0.5980 Pa). So, wind effect pressurization created by winds of less than 2 mph are not detectable by the instrumentation. Since the dataset is extremely large, it was decided to eliminate all data records for which the wind speed exceeded 1.5 mph (0.7 m/s) in order to incorporate a margin of safety.

The S-Plus interactive command shown in Figure 28 was used to strip the data records with wind speeds greater than 1.5 mph. The remaining data constituted the new dataset "Comb.Wind.LE1.5". Note that a similar interactive command had been

previously used to remove the records that included "na" fields indicating possible instrumentation problems.

Table 10. Wind Elimination Criteria

Temperature [°F]	Air Density [lb./ft. ³]	Building Surface Pressure Due to Wind Effect									
		0.25	0.5	0.75	1	1.25	1.5	1.75	2	2.25	2.5
-40	0.0978	0.00037	0.00150	0.00037	0.00059	0.00056	0.00134	0.00183	0.00239	0.00304	0.00374
-45	0.0957	0.00037	0.00147	0.00037	0.00056	0.00056	0.00131	0.00179	0.00234	0.00299	0.00365
-50	0.0946	0.00036	0.00145	0.00036	0.00053	0.00053	0.00126	0.00175	0.00231	0.00295	0.00362
-55	0.0935	0.00036	0.00143	0.00036	0.00052	0.00052	0.00122	0.00173	0.00229	0.00290	0.00358
-60	0.0923	0.00035	0.00141	0.00035	0.00051	0.00051	0.00118	0.00173	0.00226	0.00283	0.00353
-65	0.0913	0.00035	0.00140	0.00035	0.00050	0.00050	0.00115	0.00171	0.00223	0.00282	0.00349
-70	0.0903	0.00035	0.00138	0.00035	0.00050	0.00050	0.00111	0.00169	0.00221	0.00281	0.00348
-75	0.0893	0.00034	0.00137	0.00034	0.00049	0.00049	0.00108	0.00167	0.00219	0.00277	0.00342
-80	0.0882	0.00034	0.00135	0.00034	0.00049	0.00049	0.00104	0.00165	0.00216	0.00273	0.00337
-85	0.0874	0.00033	0.00134	0.00033	0.00048	0.00048	0.00101	0.00162	0.00213	0.00271	0.00334
-90	0.0865	0.00033	0.00133	0.00033	0.00047	0.00047	0.00098	0.00160	0.00210	0.00268	0.00331
-95	0.0854	0.00033	0.00131	0.00033	0.00046	0.00046	0.00094	0.00157	0.00207	0.00265	0.00327
-100	0.0844	0.00032	0.00129	0.00032	0.00045	0.00045	0.00091	0.00154	0.00204	0.00262	0.00323
-105	0.0836	0.00032	0.00128	0.00032	0.00044	0.00044	0.00088	0.00153	0.00201	0.00259	0.00320
-110	0.0827	0.00032	0.00127	0.00032	0.00043	0.00043	0.00085	0.00152	0.00197	0.00256	0.00317
-115	0.0819	0.00031	0.00125	0.00031	0.00042	0.00042	0.00082	0.00150	0.00194	0.00254	0.00313
-120	0.0810	0.00031	0.00124	0.00031	0.00041	0.00041	0.00079	0.00148	0.00191	0.00251	0.00310
-125	0.0802	0.00031	0.00123	0.00031	0.00040	0.00040	0.00076	0.00147	0.00189	0.00249	0.00307
-130	0.0794	0.00030	0.00122	0.00030	0.00039	0.00039	0.00074	0.00145	0.00187	0.00246	0.00304
-135	0.0786	0.00030	0.00120	0.00030	0.00038	0.00038	0.00071	0.00143	0.00184	0.00243	0.00301
-140	0.0778	0.00030	0.00119	0.00030	0.00037	0.00037	0.00068	0.00141	0.00181	0.00241	0.00297
-145	0.0771	0.00030	0.00118	0.00030	0.00036	0.00036	0.00066	0.00140	0.00180	0.00239	0.00293
-150	0.0763	0.00029	0.00117	0.00029	0.00035	0.00035	0.00063	0.00138	0.00178	0.00237	0.00289
-155	0.0756	0.00029	0.00116	0.00029	0.00034	0.00034	0.00061	0.00137	0.00177	0.00235	0.00285
-160	0.0748	0.00029	0.00115	0.00029	0.00033	0.00033	0.00059	0.00136	0.00176	0.00232	0.00281
-165	0.0742	0.00028	0.00114	0.00028	0.00032	0.00032	0.00056	0.00134	0.00174	0.00230	0.00278
-170	0.0735	0.00028	0.00113	0.00028	0.00031	0.00031	0.00054	0.00133	0.00173	0.00228	0.00274

```
menuSubset(data = Comb.1999.noNA, subset.expression = "Wind <= 1.5", subset.columns
= "(All Variables)", result.type = "Data Frame", subset.col.name = "subset",
save.name = "Comb.Wind.LE1.5", show.p = F)
```

Figure 28. S-Plus Interactive Command to Eliminate Wind Effect Records

3.5 Data Reorganization

The form of the data shown in Figure 27 is very useful for viewing and review. However, it is not in optimum form for building the statistical models developed in this research. These models take the form of equations that relate the observed/predicted variable, differential pressure, to the explanatory variables, outside temperature and elevation. The preferred form is a dataset with each record consisting of a field for the measured differential pressure and its associated explanatory measurements of outside temperature and elevation.

Previous research cited in Section 1 also suggests that normalizing elevation with respect to the NPL may also be useful. As noted, the NPL is dynamic in location. But, it can roughly be considered to be mid-building height.

Also, now that the data from the disparate data sources has been combined into a single dataset, there is no need for the date/time field. Recall that this field was simply a tool to insure that all concurrent data from the various data sources was properly aligned when the data was combined.

The S-Plus interactive command session shown in Figure 29 reorganizes the data from its parallel structure, each record containing a single observed variable but multiple explanatory variables, into a serial structure. In the serial structure (Table 11), each record contains an observed variable (differential pressure) and only the explanatory variables contributing to that observation.

```

# The following S-Plus interactive session is used to de-construct the combined
# data data.frame from records indexed on date/time with 8 DP readings per
# record into a new data.frame that includes the independent variables of
# elevations,
# elevation compared to mid-elevation, and OSAT and the response (dependent)
# variable
# DP in each record.

L1.dat <- as.data.frame(cbind(Comb.Wind.LE1.5[, "OSAT"], rep(9.083, 1136), rep(-
41.750, 1136), Comb.Wind.LE1.5[, "L1.DP"]))

L2.dat <- as.data.frame(cbind(Comb.Wind.LE1.5[, "OSAT"], rep(22.750, 1136), rep(-
28.084, 1136), Comb.Wind.LE1.5[, "L2.DP"]))

L3.dat <- as.data.frame(cbind(Comb.Wind.LE1.5[, "OSAT"], rep(37.750, 1136), rep(-
13.084, 1136), Comb.Wind.LE1.5[, "L3.DP"]))

L4.dat <- as.data.frame(cbind(Comb.Wind.LE1.5[, "OSAT"], rep(51.167, 1136),
rep(0.333, 1136), Comb.Wind.LE1.5[, "L4.DP"]))

L5.dat <- as.data.frame(cbind(Comb.Wind.LE1.5[, "OSAT"], rep(64.167, 1136),
rep(13.333, 1136), Comb.Wind.LE1.5[, "L5.DP"]))

L6.dat <- as.data.frame(cbind(Comb.Wind.LE1.5[, "OSAT"], rep(76.667, 1136),
rep(25.833, 1136), Comb.Wind.LE1.5[, "L6.DP"]))

L7.dat <- as.data.frame(cbind(Comb.Wind.LE1.5[, "OSAT"], rep(89.000, 1136),
rep(38.167, 1136), Comb.Wind.LE1.5[, "L7.DP"]))

L8.dat <- as.data.frame(cbind(Comb.Wind.LE1.5[, "OSAT"], rep(101.667, 1136),
rep(50.833, 1136), Comb.Wind.LE1.5[, "L8.DP"]))

Gru.dat <- as.data.frame(rbind(L1.dat, L2.dat, L3.dat, L4.dat, L5.dat, L6.dat,
L7.dat, L8.dat))

names(Gru.dat) <- c("OSAT.F", "Elev.Ft", "Elv.NPL", "DP.InH2O")

write.table(Gru.dat, file="e:/Ophd/grueningdata/combineddata/GruDat.csv", sep=",",
dimnames.write="col")

mode(Gru.dat[,1])
[1] "numeric"

mode(Gru.dat[,2])
[1] "numeric"

mode(Gru.dat[,3])
[1] "numeric"

mode(Gru.dat[,4])
[1] "numeric"

# End of interactive session to convert data

```

Figure 29. S-Plus Interactive Session to Create Serial Dataset

The differential pressure readings, as recorded by the instrumentation system, carried many digits to the right of the decimal point. Six of these digits are displayed in

Figure 27. But do all of these digits present significant data? The differential pressure transmitter possessed a resolution of only 0.0025 in. H₂O. So, at best, the pressure data is only significant to 4-decimal places. Because the resolution is 0.0025 rather than 0.0001, an argument could be made that the pressure readings should be rounded to the nearest 0.001 in. H₂O. However, due to other 'safety' factors already incorporated into the data, the pressure readings were rounded to 4-decimal place resolution using the S-Plus interactive command session shown in Figure 30.

```
Gru.dat.rnd <- as.data.frame(cbind(Gru.dat[,1],
  Gru.dat[,2], Gru.dat[,3], round(Gru.dat[,4],4)))

names(Gru.dat.rnd) <- c("OSAT.F", "Elev.Ft", "Elv.NPL",
  "DP.InH2O")

write.table(Gru.dat.rnd,
  file="e:/Ophd/grueningdata/combineddata/GruDatRnd.csv",
  sep=",", dimnames.write="col")
```

Figure 30. S-Plus Interactive Session to Round Data

Table 11 shows an excerpt from the dataset in its final form. The entire dataset contains slightly more than 9,000 records (data points).

Table 11. Serial Structure Dataset Excerpt

OSAT.F	Elev.Ft	Elv.NPL	DP.InH2O
10	9.083	-41.75	-0.0163
11	9.083	-41.75	-0.0275
13	9.083	-41.75	-0.0204
...
...
...
-22	22.75	-28.084	-0.006
-22	22.75	-28.084	0.0012
-26	22.75	-28.084	-0.025
...
...
...
10	37.75	-13.084	0.0029
7	37.75	-13.084	0.0071
1	37.75	-13.084	0.001
...
...
...
-2	51.167	0.333	0.0271
-2	51.167	0.333	0.0283
-2	51.167	0.333	0.0232
...
...
...
-26	64.167	13.333	0.0952
-25	64.167	13.333	0.0915
-25	64.167	13.333	0.101
...
...
...
-28	76.667	25.833	0.1545
-30	76.667	25.833	0.1077
-32	76.667	25.833	0.1554
...
...
...
-35	89	38.167	0.189
-35	89	38.167	0.1586
-34	89	38.167	0.1854
...
...
...
13	101.667	50.833	0.1289
15	101.667	50.833	0.1308
15	101.667	50.833	0.1213

3.6 Data Validation

The final step in analyzing the data prior to attempting to fit the data to a statistical model is to check the validity of each data point. Data points that were recorded when the instrument system was experiencing problems have already been eliminated as described in previous sections. However, it is possible that some of the remaining data points are not “good” representations of the data. For example, a particular differential pressure reading may be erroneous due to a momentary blockage in a sensor tube, a breeze at the tube opening caused by something moving past the port, or the opening/closing of the door across which the differential pressure is read at the exact time the reading was recorded.

In statistical parlance, these points are known as *outliers*. An outlier is a point that has a disproportionate influence on the statistical fit of the data. Consider the simple least-squares linear model shown in Figure 31.

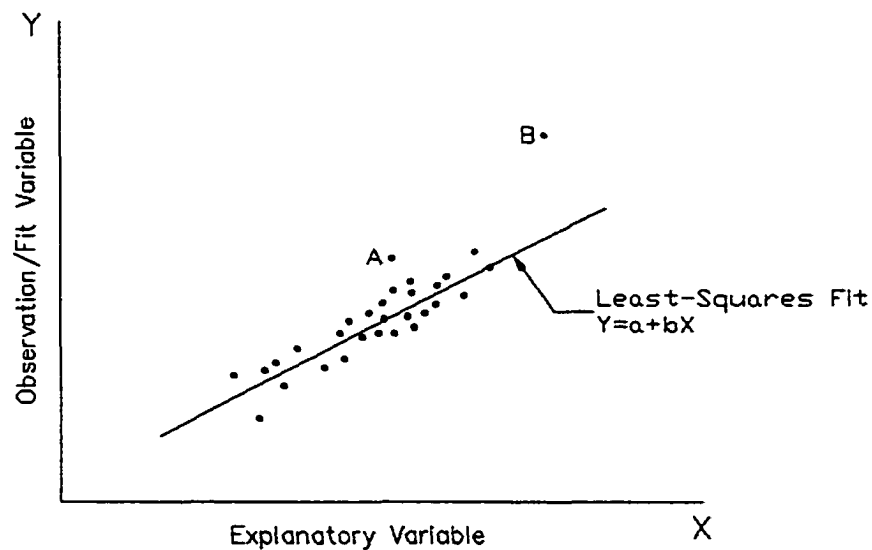


Figure 31. Outlier Visualization

In this illustration, Point A is significantly separated from the main cluster of data in the Y direction. This point will cause the final fitted line to be “pulled” closer to itself than the other points which are generally in the uniform cluster of data. This would cause the intercept term, a , to be different than it would be if Point A did not exist.

Point B is separated from the general data cluster in both the X and Y directions. This point will tend to “leverage” the fitted line, drawing the right end toward Point B. This would cause a shift in the fitted line not only in the intercept term, a , but also a significant change to the slope, b . The fitted line would be quite different if Point B were not included in the dataset.

It’s easy to see from this illustration why these points are called *outliers*. They lay well outside the cluster of the remainder of the dataset. These are the points that can significantly influence the fit of the line. However, just because a point is an outlier does not mean it is a “bad” point and should automatically be removed from the dataset. Outliers should be closely evaluated to determine if they are erroneous points or if they may be the most important points in characterizing the data.

One statistical tool used to identify outliers in a dataset is the Cook’s Distance Method (Cook’s-D). In the Cook’s Distance Method, multiple simple linear regressions are performed on the dataset. First a fit is developed using all of the points in the dataset. Then a single point is removed and the regression is repeated. An index is created representing the difference in the fit between these two models. This index is the Cook’s-Distance. This procedure is repeated removing and replacing each point in the dataset thus creating a Cook’s-D index for each data point. If a point’s Cook’s-D is greatly outside the norm, then it is a point of high influence and should be evaluated for its validity. More detail on the Cook’s Distance Method, including discussions of what might be considered “greatly outside the norm”, can be

found in most undergraduate level statistics books such as the text by Neter et al. (1996).

A Cook's-D analysis of the dataset is presented in Figure 32. Three points are identified as outliers (label with the sequential point number within the dataset) requiring further evaluation.

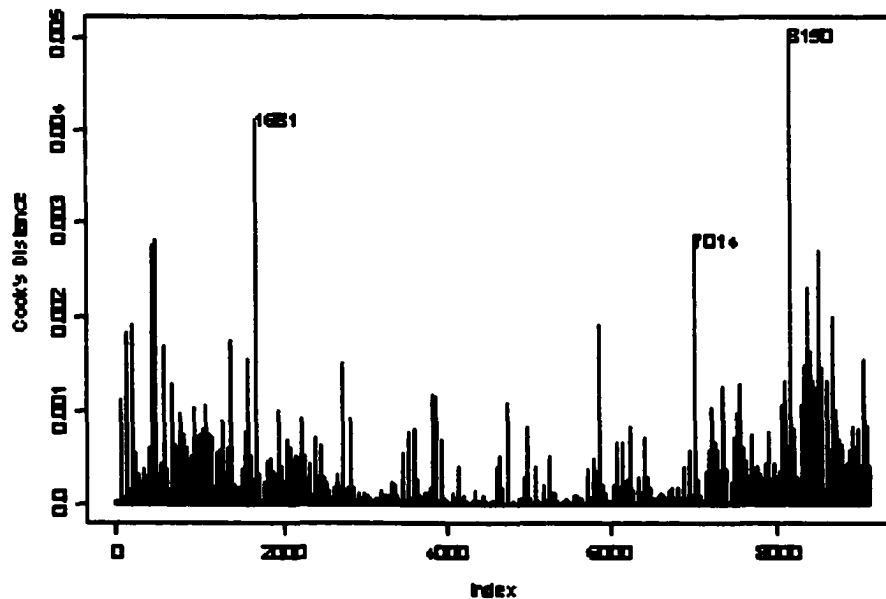


Figure 32. Cook's-D Evaluation of Data Points

Table 12 shows the details for each of these points.

Table 12. Cook's-D Influential Point Details

Point	D.P.	OSAT	Elevation
1681	-0.1920	-42	22.750
7014	0.3416	-33	89.000
8150	0.3962	-33	101.667

There are 20 points with similar temperature and elevation data to Point 1681. The differential pressure range for all of these points except 1681 is -0.01 to -0.04 . The value for point 1681 is far outside the norm with no apparent justification. Possibly a door opened/closed near the exact time the reading was recorded. Since there is no justification for this aberrant reading, it was eliminated from the data set.

A similar analysis found 12 points similar to 7014 with a differential pressure range of 0.08 to 0.20 . There were also 12 points similar to 8150 with differential pressures ranging from 0.14 to 0.26 . Again, there was no reasonable explanation for the vastly different pressures recorded for points 7014 and 8150, so these points were also eliminated from the dataset.

This completed the data processing and validation. The next phase of the research uses this data to create statistical models and compare these models to the predictions of buoyancy effect pressurization obtained from Eq. (7).

4. Statistical Models

The following subsections describe the statistical models that were fit to the data. These models range from a simple linear regression to several more complex models. A detailed description is presented for each case including analysis of whether any of the model's governing assumptions were violated, and any problems noted with the resulting data fit. Each subsection includes a comparison of the particular model's prediction to the actual data and to the prediction made by the ASHRAE recommended method represented by Eq. (7).

4.1 Simple Additive Model

The first model considered was a simple additive model. This type of model is a least-squares fit method where the response (dependent) variable is equal to the simple sum of the explanatory (independent) variables.

The response variable is the differential pressure at each elevation. The explanatory variables are the outside temperature and the elevation at which the differential pressure is measured. As discussed earlier, the models developed in this dissertation will reference the elevation to the building mid-height. This is a well defined location and avoids the problem of locating the neutral pressure level. The general form of the simple additive model is:

$$P = a + bH + cT \quad (12)$$

where: P = differential pressure [in. H₂O]
 a = intercept parameter
 b = slope parameter (w.r.t. H)
 H = elevation from mid-building height [ft]
 c = slope parameter (w.r.t. T)
 T = outside temperature [°F]

The S-Plus integrated development environment was used to fit the data to the simple additive model. The resultant report is shown in Figure 33.

```

*** Linear Model ***

Call: lm(formula = DP.InN20 ~ Elev.MPL + OSAT.F, data = Gru.LM, na.action = na.omit)
Residuals:
    Min       1Q   Median       3Q      Max
-0.1599 -0.02991 -0.006234  0.02756  0.1612

Coefficients:
            Value Std. Error  t value Pr(>|t|)
(Intercept)  0.0525   0.0004    119.8503  0.0000
      Elev.MPL  0.0019   0.0000    137.6816  0.0000
        OSAT.F -0.0006   0.0000    -59.6890  0.0000

Residual standard error: 0.03998 on 9082 degrees of freedom
Multiple R-Squared:  0.7126
F-statistic: 11260 on 2 and 9082 degrees of freedom, the p-value is 0

```

Figure 33. S-Plus Additive Model Report

This report lists the values for the model's parameters (a, b, & c) in the table under the "Value" heading in the lower half of the report. Therefore, the simple additive model that best fits the data collected is:

$$P = 0.0525 + 0.0019H - 0.0006T \quad (13)$$

The report also presents some diagnostics about the fit of this model. The "t value" and "Pr (>|t|)" columns are tools used to determine whether the values of the parameters (coefficients) listed could actually be zero instead of the values calculated by the regression. If these values were zero, this would indicate that the differential pressure was not a function of the explanatory variable. From the physical nature of the problem, this would indicate a "bad" model. This regression results in large absolute t-values and the probability that any coefficient is actually zero is less than 0.01%. Therefore, the observed variable, differential pressure, is a function of the explanatory variables, elevation from mid-building height and outside temperature.

In-depth information about the t-value and p-value, how they are calculated, and how they are interpreted, can be found in most undergraduate and graduate level statistics texts such as Neter et al. (1996).

The “R-squared” (coefficient of multiple determination) diagnostic for the model fit also gives some insight into how well the observed data fits the model equation. This is a measure of how the explanatory variables reduce the variation in the response variable. While a large value for R^2 does not guarantee that the fit is good, a large R^2 , in conjunction with other indicators, can add confidence in using the model.

So, from the information presented in the model report (Fig. 33), it appears that Eq. (13) represents a good fit to the data. However, this model was fit based on certain assumptions inherent in the S-Plus programming (and similar underlying assumptions from basic statistical methods). In statistical model fitting, an error or residual is defined as the difference between the observed response and the response predicted by the model for each set of explanatory variables. It is assumed that the errors or residuals for each point are normally distributed, have a random distribution about zero, and a uniform variance. The easiest way to evaluate this criteria is to plot the residuals against the predicted values.

Figure 34 shows this plot for the simple additive model represented by Eq. (13). It is obvious that the error distribution is not random about zero. There is a definite concave curvature to the plot. This indicates that the data does not fit a simple additive model (the assumptions on which the model is based have been violated). However, the total variance of the errors is quite small (less than -0.2 to $+0.2$) so it might be worthwhile to see how this model compares to the observed data and the predictions made by the recommended ASHRAE method.

Plotting a single response variable against two explanatory variables results in a three dimensional plot that is very difficult to use and interpret. Therefore, the information will be presented in a series of plots (Fig. 35 – 40). Each plot will show the response variable, differential pressure, plotted against the explanatory variable, distance from mid-building height. The series of plots will encompass several discrete values of the other explanatory variable, outside air temperature. The data collected provides data points from -45°F outside temperatures to above the 70°F inside temperature at which the stack effect pressurization reverses. Plotting the comparisons at 20°F increments from -40°F to $+60^{\circ}\text{F}$ provides a ‘good picture’ of the results. One deviation from this scenario occurs. There was insufficient data at $+10^{\circ}\text{F}$ to provide a meaningful plot. So, the data for $+15^{\circ}\text{F}$ was plotted instead of data at the $+10^{\circ}\text{F}$ and $+30^{\circ}\text{F}$ increments. One last step to add to the clarity of the plots is that only five randomly selected observations are shown. This reduces the clutter on the plots but does not affect the trend shown.

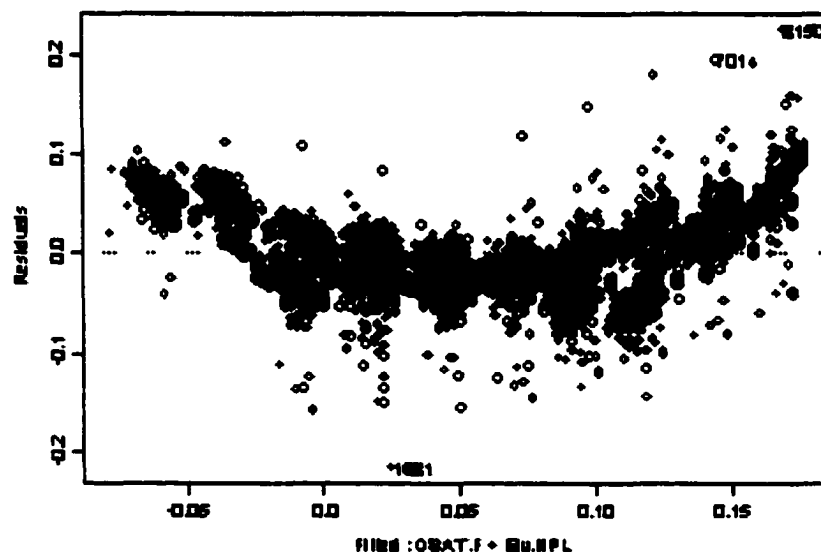


Figure 34. Additive Model - Residual vs. Fit Plot

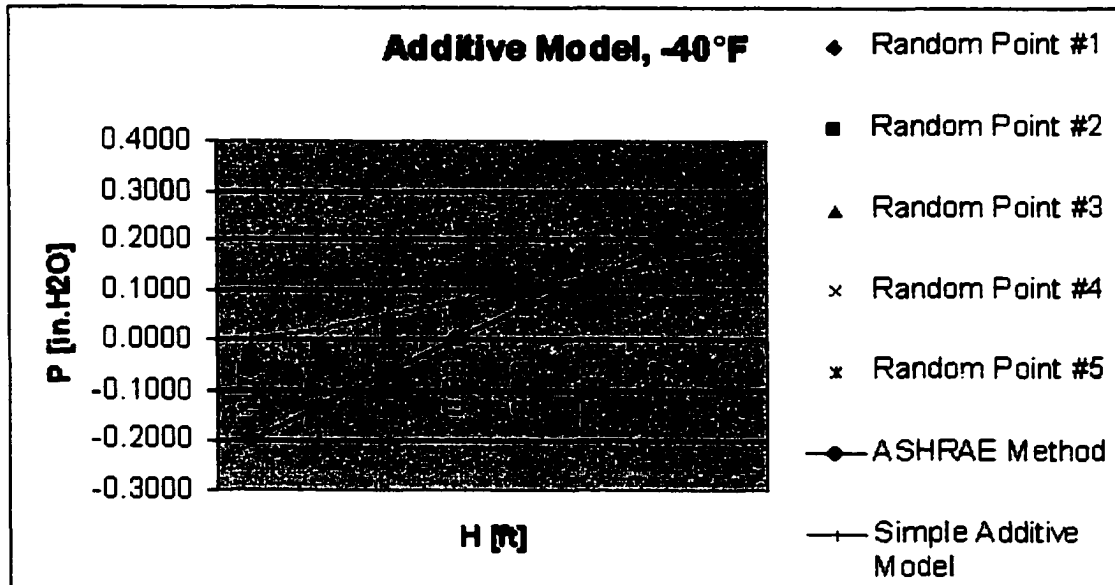


Figure 35. Additive Model Comparison at -40°F

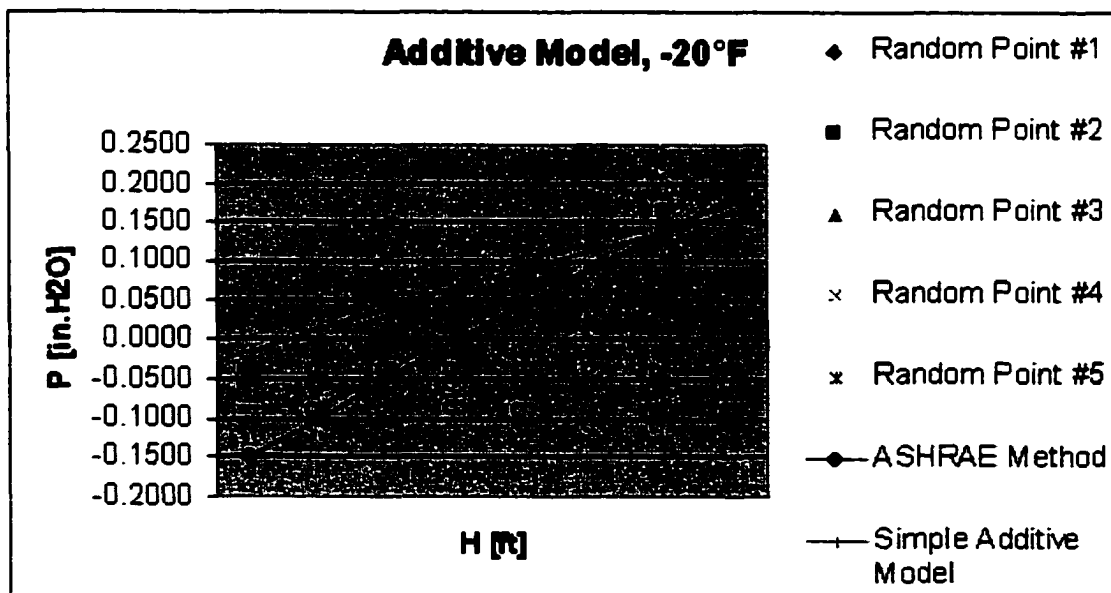


Figure 36. Additive Model Comparison at -20°F

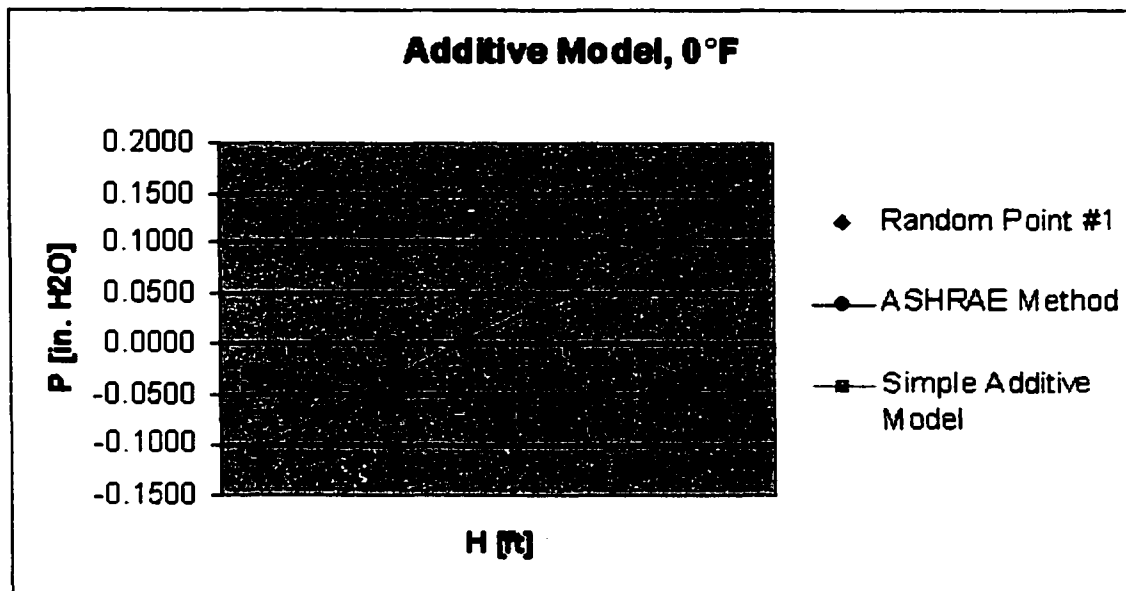


Figure 37. Additive Model Comparison at 0°F

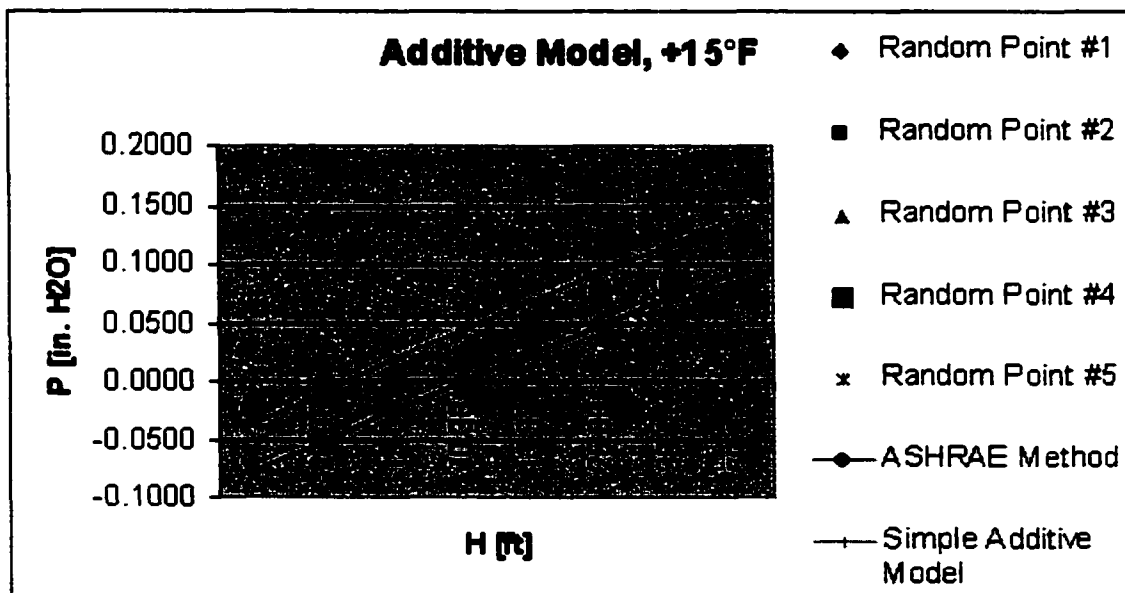


Figure 38. Additive Model Comparison at +15°F

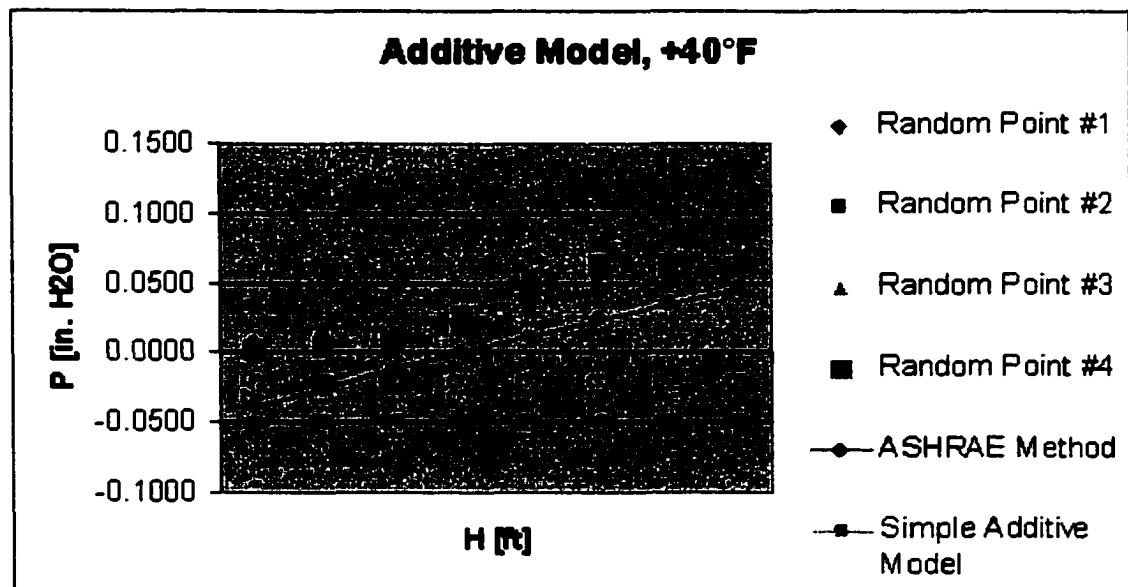


Figure 39. Additive Model Comparison at +40°F

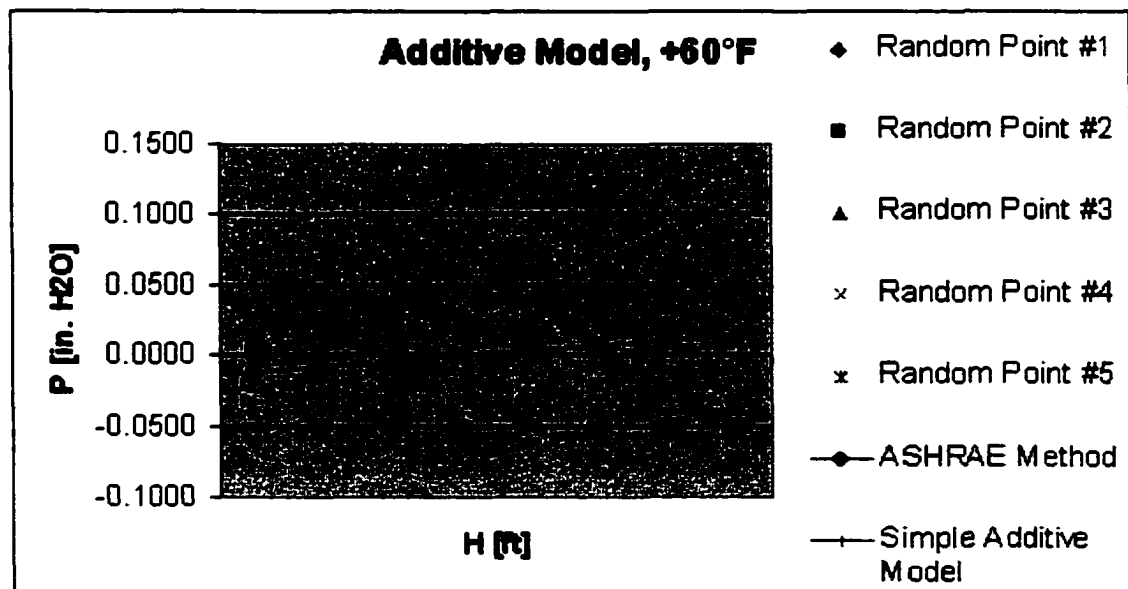


Figure 40. Additive Model Comparison at +60°F

These plots show that the Simple Additive Model provides a better match to the data at the lower outside air temperatures than does the ASHRAE recommended method. This is especially true at the lower elevations where the ASHRAE Method can be seen to be overly conservative. Some of this difference can be attributed to the fact that the HVAC systems were operational during data collection. This tended to depress the NPL due to the outside ventilation air introduced. At the higher outside air temperatures, +40°F and +60°F, neither model is very close to the observed pressure readings. But it also should be noted that, at these outside air temperatures, the buoyancy driving force is low and the magnitude of the differential pressure is also much smaller than at the lower outside air temperatures. Errors in predictions versus actual observations are less critical at these points.

4.2 Transformed Additive Model

One 'statistical trick' to try to correct the residuals vs. fit curvature found in the previous model is to transform the explanatory or response variables. A standard practice to correct the concave curvature is to fit the natural logarithm of the explanatory variables to the response variable.

Unfortunately, the explanatory variable for elevation, H , is actually the elevation difference from the mid-building height. This means that half of the values are negative and, thus, have no valid logarithm. Therefore, a transformed additive model was attempted using the actual elevation from lowest level as the explanatory elevation variable. This avoids the logarithm of a negative value problem but precludes direct comparison to the ASHRAE recommended method since it is based on the elevation from NPL approach.

Taking the logarithm of the temperature explanatory variable is also a problem since many of the temperatures are also negative values. But, this is easily solved by

changing the temperature scale from the Fahrenheit scale to the Rankine (absolute) temperature scale.

The resulting transformed additive model results in an equation of the following form:

$$P = a + b\text{Ln}(h) + c\text{Ln}(T) \quad (14)$$

where: P = differential pressure [in. H₂O]
 a = intercept parameter
 b = slope parameter (w.r.t. h)
 h = elevation from building base [ft]
 c = slope parameter (w.r.t. T)
 T = outside temperature [°R]

The S-Plus integrated development environment provided the report shown in Figure 41 for this transformed model.

```

*** Linear Model ***

Call: lm(formula = DP.InH2O ~ ln.elev.ft + ln.osat.R, data = Gru.xfrm.LM,
na.action = na.omit)

Residuals:
    Min     1Q   Median     3Q    Max
-0.2347 -0.03015 -0.01105  0.0282  0.2563

Coefficients:
              Value Std. Error  tvalue Pr(>|t|)
(Intercept)  1.5814   0.0351  45.0684  0.0000
ln.elev.ft   0.0691   0.0006 106.5026  0.0000
ln.osat.R   -0.2907   0.0057 -51.0690  0.0000

Residual standard error: 0.04695 on 9085 degrees of freedom
Multiple R-Squared: 0.6056
F-statistic: 6975 on 2 and 9085 degrees of freedom, the p-value is 0

```

Figure 41. S-Plus Transformed Additive Model Report

This model provides high p-values and low standard error estimates. But the plot of residuals vs. fit for this model (Fig. 42) displays the same non-random distribution problems as the original Simple Additive Model. In addition, the errors tend to be biased to the right end of the plot. This is a characteristic of the logarithmic transformation that sometimes occurs. So the transformed data model is actually worse than the Simple Additive Model. Therefore, this model was not pursued.

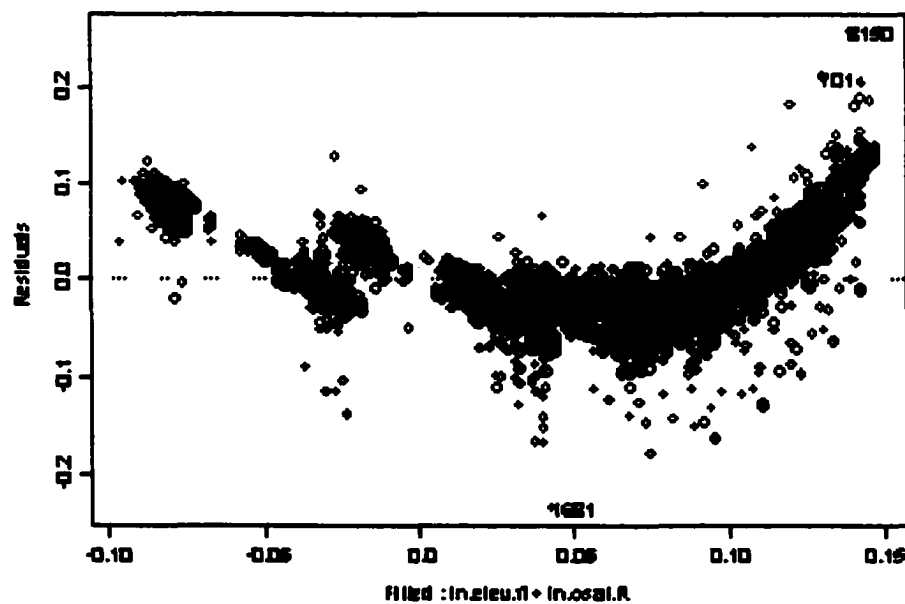


Figure 42. Transformed Additive Model - Residual vs. Fit Plot

4.3 Nonlinear Multiplicative Model

The equation recommended by ASHRAE, Eq. (7), to estimate buoyancy effect pressurization suggests that a multiplicative nonlinear model may fit the data. This model has the form:

$$P = a + bHT \quad (15)$$

where: P = differential pressure [in. H₂O]
 a = intercept parameter
 b = slope parameter
 H = elevation from mid-building height [ft]
 T = outside temperature [°R]

It is interesting to note that the absolute temperature scale, °R, must also be used for the explanatory temperature variable for this model. If the Fahrenheit scale is used, there are times when the temperature value may be zero. This causes a discontinuity in the model. Since a temperature value of zero will not occur on the Rankin scale, the discontinuity problem is resolved.

This model form was constructed in the S-Plus integrated development environment. The result is the report shown in Figure 43.

```

*** Nonlinear Regression Model ***

Formula: DP.InH2O ~ b0 + b1 * Elev.NPL *(OSAT.F +460)

Parameters:
  Value Std. Error t value
b0 4.73372e-002 5.48123e-004 86.3623
b1 3.79003e-006 3.77604e-008 100.3700

Residual standard error: 0.0513508 on 9083 degrees of freedom

Correlation of Parameter Estimates:
  b0
b1 -0.184

```

Figure 43. S-Plus Multiplicative Model Report

The standard error values of 5.48×10^{-4} and 3.78×10^{-8} are very small and t-values of 86 and 100 are considered large. Therefore, these diagnostics show this model to be a

“good” representation of the data. Figure 44 shows the residuals versus fit plot for this model.

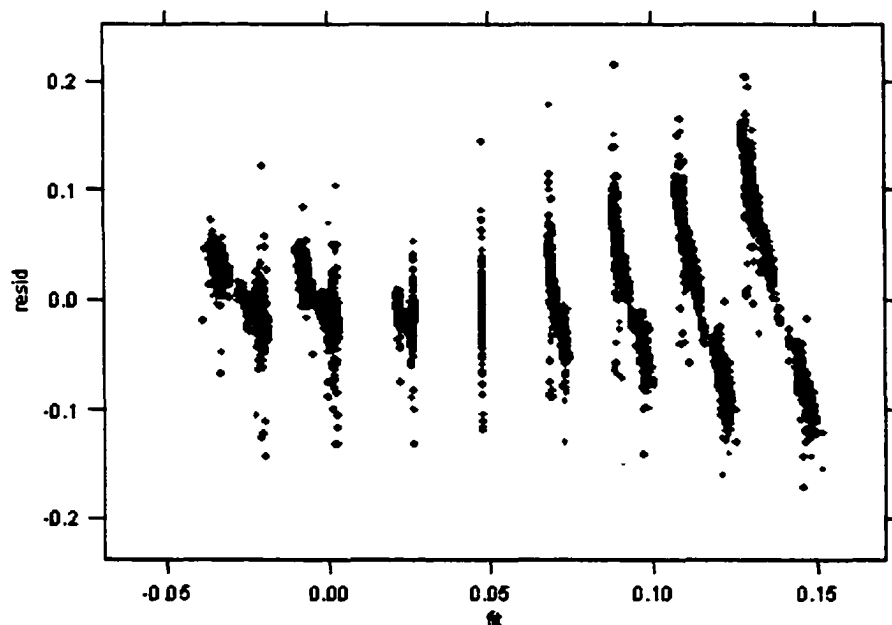


Figure 44. Multiplicative Model - Residual vs. Fit Plot

This plot shows that the residuals are fairly evenly distributed above and below the zero-line. This indicates that the model type is valid.

The “banding” on this plot is an interesting result of the data. Note that there are eight distinct bands. These correspond to the eight distinct levels at which the elevation explanatory variable was measured. While temperature varies smoothly throughout all possible values, the elevation variable takes on a specific value at the level of each differential pressure sensor port. This explains the banding effect seen in Figure 44.

There is also a slight ‘bugling’ of the data toward the right. This indicates that the residual variance is not uniform. But this can also be explained by the physical nature of the data collection design. The data toward the left of the plot represents the lower floors. Since the two lowest floors are below ground, it should be expected that the air flow would be more restricted than for those floors directly open to the outside environment. This restriction in air movement will compress the variation in the data for the lower levels.

Therefore, from the diagnostics, this multiplicative model appears to be a good fit to the data. From the model report (Fig. 43) we obtain the following equation:

$$P = (4.73372 \times 10^{-2}) + (3.79003 \times 10^{-6})HT \quad (16)$$

Figures 45 through 50 show the comparison of this model to the ASHRAE recommended method and actual observed data.

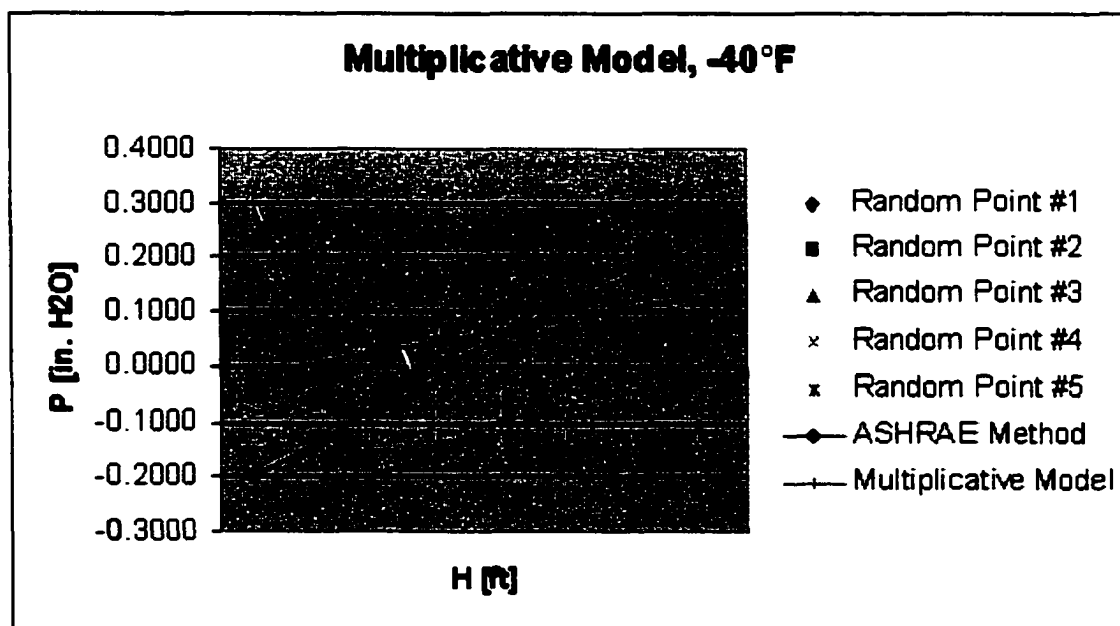


Figure 45. Multiplicative Model Comparison at -40°F

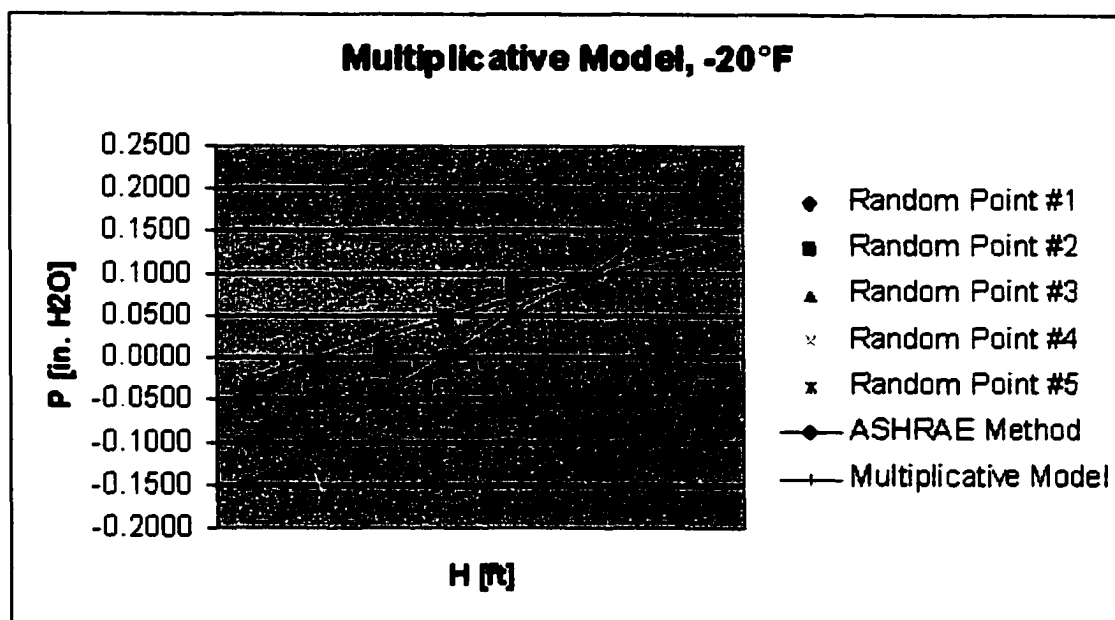


Figure 46. Multiplicative Model Comparison at -20°F

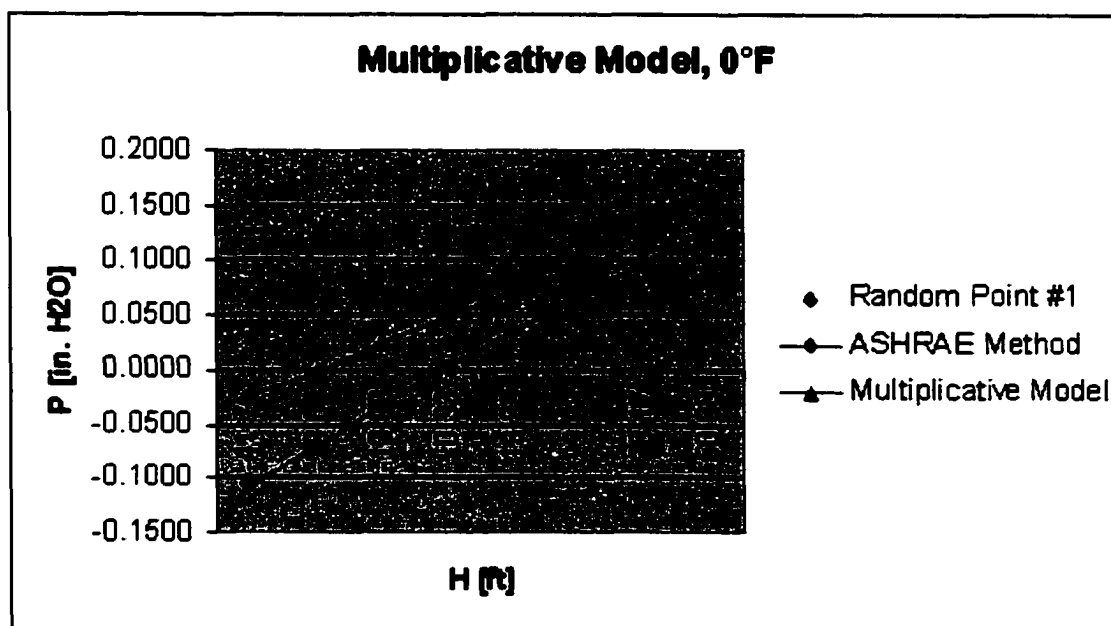


Figure 47. Multiplicative Model Comparison at 0°F

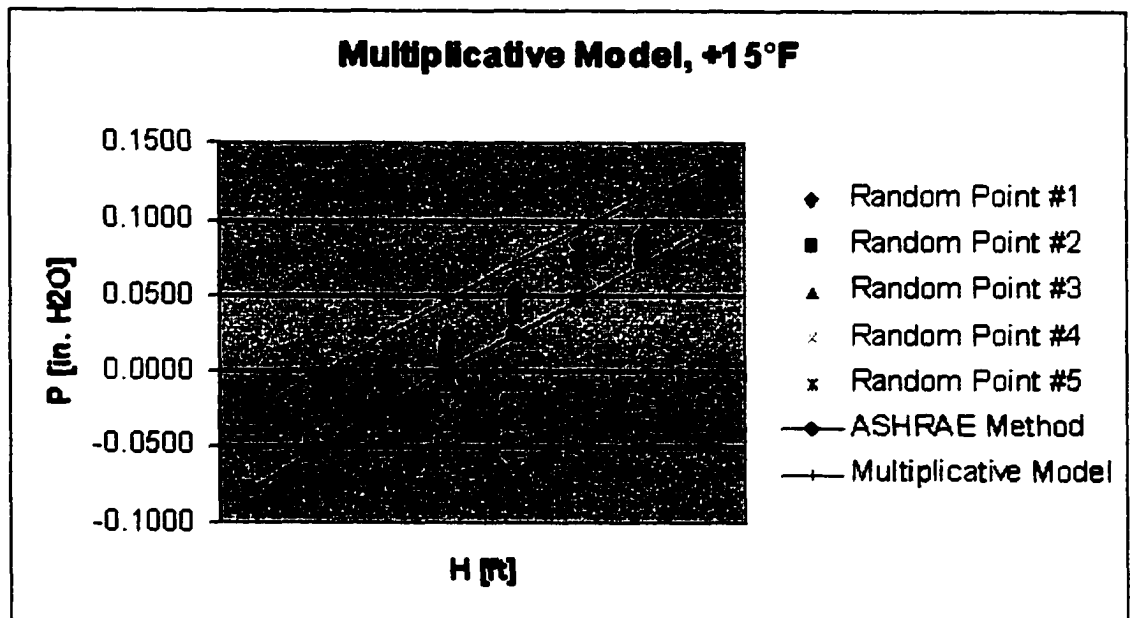


Figure 48. Multiplicative Model Comparison at +15°F

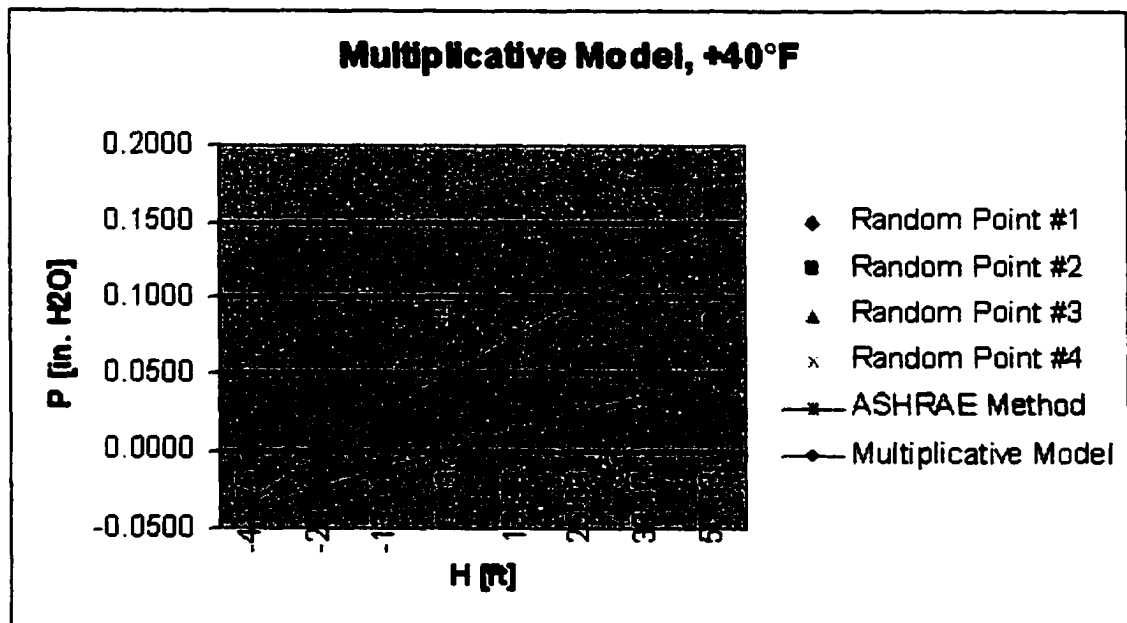


Figure 49. Multiplicative Model Comparison at +40°F

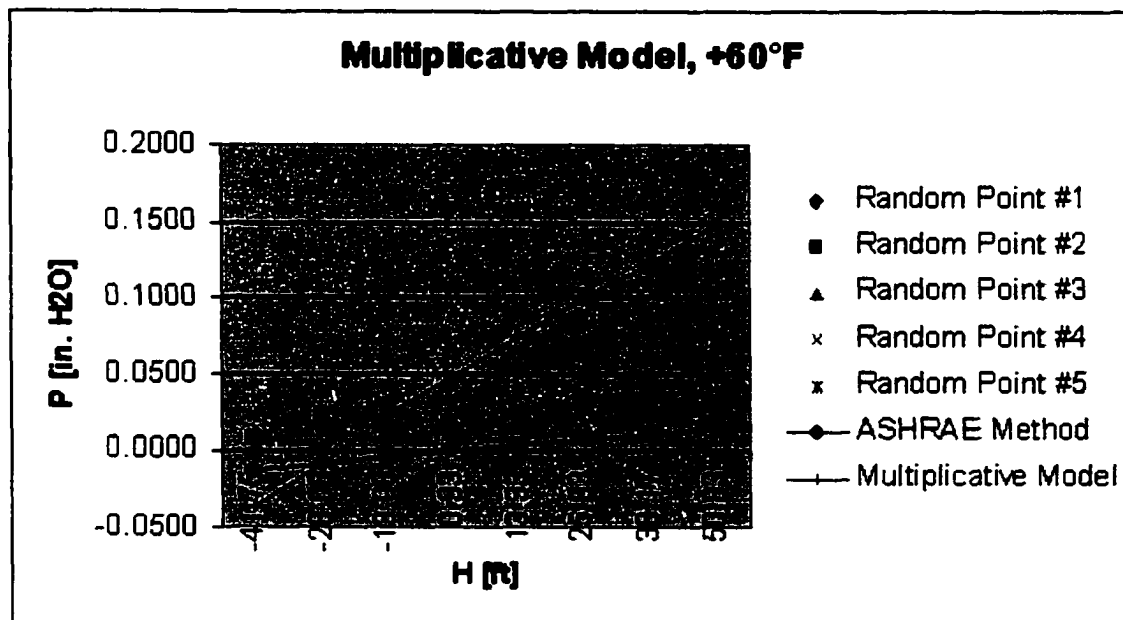


Figure 50. Multiplicative Model Comparison at +60°F

These plots show that the multiplicative model provides a better fit to the data than the ASHRAE recommended method at the lower outside air temperatures for the lower (more negative) stories of the building. However, the multiplicative model tends to underestimate the positive pressures that occur at the upper elevations of the building. The ASHRAE Method tends to provide a more conservative estimate for the median range of temperatures (the 0°F to 40°F range). This would provide a measure of safety in estimating the infiltration load to be offset by the heating system. However, too great an overestimation of infiltration, evidence of which is shown in the colder temperature plots, could result in vastly over-sized heating equipment with its associated higher initial cost and controllability problems. Neither model does a very good job of matching the data at the 60°F outside temperature condition. However, since differential pressures in this temperature range are small, this will probably not be a significant detriment during the design process.

4.4 Nonlinear Inverse Temperature Model

Previous research by Lee et al. (1985) suggests that the differential pressure displays an inverse relationship to the absolute outside air temperature. This would lead to a model of the form shown in Equation 17.

$$P = a + b \left(\frac{H}{T} \right) \quad (17)$$

where: P = differential pressure [in. H₂O]
 a = intercept parameter
 b = slope parameter
 H = elevation from mid-building height [ft]
 T = outside temperature [°R]

Again, with this model, it is imperative that the absolute temperature scale be used to avoid discontinuities in the model due to divisions by zero.

Using the S-Plus integrated development environment to construct a nonlinear model from the dataset yielded the model report shown in Figure 51.

```

*** Nonlinear Regression Model ***

Formula: DP.InH2O ~ b0 + b1 * (Elv.NPL/(OSAT.F + 460))

Parameters:
  Value Std. Error t value
b0 0.0460443 0.000458194 100.491
b1 0.9354750 0.006909230 135.395

Residual standard error: 0.0429259 on 9083 degrees of freedom

Correlation of Parameter Estimates:
  b0
b1 -0.184

```

Figure 51. S-Plus Nonlinear Inverse Temperature Model Report

The standard errors (0.00046 & 0.0069) and t-values (100 & 135) for this model are excellent. But, the residual versus fit plot also needs to be checked to ensure that the assumptions on which the nonlinear model are based were not violated. This plot is shown in Figure 52.

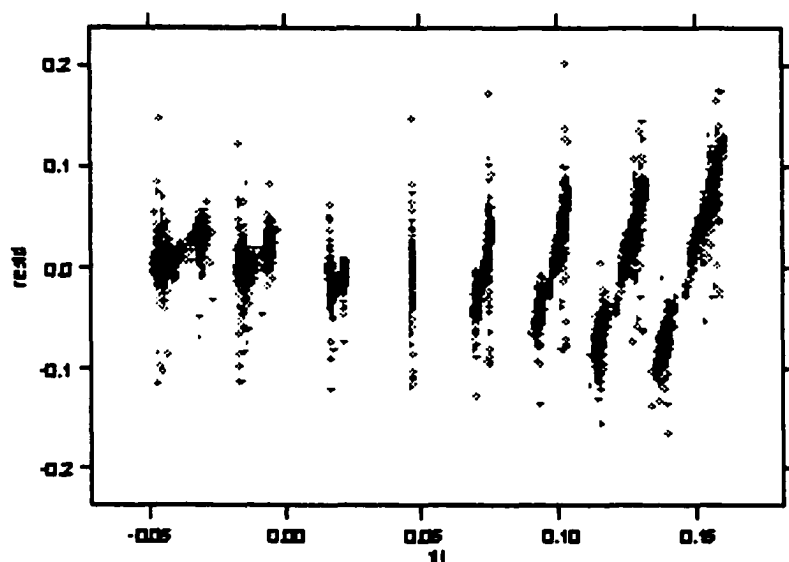


Figure 52. Inverse Temperature Model - Residual vs. Fit Plot

This plot shows a similar banding effect as the multiplicative model. Again, this is caused by the fact that while the temperature varies continuously over its range, the elevation variable is limited to eight distinct values. Thus, the eight data bands. Similar arguments also hold for the difference in residual variance (bugling to the right) although the bugling appears less perceptible than it was for the multiplicative model.

The above diagnostics show that this nonlinear inverse temperature model is the best of the statistical models constructed to this point. The resulting equation for buoyancy effect pressurization is given in Equation (18).

$$P = (0.0460443) + (0.935475) \left(\frac{H}{T} \right) \quad (18)$$

Figures 53 through 58 show the plots for this model compared to the actual observed data and the ASHRAE recommended method.

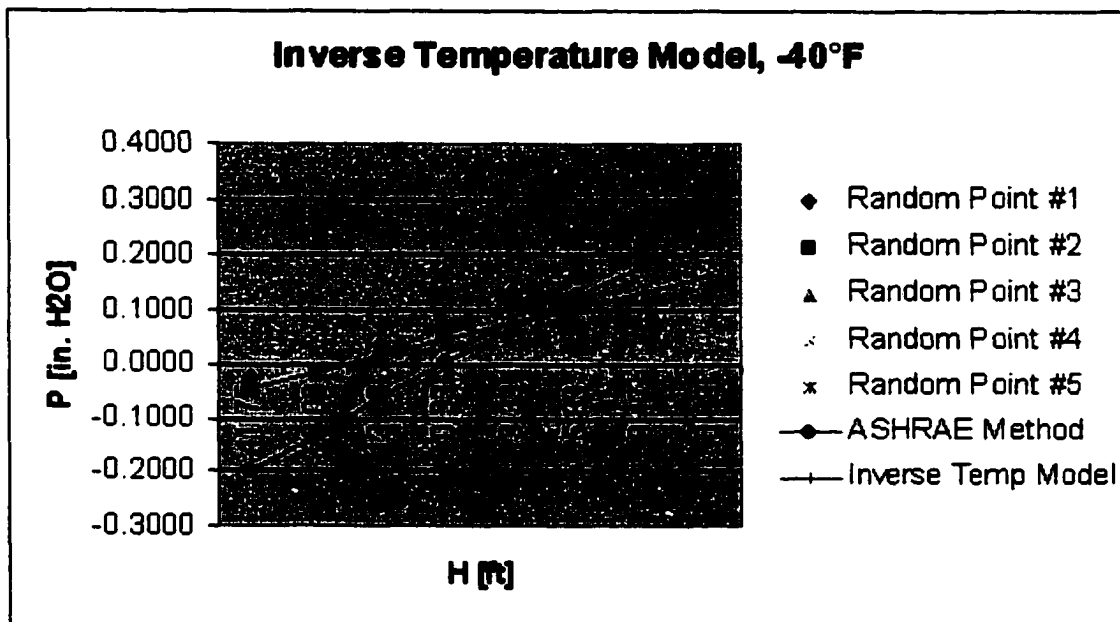


Figure 53. Inverse Temperature Model Comparison at -40°F

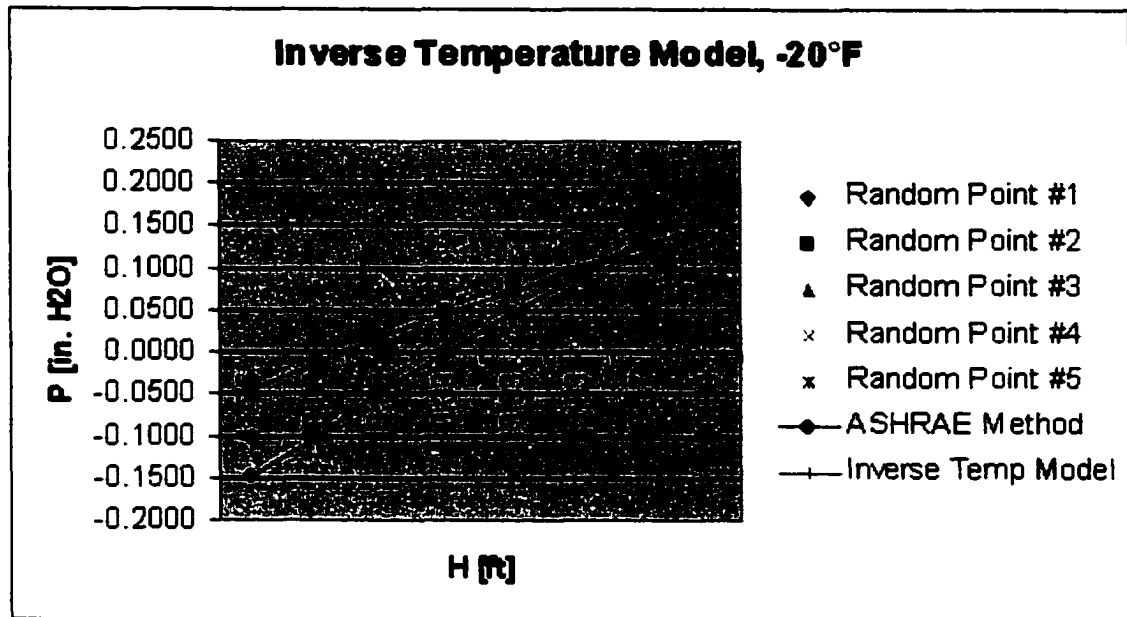


Figure 54. Inverse Temperature Model Comparison at -20°F

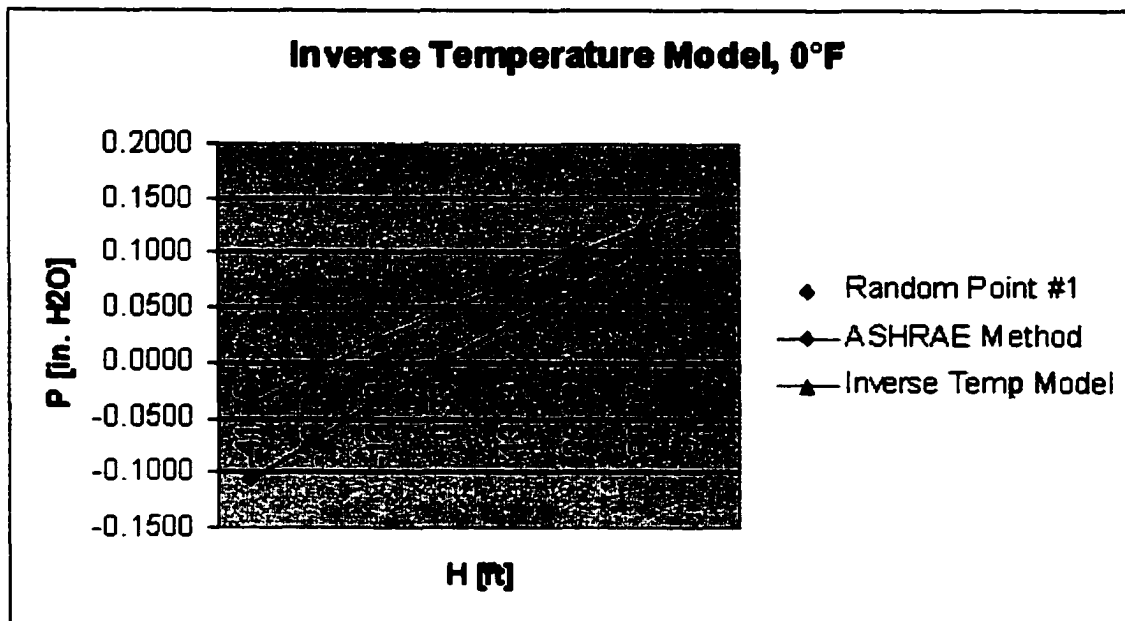


Figure 55. Inverse Temperature Model Comparison at 0°F

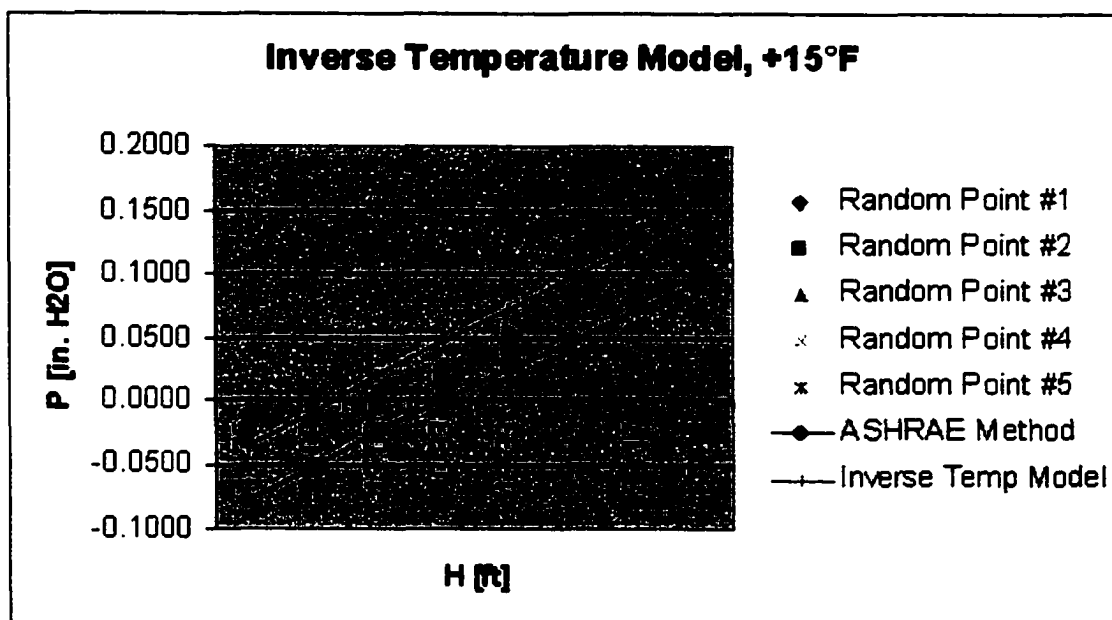


Figure 56. Inverse Temperature Model Comparison at +15°F

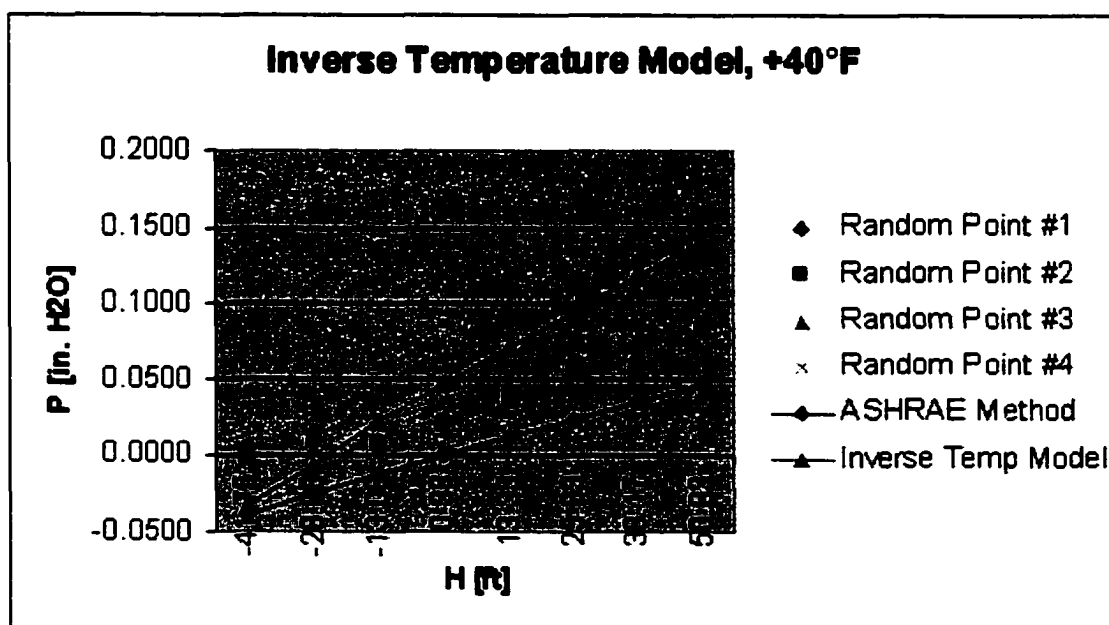


Figure 57. Inverse Temperature Model Comparison at +40°F

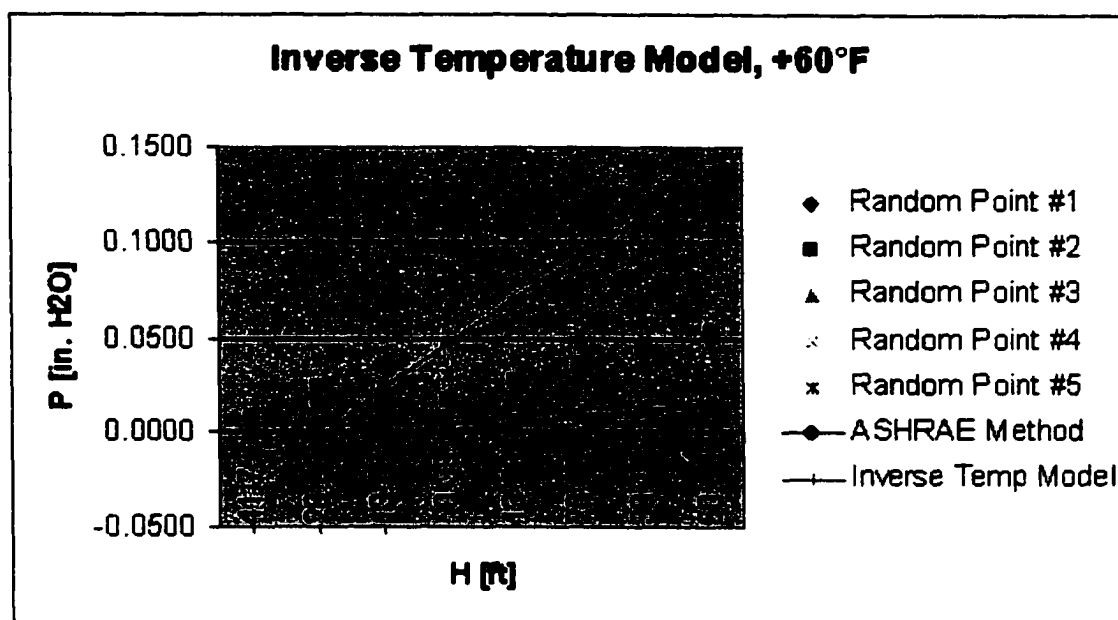


Figure 58. Inverse Temperature Model Comparison at +60°F

This model does a fine job of representing the observed differential pressures up to an outside temperature of around 15°F. It is much closer than the ASHRAE Method at the extreme cold temperatures and lower building levels. At higher temperatures, this model diverges from the observed data at the higher building elevations. However, as explained before, the buoyancy pressurization at higher temperatures are not a critical factor to the sizing of building systems.

4.5 Temperature Ratio Model

The three previously developed statistical models, the simple additive model, the nonlinear multiplicative model, and the nonlinear inverse temperature model, were all good simple statistical models to try to apply to the problem of buoyancy effect pressurization. But they did not account for the physical nature of the relationships between the variables very well. As a result, they all had problems in representing

the data. This was extremely evident at the higher outside air temperatures. The slopes of the lines created by these model equations did not match the observed data.

It can be seen from the comparison plots, that the ASHRAE Method seems to fit the slope of the data better than the simple statistical models created. That is, the slope of the line for the ASHRAE Method seems to parallel the slope of the actual data. However, as can also be seen, the ASHRAE Method results in an estimation of buoyancy pressurization that is significantly lower than observed from the actual building data. This offsetting of the line from the actual data was surmised to be caused by the problem in identifying the NPL for the test building. The ASHRAE Method plots were constructed based on the NPL being located at the building mid-height. As discussed earlier, this is often the assumption made, especially in new building design, when there is no better way to establish the location of the NPL. However, variations of envelope opening distribution over the vertical height of the building and equipment pressurization effects often move the NPL away from the idealized mid-height location.

Therefore, a statistical model which more closely resembles the ASHRAE Method as given in Eq. (7) may provide better results. One form for this model is:

$$P = a + bH\tau \quad (19)$$

where: P = differential pressure [in. H₂O]
 a = intercept parameter
 b = slope parameter
 H = elevation from mid-building height [ft]
 $\tau = \frac{T_i - T_o}{T_o}$; all T's in °R

In this formulation, the intercept parameter, a , is intended to adjust for the bias created by assuming that the NPL is at the building mid-height. The slope parameter, b , accounts for the gravimetric effects. It is a combination of the density and acceleration due to gravity that is found in the ASHRAE Method. The temperature ratio term, τ , is the same as the term in Eq. (7).

This nonlinear model was constructed and run against the dataset using the S-Plus integrated development environment. Figure 59 shows the resulting model report.

```

1799.63 : 0.01 0.1
6.19464 : 0.0468462 0.0136469

*** Nonlinear Regression Model ***

Formula: DP.InH2O ~ b0 + b1 * Elv.NPL * tau

Parameters:
      Value   Std. Error t value
b0 0.0468462 0.0002770540 169.087
b1 0.0136469 0.0000533694 255.706

Residual standard error: 0.0261109 on 9086 degrees of freedom

Correlation of Parameter Estimates:
      b0
b1 -0.151

```

Figure 59. S-Plus Temperature Ratio Model Report

The standard error values and t-values in this report indicate a ‘good’ model. But the residual vs. fit plot (Figure 60) show a distinct concave curvature rather than an even distribution of the residuals above and below the zero line. This indicates that a nonlinear model of this form is not strictly appropriate for the data. However, as was the case with the simple additive model, the residual range is very small, roughly between +0.1 and -0.1, so it still may be a good idea to see how this model compares to the data. From the report (Fig. 59), the fitted model is:

$$P = 0.0468462 + 0.0136469H\tau \quad (20)$$

Figures 60 through 65 show the comparison of this model to the ASHRAE Method and the actual data.

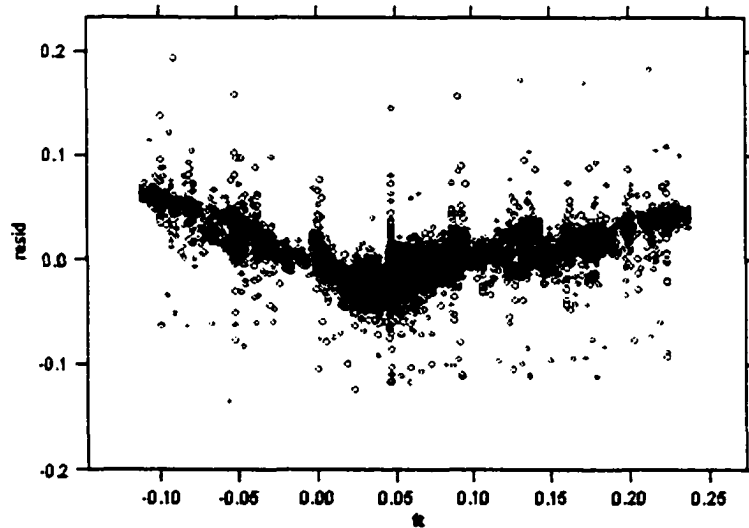


Figure 60. Temperature Ratio Model – Residual vs. Fit Plot

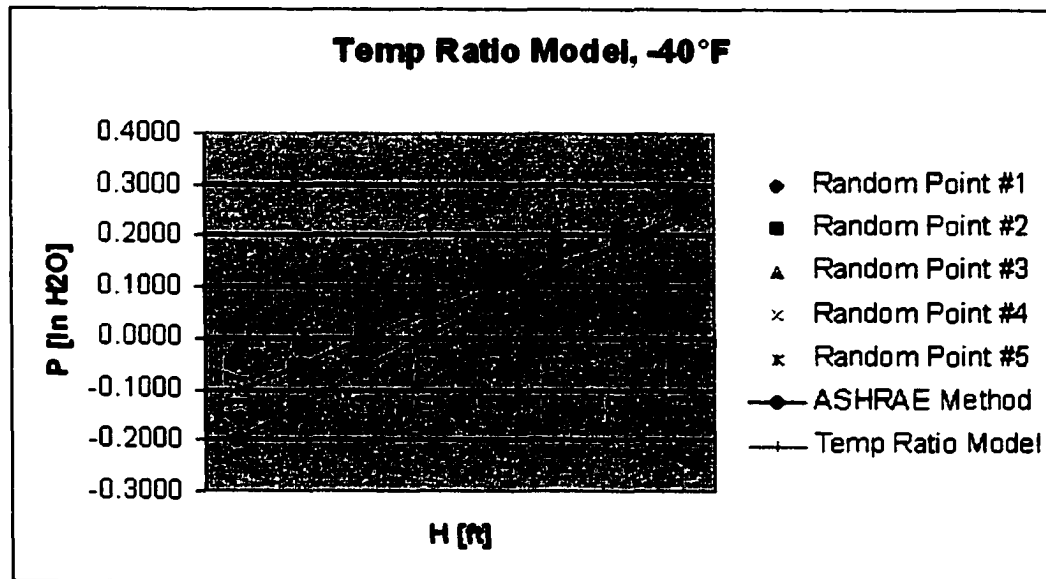


Figure 61. Temperature Ratio Model Comparison at -40°F

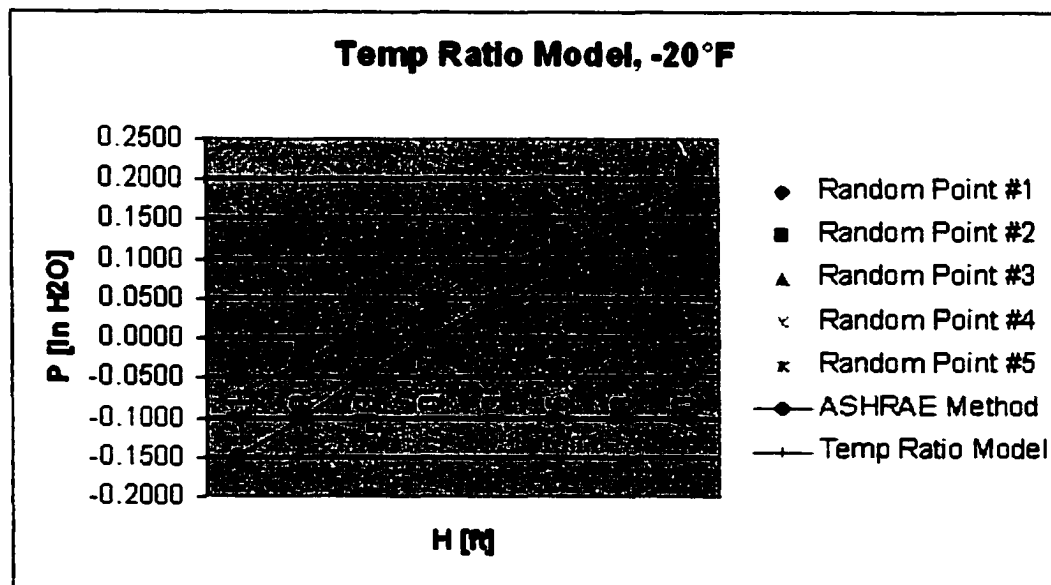


Figure 62. Temperature Ratio Model Comparison at -20°F

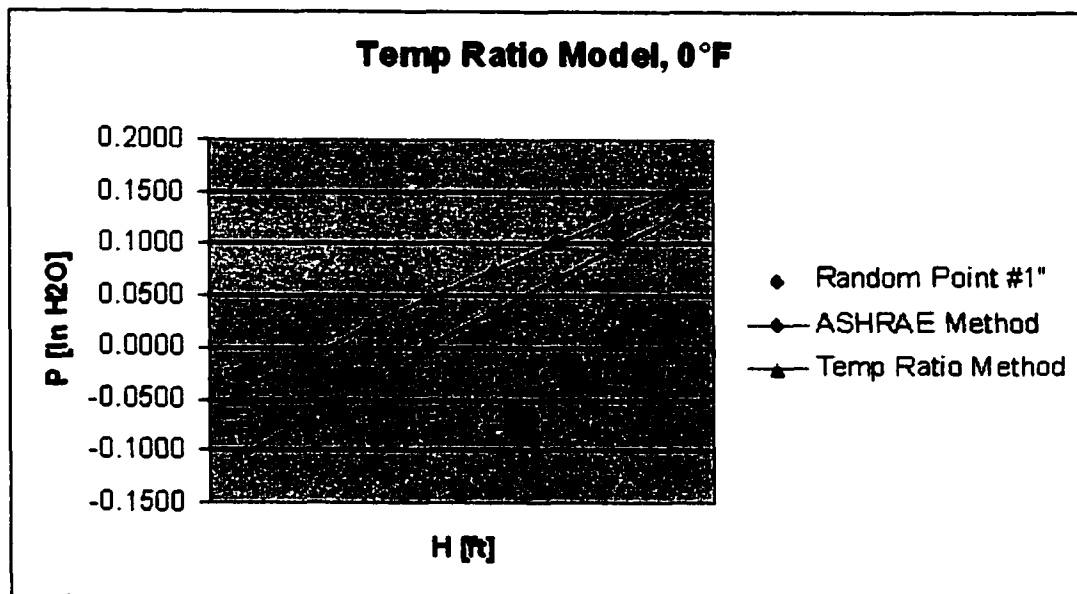


Figure 63. Temperature Ratio Model Comparison at 0°F

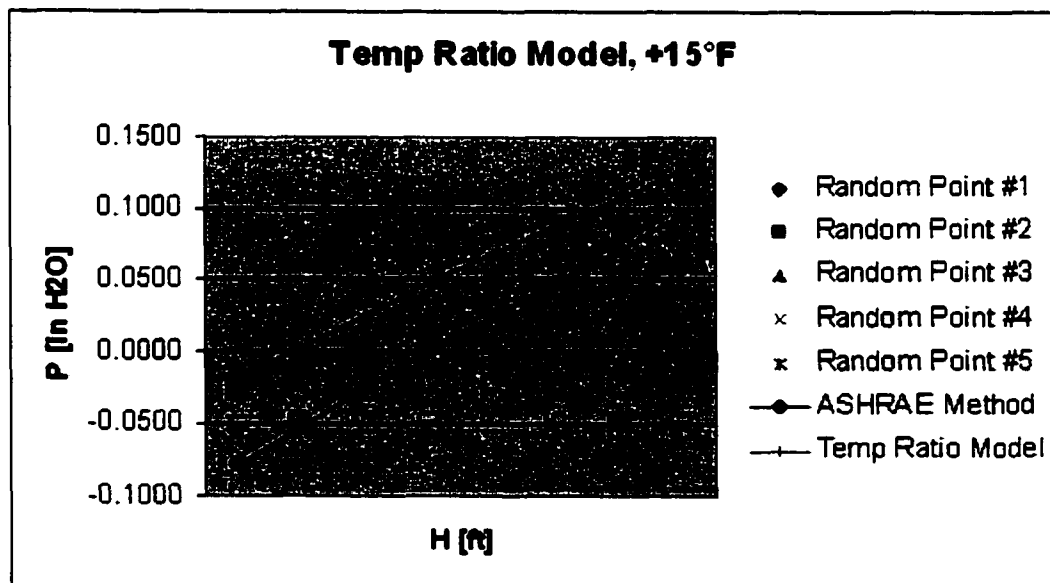


Figure 64. Temperature Ratio Model Comparison at +15°F

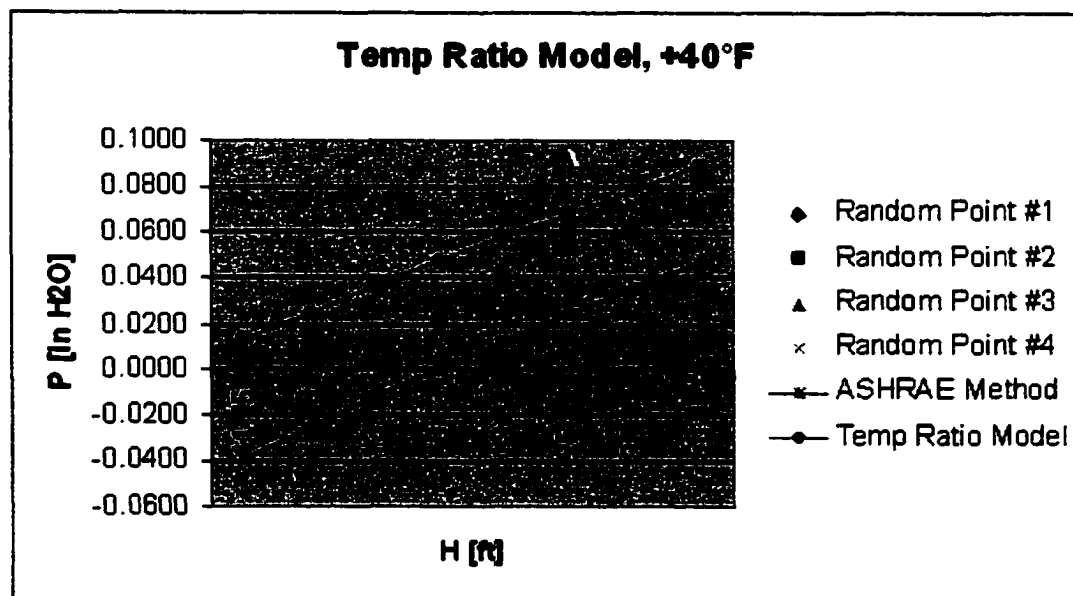


Figure 65. Temperature Ratio Model Comparison at +40°F

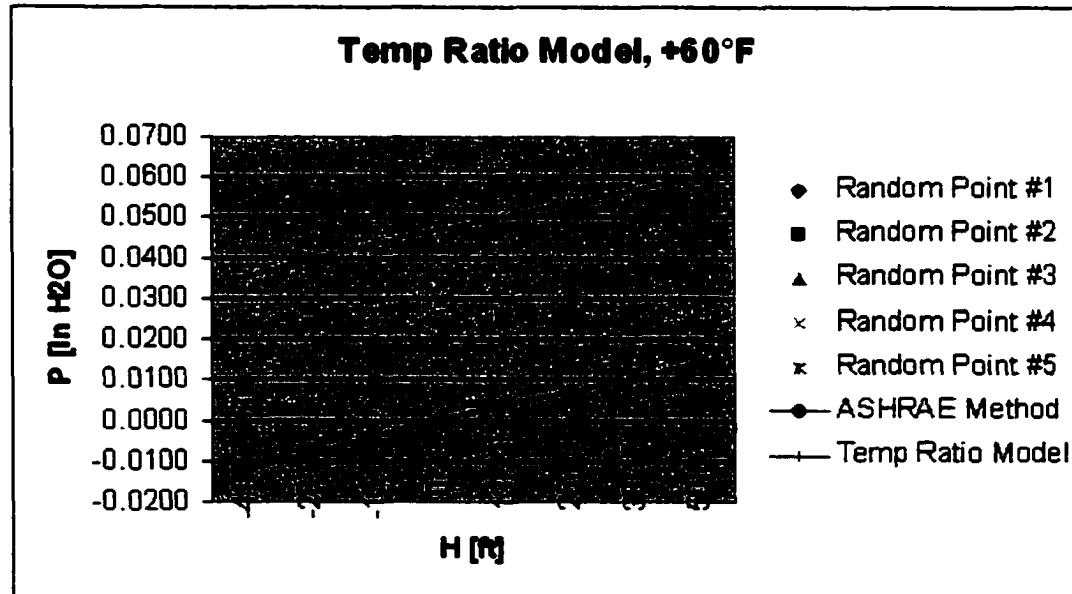


Figure 66. Temperature Ratio Model Comparison at +60°F

The plots show that this model, although not strictly correct from a statistical standpoint, does a fairly good job of representing the data. The slopes are much closer to matching the general slope of the observed data than the previous models although there is still divergence, especially at the higher temperatures. Also, this model, like the previous models, tends to overestimate the pressure differential at higher outside air temperatures.

These results suggest that a problem still remains in the inability to locate the NPL over the range of outside air temperatures encountered. The fact that the fit gets worse as the outside air temperature increases suggests that the location of the NPL may be a function of the outside air temperature. As discussed in Section 1, this should not be the case. But the plot of the NPL location from the observed data (Fig. 7) suggests that there may be a weak functional relation between NPL and temperature. The next model will attempt to incorporate this relation.

4.6 Additive Temperature Ratio Model

To account for a temperature relation in the location of the NPL, an additive temperature ratio model was constructed.

$$P = a\tau + bH\tau \quad (21)$$

where: P = differential pressure [in. H₂O]
 a = intercept parameter
 b = slope parameter
 H = elevation from mid-building height [ft]
 $\tau = \frac{T_i - T_o}{T_o}$; all T's in °R

In this model, the intercept term is multiplied by the temperature ratio term, τ , to account for a functional relation between the temperature and the location of the NPL. The slope parameter, b , continues to account for the gravimetric effects as it did in the previous model and the elevation is referenced to the mid-building height rather than the location of the NPL. The resultant S-Plus report for this model run against the dataset is shown in Figure 67.

```

24.5243 : 0.05 0.01
4.85303 : 0.289058 0.0132691

*** Nonlinear Regression Model ***

Formula: DP.InH2O ~ b0 * tau + b1 * Elev.NPL * tau

Parameters:
      Value   Std. Error t value
b0 0.2890580 0.0014635900 197.499
b1 0.0132691 0.0000475198 279.233

Residual standard error: 0.0231111 on 9086 degrees of freedom

Correlation of Parameter Estimates:
      b0
b1 -0.185

```

Figure 67. S-Plus Additive Temperature Ratio Model Report

The standard error and t-values shown in this report indicate that this model is a 'good' fit for the data. The Residual vs. Fit plot for this model (Fig. 68) also indicates a good model fit. The non-random pattern seen in the previous model is gone and the residuals are evenly distributed about the zero line with a fairly even variance throughout the data range.

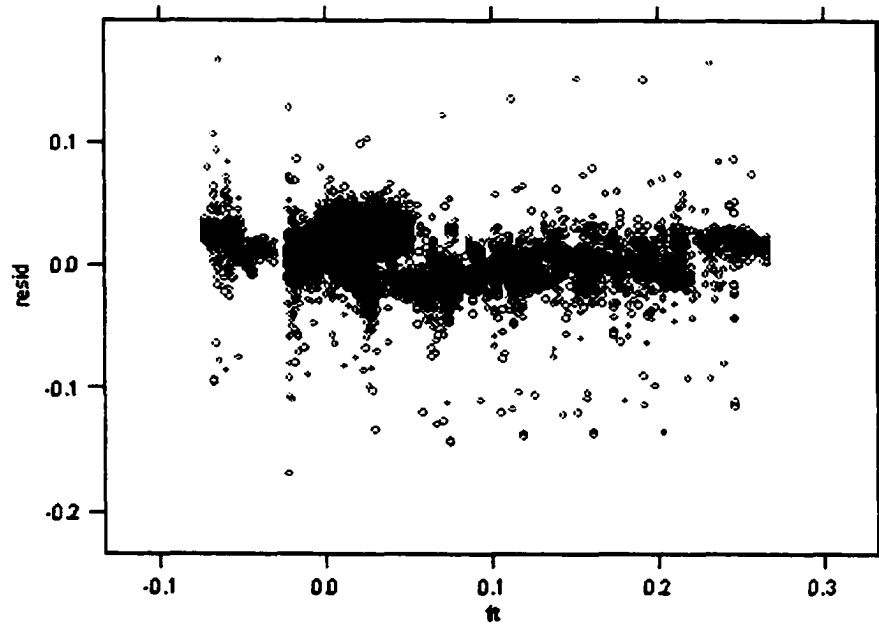


Figure 68. Additive Temperature Ratio Model – Residual vs. Fit Plot

Therefore, the additive temperature ratio model represented by Equation 22 was compared to the actual data and the ASHRAE Method in Figures 69 through 74.

$$P = 0.289058\tau + 0.0132691H\tau \quad (22)$$

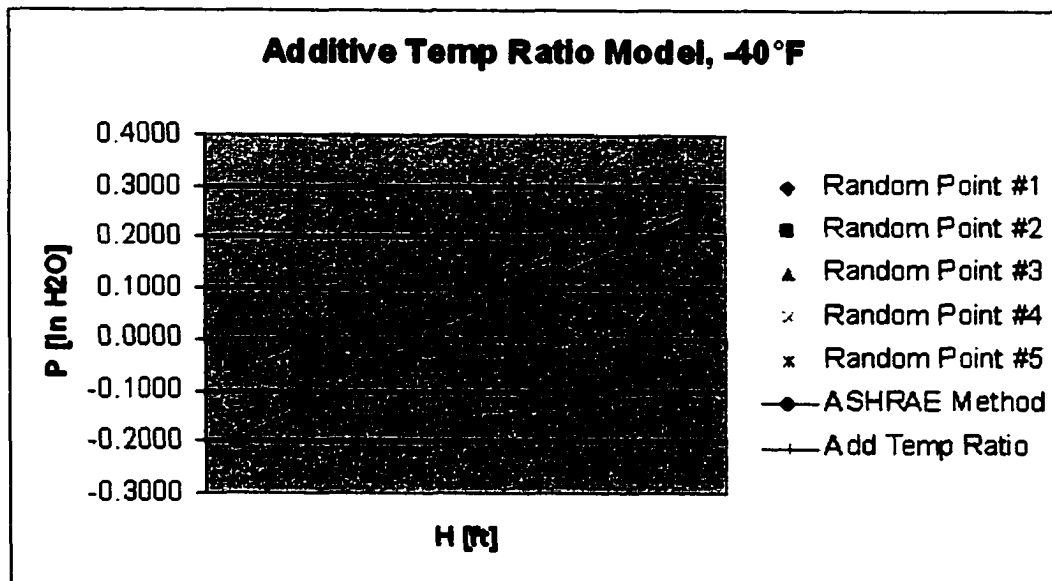


Figure 69. Additive Temperature Ratio Model Comparison at -40°F

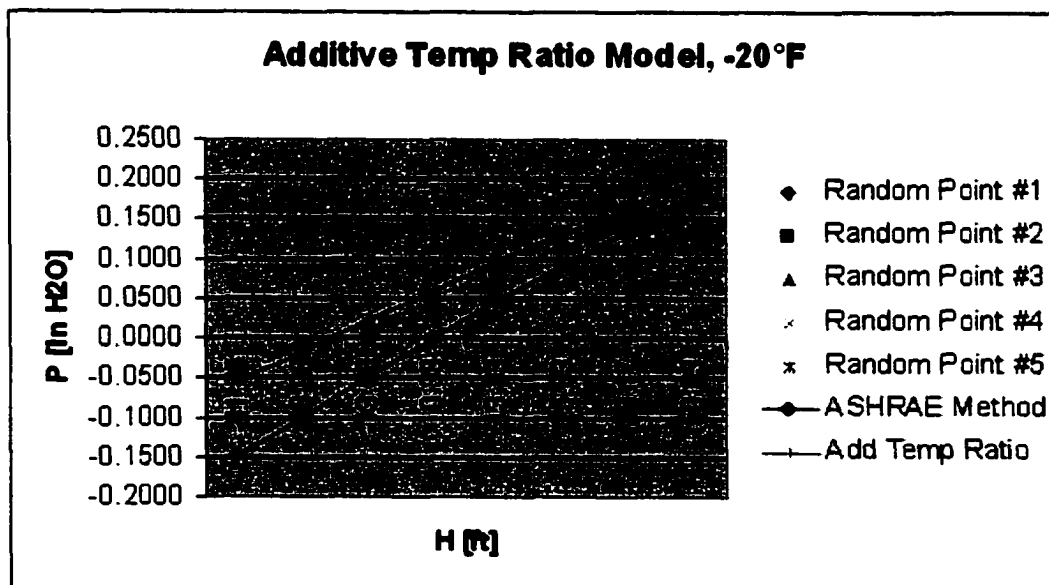


Figure 70. Additive Temperature Ratio Model Comparison at -20°F

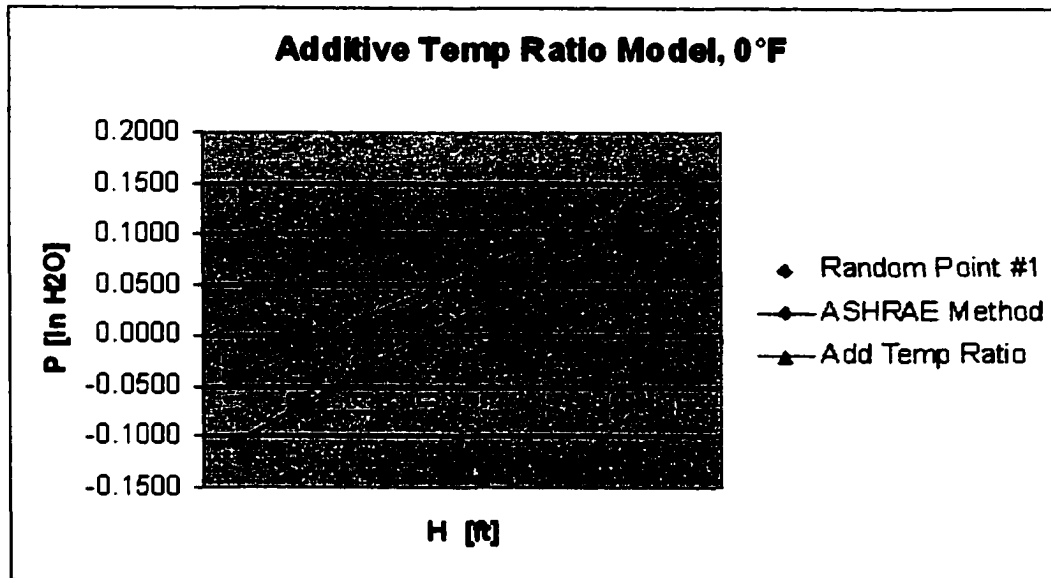


Figure 71. Additive Temperature Ratio Model Comparison at 0°F

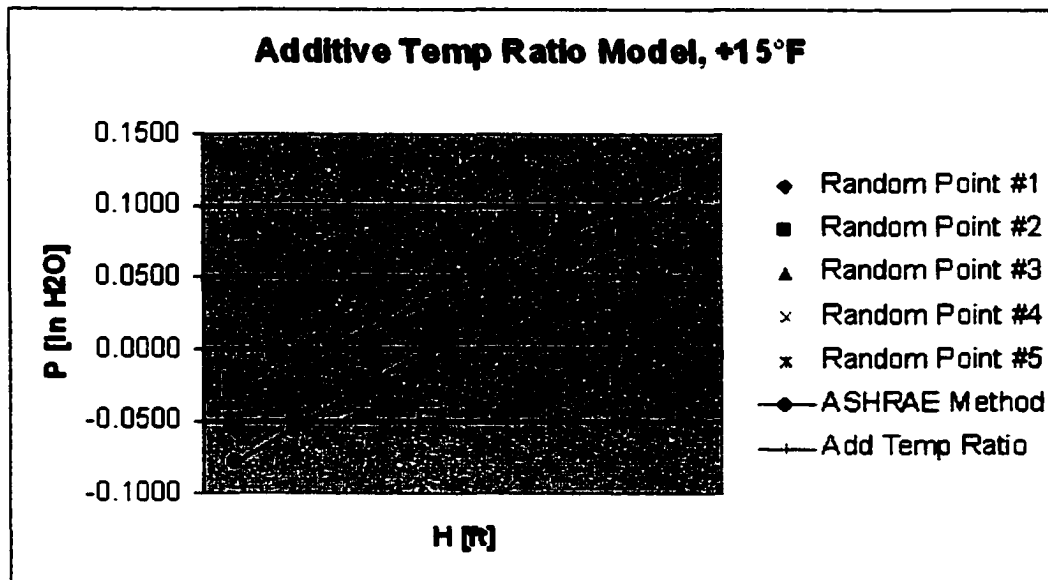


Figure 72. Additive Temperature Ratio Model Comparison at +15°F

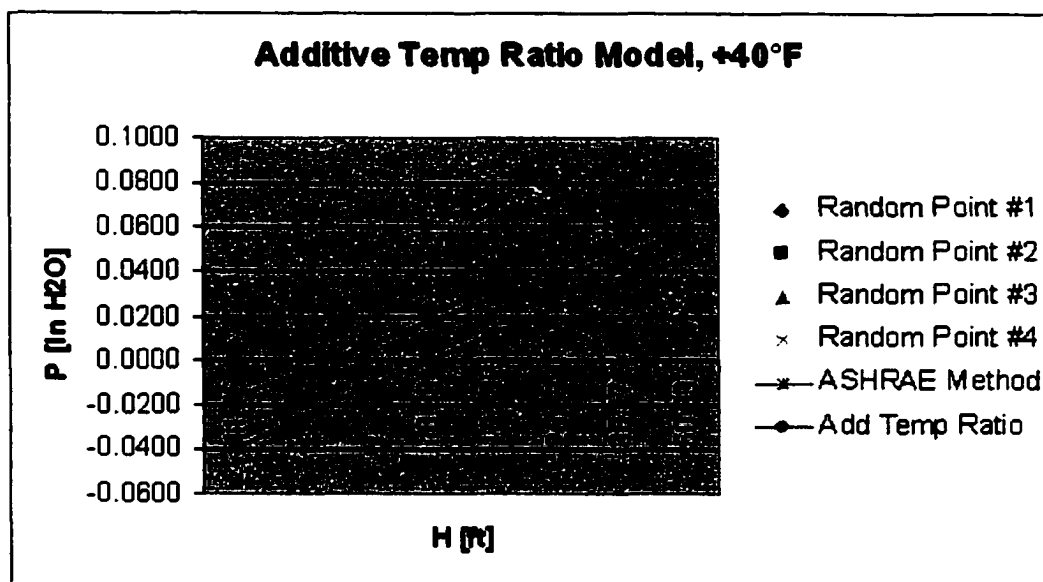


Figure 73. Additive Temperature Ratio Model Comparison at +40°F

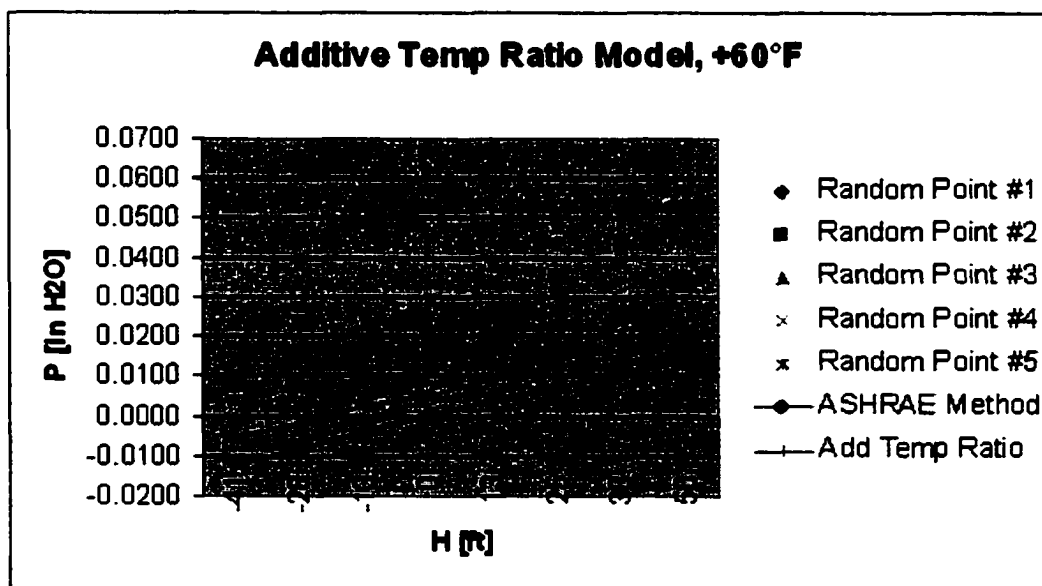


Figure 74. Additive Temperature Ratio Model Comparison at +60°F

The plots show that the slope of the line for this model is generally close to the trend shown by the actual data. It also closely approximates the slope of the line given by

the ASHRAE Method. However, the predictions from this model are significantly offset below the actual data which was a problem originally observed with the ASHRAE Method. But a consistent offset below the observed data can be handled by introducing an independent intercept parameter to the model.

4.7 Additive Temperature Ratio with Intercept Model

The plots for the last model suggest that the introduction of an intercept term to the model might help to adjust the offset so that the model more closely represents the observed data. In essence, this intercept term is simply an adjustment to account for the difference between the actual location of the NPL and the mid-height reference used for the elevation variable in the model. This model would take the form shown in Eq. (23):

$$P = a + b\tau + cH\tau \quad (23)$$

where: P = differential pressure [in. H₂O]
 a = intercept parameter
 b = NPL temperature relation parameter
 c = slope parameter
 H = elevation from mid-building height [ft]
 $\tau = \frac{T_i - T_o}{T_o}$; all T's in °R

A nonlinear model of this form was built in S-Plus and fit to the data. The report, shown in Figure 75, displays good standard error and t-values for this model. The Residual vs. Fit plot (Fig. 76) indicates that the model is statistically valid.

```

9.06244 : 0.05 0.01 0.01
3.34144 : 0.022188 0.181938 0.0132691

*** Nonlinear Regression Model ***

Formula: DP.InH2O ~ b0 + b1 * tau + b2 * Elv.NPL * tau

Parameters:
      Value  Std. Error  t value
b0 0.0221880 0.0003461030  64.1082
b1 0.1819380 0.0020656700  88.0770
b2 0.0132691 0.0000394329 336.4990

Residual standard error: 0.019178 on 9085 degrees of freedom

Correlation of Parameter Estimates:
      b0      b1
b1 -8.09e-001
b2  2.77e-009 -1.09e-001

```

Figure 75. S-Plus Additive Temperature Ratio w/Intercept Model Report

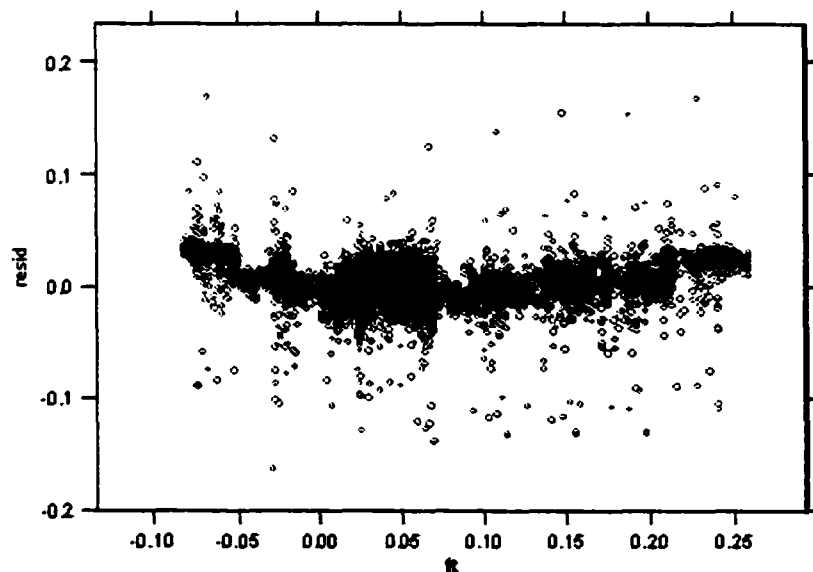


Figure 76. Additive Temperature Ratio w/Intercept Model – Residual vs. Fit Plot

From the information in the model report (Fig. 75), the equation for this fitted model is:

$$P = 0.022188 + 0.181938\tau + 0.0132691H\tau \quad (24)$$

Figures 77 through 82 show the comparison plots for this model.

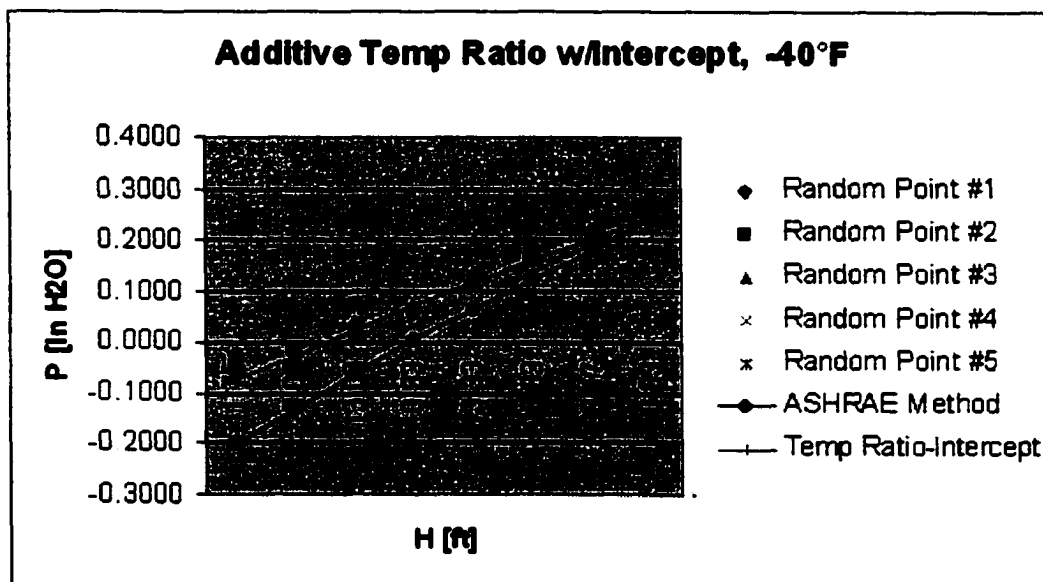


Figure 77. Additive Temperature Ratio w/Intercept Model Comparison at -40°F

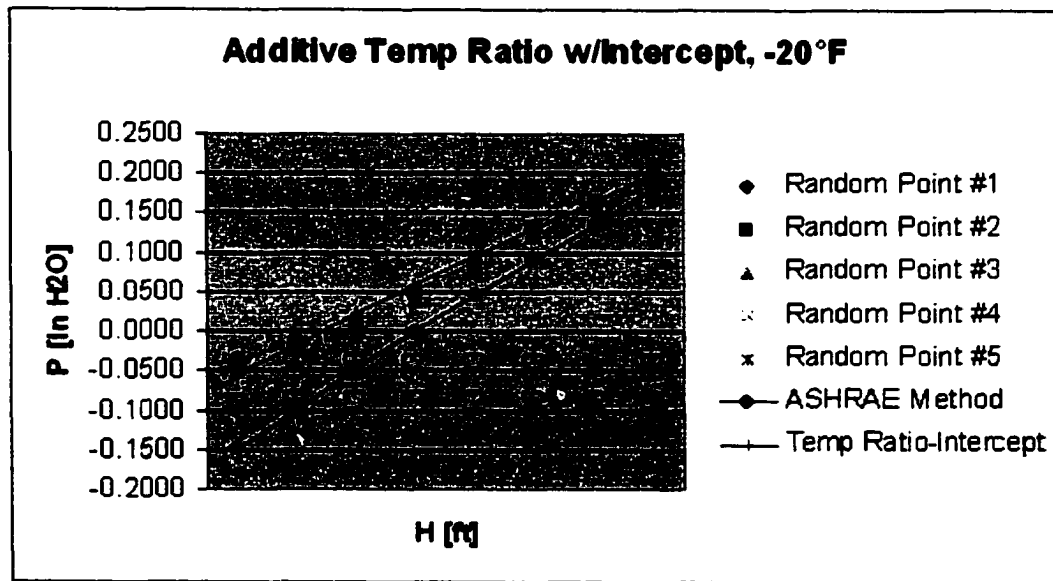


Figure 78. Additive Temperature Ratio w/Intercept Model Comparison at -20°F

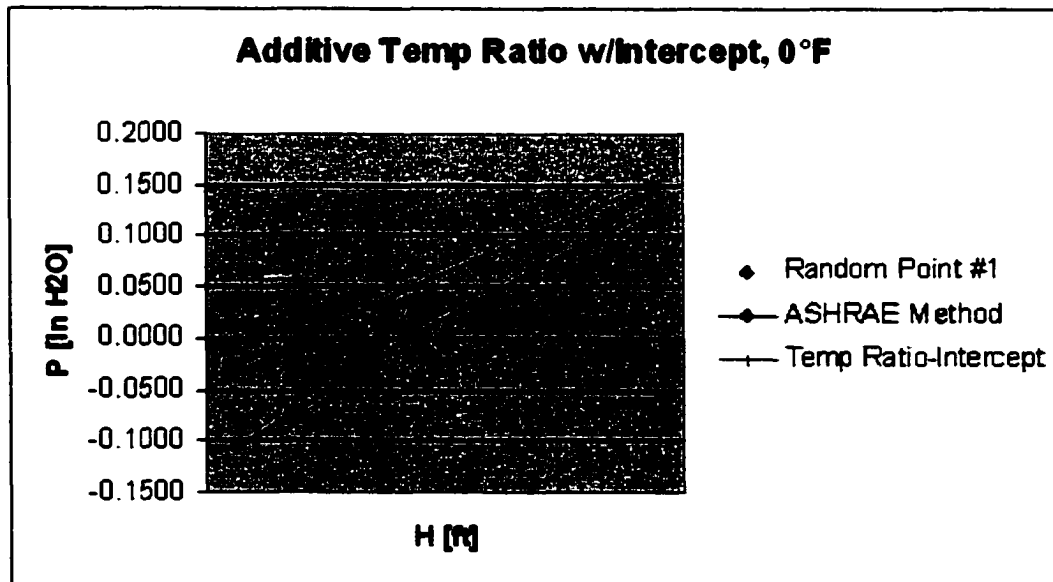


Figure 79. Additive Temperature Ratio w/Intercept Model Comparison at 0°F

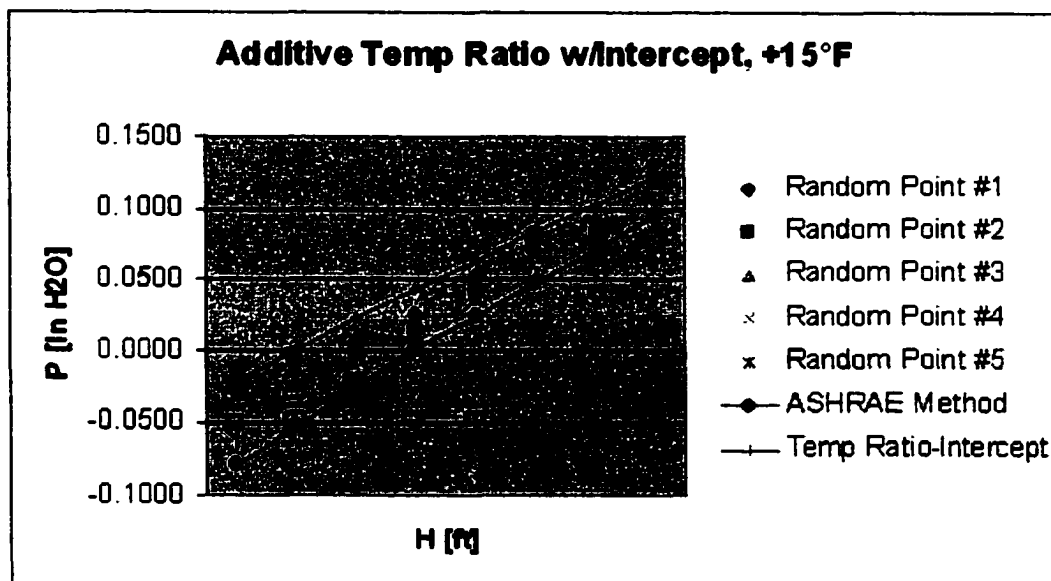


Figure 80. Additive Temperature Ratio w/Intercept Model Comparison at +15°F

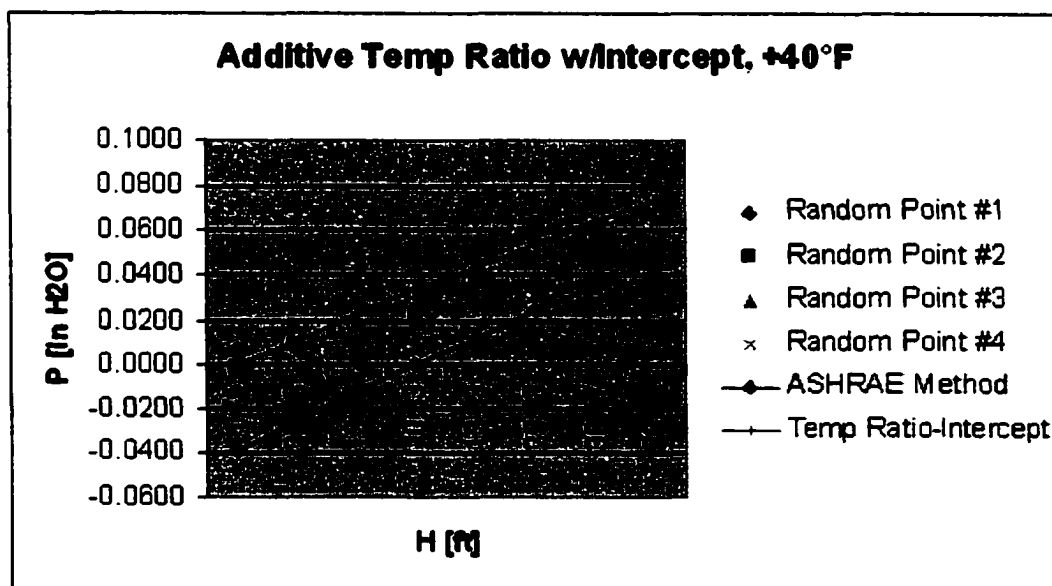


Figure 81. Additive Temperature Ratio w/Intercept Model Comparison at +40°F

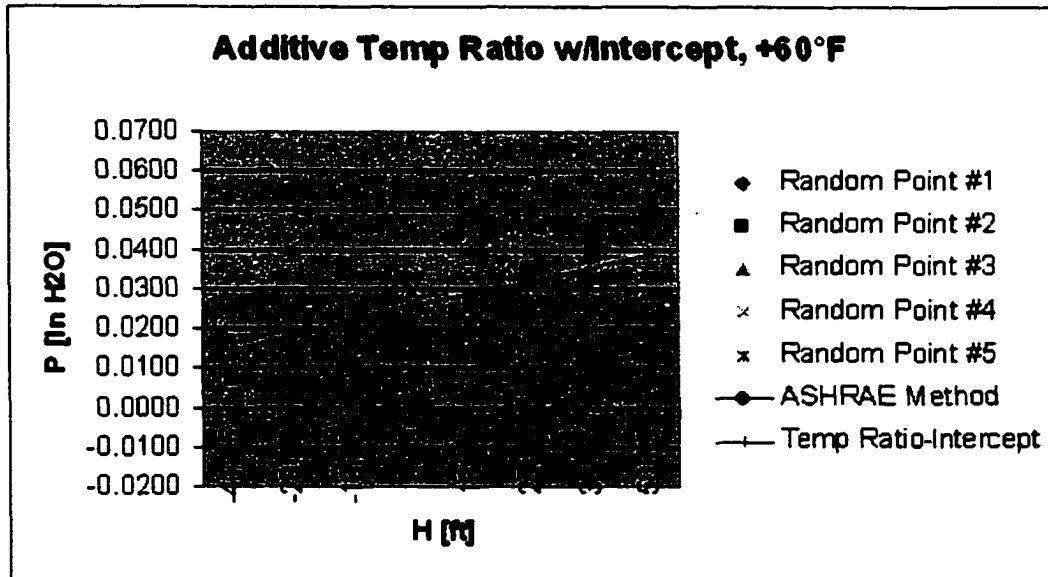


Figure 82. Additive Temperature Ratio w/Intercept Model Comparison at +60°F

The plots show this model does an excellent job in representing the data over the entire range of outside temperatures. The slope of the model line closely approximates the slope of the ASHRAE Method and also the trend of the actual observed data. The offset present in the previous models has been accounted for by the intercept term and the model plot is a good fit for the data at all temperatures.

5. Conclusions

5.1 Shortcomings of ASHRAE and Other Previous Methods

The comparison of the data collected from the test building to the buoyancy pressurization predicted by the ASHRAE Method reveals that the ASHRAE Method, Eq. (7), tends to significantly overestimate the negative pressure gradients that will exist across the envelope below the neutral pressure level at extremely cold outside air temperatures. Some of the observed difference can be attributed to the fact that the HVAC system was introducing outside air ventilation during the data collection period and, thus, equipment pressurization effects were also present. Equipment effect pressurization, as discussed in Section 1, tends to displace the neutral pressure level from the mid-height of the building. Therefore, a better explanation of the ASHRAE Method shortcomings is the problem with properly identifying the NPL and the fact that the NPL does not remain in the same location over all environmental and building conditions.

Locating the NPL in a building is difficult due to all of the considerations that affect the location. The data collected shows that the location moves due to outside temperature. It is also dependent on the location, type, and distribution of openings in the external building envelope and the air flow pathways vertically within the building. Accounting for these factors is difficult in an existing building. It is even more difficult for a new building when only the plans are available and the quality of construction, and thus air flow pathways, can only be estimated. The requirement to know the location of the NPL to determine buoyancy effect pressurization is a major problem with the ASHRAE Method. The models developed in this research avoid this problem by referencing building elevation to the mid-height elevation rather than the location of the NPL.

The ASHRAE Fundamentals Handbook does state that the differential pressure predictions resulting from the use of Eq. (7) are a worst case prediction. That

assertion is definitely borne out by the data collected in this research. However, extremely large overestimation of building negative pressure gradients can lead to over-sizing of building and zone heating equipment. If the zone heating equipment is over-sized to account for an infiltration load that was overestimated, the temperature in the space will be more likely to “swing” about the space setpoint temperature. This is especially true at partial load (off-peak) conditions. That is, times when the outside air temperature is not as cold as the design temperature. As the temperature in the space drops below setpoint, the HVAC control system will provide heat to the space. However, if the equipment is over-sized, it will tend to supply more heat than is necessary. The temperature will then swing above setpoint and the heat will cycle off. This instability in space temperature can continue with the system never quite managing to attain setpoint conditions. This can cause early failure due to repeated cycling of system components. It also causes occupant discomfort as the space temperature cycles rather than stabilizing at the desired setpoint.

The observed data should also dispel the notion that the outside air ventilation brought in by the HVAC system to meet building code requirements can positively pressurize the entire building, thus eliminating the need to account for infiltration loads in system design. Over six percent excess outside air was being introduced to the test building during the data logging periods. Still, significant negative pressure gradients existed at the lower levels during the heating season. The fact that the original building design did not consider this infiltration load is what caused the fire sprinkler system to freeze and damage the building. This was one of the original factors that led to this research effort.

5.2 Models Developed in this Research

Of the new models developed in this research, the additive temperature ratio with intercept model, Eq. (24), is the best. Predictions from this model do an excellent job of matching the observed data at all temperature ranges. To some extent, this should

be expected since the model is based on the observed data. More will be said about this in the Recommendations section of this dissertation. The major advantage of using this model during building/system design is that the location of the neutral pressure level is not required. The only required parameters are the inside and outside temperatures and the building's mid-height elevation. All of these parameters are readily obtainable from location and design sources.

This research reinforces the fact that the interaction between a building and its physical environment is extremely complex. While models can simplify analysis of certain design aspects, they also tend to introduce errors from reality due to the assumptions made in constructing the model. This research provides at least one more tool that can be used during building design to try to accurately predict building pressurization due to buoyancy effect.

6. Recommendations

This first recommendation is to make the Additive Temperature Ratio with Intercept Model more robust. The nonlinear statistical fit done for this dissertation was based on data from a single building. Data needs to be collected from many more buildings exposed to extremely cold temperatures to ensure that the model parameters provide good differential pressures for a general building exposed to the extreme environment.

The buildings from which the additional data is collected should also vary in height. This will strengthen the relation of the prediction to the explanatory elevation variable.

Buildings for future study should also be totally above ground. The lower two levels for this dissertation were below grade. This caused several potential problems.

The lower two levels were only exposed to the outside air temperature in the vicinity of the emergency stairwell fire exits. At times the temperature in the stairwell could be higher or lower than the ambient outside air temperature. Even though the stairwell was open to the environment, the temperature could be warmer than the general outside air temperature due to opening of the two lower level doors admitting warm building air into the space. Also, heat transfer from the surrounding ground, which is warmer than the outside air, would tend to make the temperature in the stairwell warmer than the ambient outside air. Conversely, after an extreme outside cold temperature period, cold air would be trapped in the stairwell. Since this air was colder, thus denser, than the ambient outside air, it tended to be trapped in the stairwell until flushed out by opening a door into the stairwell or until the heat transfer from the surrounding ground caused the trapped air to warm.

Since these levels were below grade, they had no windows. This means that the flow pathways were fewer than for those levels above grade that had windows. However, the foundation's walls below grade in the test building are known to have structural cracks that would provide pathways for air flow that are not present in the walls above grade. The air flow pathways below grade are more constricted than those above grade since the air moving through the below grade paths must also migrate through the earth surrounding the foundation walls.

All of these factors appear to have caused a slight decrease in the slope of the pressurization line for the below grade levels that can be observed in all of the data plots.

The more robust model should also include one or two more explanatory variables or factors. These would be some sort of rating system for the building. One factor could rate the condition of the envelope. In essence, this would be a weighting factor describing the quantity, size, and shape of the cracks, joints, and holes in the envelope. A second factor may weight the number of window and door openings and their distribution within the envelope. It is easy to presume that a reinforce concrete bunker with a single fire-sealed door should present fewer air flow paths across its envelope than a curtain walled office building with glass walls making up half of its exterior skin and many access doors at several levels.

It is also recommended that the test buildings be ones that allow data to be collected when the outside air ventilation system is not introducing equipment pressurization effects. This way, any pressure gradients can be solely attributed to the buoyancy effect. This assumes that wind effect is removed in a similar manner as was done with this research. Ideally, the building would have a heating system separate from the fan systems of the building. That way the inside temperatures could be easily maintained during data collections without any ventilation system effect. Under these

test conditions, the intercept term in Eq. (24) would be solely due to the air flow path distribution. It would represent the difference between the mid-building height and the neutral pressure level caused by buoyancy effect pressurization. In this manner, the actual location of the NPL could be located.

In researching references for this dissertation, very few references were found dealing specifically with equipment effect pressurization. Buildings could be tested as described earlier with outside ventilation turned off and the data fit to the Additive Temperature Ratio with Intercept Model. The same buildings could then be tested with various amounts of outside air ventilation being introduced to the structure. This should result in a change to the intercept term only. The introduction of outside air should tend to positively pressurize the entire structure and bias the pressurization plot upward but with the same slope. From this type of testing, a model could be developed solely for equipment effect pressurization. This would be another very helpful design tool for facilities design.

Much of the previous research on buoyancy effect building pressurization found that air flows across the building envelope adhere to what would be seen from a rigorous fluid dynamics analysis of the flowing air, pressure gradients, and flow paths. But some of the reason that the ASHRAE Method overestimates the pressure difference at extremely low temperatures may be tied to changes in the air flow at extreme low temperatures. It seems reasonable to assume that the fluid properties of the air (density, viscosity) don't deviate from their accepted variations with temperature. The "extremely cold" temperature reference, is in respect to temperatures experienced in building design. The temperatures are nowhere near the liquefaction temperatures that would cause great changes in the fluid properties of air. This leads to the conclusion that differences may exist due to changes in the flow paths. The changes in the openings (size, shape, edge condition) across the envelope may not behave linearly at the extremely cold outside temperatures. The earlier research was based

on building models that had uniform and regular air flow paths (generally drilled holes). It is easy to surmise that these would expand and contract differently with changes in temperature than the actual cracks, joints, and irregular holes present in the test building's envelope. Future research could look at how air flow paths similar to those in actual buildings change as their temperature exposure changes. Examples of such openings include: irregular spalling and cracking in concrete walls, linear expansion joints filled with various sealants, corners where expansion joints meet, joints between window assemblies and wall assemblies, and joints between door assemblies and wall assemblies.

As mentioned in Section 1.5, future modeling may include a computational fluid dynamics (CFD) approach. Presently this approach is generally reserved for high value building designs or analysis of non-standard building systems. These are generally the situations in which the added time and cost of CFD analysis can be justified.

One area presently using CFD analysis is modeling natural ventilation in a building. Chen and Li (undated) compared the results of a CFD model to a laboratory scale model of the natural ventilation in a single-zone building. Their results showed that the CFD model closely represented the scale model. Interestingly, the results showed multiple possible flow patterns within the building for the same sets of initial and boundary conditions. The model represented in this research dealt with a heat source at the floor level and the flow that it induced from air inlets at the floor perimeter to a single outlet at the zone's ceiling.

Alexander, et al. (1997) compared the analysis of a naturally ventilated atrium using CFD analysis to model wind tunnel testing. Atria are a non-standard building design element in which air flow patterns can be difficult to analyze. They tend to be large open spaces with little to no restriction to flow in either the horizontal or vertical

direction. They are often open to several building levels, thus causing a short circuit in the vertical flow of air through the structure. This particular analysis considered pressurization due to both wind and buoyancy effects for a naturally ventilated atrium. The building design being considered was a six-story office complex with the atrium connecting levels one through five. The office space was mechanically ventilated but the atrium would be naturally ventilated to control atrium temperatures. The design called for buoyancy effect to draw air upward through the atrium from inlets at the lowest level to an exhaust on the face of the highest level. The analysis was undertaken to insure that prevailing winds would not set up counter flows where air tended to enter at the high level vent and flow downward through the atrium to the low level vents. The analysis showed that the prevailing winds would set up this undesirable counter-flow condition. This required the design of an exit vent device for the upper outlet to counteract the impingement of the prevailing wind. The wind effect and device design were analyzed using both wind tunnel modeling techniques and commercially available CFD code. Both methods yielded different results but similar trends in the wind pressurization effect. Due to computing limitations, the CFD model had to be limited to a two dimensional model. This meant that only wind flow directly into the atrium's face was considered, quartering winds could not be modeled. Also, the CFD solutions never fully converged. They reached a steady, oscillating state, which was interpreted to represent the unsteady nature of the flow being modeled.

Beausoleil-Morrison, et al. (2001) describes the use of CFD integrated into a total building energy model. This analysis combined commonly used nodal modeling of a building with CFD modeling to account for air flow within zones and across building boundaries. An algorithm similar to SIMPLE cited earlier in this dissertation was used as the solution engine for the CFD code. Nodal analysis generally breaks the building into discrete zones or nodes to which energy conservation principles are applied. A limitation to this type of analysis is that only energy flows from zone

(node) to zone. In a real world building, air also flows from zone to zone (including across building boundaries). The research cited here, applied CFD methods to account for air flow through doors, windows, cracks, and other openings. Models of this combined nature help to predict not only energy consumption but also ventilation efficacy within the building.

These examples show that CFD can be a tool for modeling buoyancy effect pressurization. But they also show that there is a long way to go before CFD models will represent real world buildings and be useful tools for the consulting engineer in the day to day design of facilities.

Appendix A – Data

The CD-ROM included in this Appendix contains all of the data used in this research. The data is presented in many forms as described in earlier sections from raw data to various forms of processed data. In addition, an electronic version of this dissertation is present on the CD-ROM along with all of the figures and tables.

REFERENCES

- Alexander, D.K., Jenkins, H.G., Jones, P.J. (1997). "A Comparison of Wind Tunnel and CFD Methods Applied to Natural Ventilation Design".
- American Society of Heating Refrigeration, and Air Conditioning Engineers. *1997 ASHRAE Handbook – Fundamentals, Inch-Pound Edition*, American Society of Heating, Refrigeration, and Air Conditioning Engineers, Inc., 1791 Tullie Circle, N.E., Atlanta, GA 30329.
- American Society of Heating Refrigeration, and Air Conditioning Engineers. *Cooling and Heating Load Calculation Manual* (undated), ASHRAE GRP 158, American Society of Heating, Refrigeration, and Air Conditioning Engineers, Inc., 1791 Tullie Circle, N.E., Atlanta, GA 30329.
- Bargar, H.E. & Das, D.K. (2001). "Stack Effect Infiltration in Extreme Cold Climates" *Proceedings of the 52nd Arctic Science Conference*, Anchorage, AK, Sept 12-15, 2001, p. 31.
- Bargar, H.E. & Das, D.K. (2002). "Building Pressurization in Extreme Cold Climates" *Proceedings of the 11th International Conference on Cold Regions Engineering*, Anchorage, AK, May 20-22, 2002, p. 519-530.
- Beausoleil-Morrison, I., Clarke, J., Denev, J., Macdonald, I.A., Melikov, A., & Stankov, P. (2001). "Further Development in the Conflation of CFD and Building Simulation", *Seventh International IBPSA Conference*, Rio de Janeiro, Brazil, August 13-15, 2001.
- Chen, Z. & Li, Y. (undated). "Flow Bifurcations of Buoyancy Driven Natural Ventilation in a Single-Zone Building".

Fluid Dynamics International (undated), 1600 Orrington Avenue, Suite 400, Evanston, IL 60201.

Innovative Research, Inc. (undated), 2800 University Avenue SE, Minneapolis, MN 55414.

Insightful, Inc. (formerly Mathsoft, Inc.)(undated), 1700 Westlake Avenue North, Suite 500, Seattle, WA 98109-3044.

Kiel, D.E. & Wilson, D.J. (1986). "Gravity Driven Air Flows through Open Doors" *Paper 15, 7th AIC Conference*, Stratford-upon-Avon, UK, 29 Sept – 2 Oct 1986.

Lee, B.E., Husain M., & Soliman, B. (1980). "Predicting Natural Ventilation Forces upon Low-Rise Building" *ASHRAE Transactions* 22(2):35-39.

Lee, K.H., Lee, Y., & Tanaka, H. (1985). "Thermal Effect on Pressure Distribution in Simulated High-Rise Buildings: Experiment and Analysis" *ASHRAE Transactions* 91(2):530-544.

Lee, K.H., Tanaka, H., & Lee, Y. (1988). "Thermally Induced Pressure Distribution in Simulated Tall Buildings with Floor Partitions" *ASHRAE Transactions* 94(1):228-242.

Malik, N. (1978). "Field Studies of Dependence of Air Infiltration on Outside Temperature and Wind" *Energy and Buildings* 1(1997/98):281-292.

McQuiston, F.C., Parker, J.D., & Spitler, J.D. (2000). *Heating, Ventilating, and Air Conditioning Analysis and Design, 5th Edition*, John Wiley & Sons, Inc., 605 Third Ave., New York, NY 10158-0012.

Min, T.C. (1958). "Winter Infiltration through Swinging-Door Entrances in Multi-Story Buildings" *ASHRAE Transactions* 64:421-446.

Modera, M.P., Dickerhoff, D., Jansky, R., & Smith, B. (1991). "Improving the Energy Efficiency of Residential Air Distribution Systems in California" *Report LBL-30866*, Lawrence Berkeley National Laboratory, Berkeley, CA.

Neter, J., Kutner, M.H., Nachtsheim, C.J., & Wasserman, W. (1996). *Applied Linear Statistical Models, 4th Edition*, Irwin/McGraw-Hill, Inc., Burr Ridge, IL.

Patankar, S. V. (1980). *Numerical Heat Transfer and Fluid Flow*, McGraw-Hill Book Company, PO Box 182605, Columbus, OH 43218-2605.

Phillips, J. (1997). Personal Communication, Physical Plant Director, University of Alaska Fairbanks, Fairbanks, AK.

Swami, M.V. & Chandra S. (1988). "Correlations for Pressure Distribution on Buildings and Calculation of Natural-Ventilation Air Flow" *ASHRAE Transactions* 94(1):243-266.

Tamura, G.T. & Wilson, A.G. (1966). "Pressure Differences for a Nine-Story Building as a Result of Chimney Effect and Ventilation System Operation" *ASHRAE Transactions* 72(1):180-189.

Tamura, G.T. & Wilson, A.G. (1968). "Pressure Differences Caused by Wind on Two Tall Buildings" *ASHRAE Transactions* 74(2):170-181.

Tamura, T.G. & Shaw, C.Y. (1976). "Studies on Exterior Wall Air Tightness and Air Infiltration of Tall Buildings" *ASHRAE Transactions* 82(1):122-134.

NOTE TO USERS

**The CD is not included in this original manuscript.
It is available for consultation at the author's
graduate school library.**

This reproduction is the best copy available.

UMI